Exclusion Based Sample Preparation Enabling Multiple Analyte Interrogation

By

Lindsay Strotman

A dissertation submitted in partial fulfillment of

the requirements for the degree of

Doctor of Philosophy

(Biomedical Engineering)

at the

University of Wisconsin-Madison

2014

Date of final oral examination: 3/05/14

This dissertation is approved by the following members of the Final Oral Committee:
David J. Beebe, Professor, Biomedical Engineering
Elaine Alarid, Professor, Oncology
Richard Burgess, Professor Emeritus, Oncology
Linda Schuler, Professor, Comparative Biosciences
Lloyd Smith, Professor, Chemistry

Abstract

Sample preparation is critical and necessary in most analytical processes to isolate and enrich components of interest from a sample matrix. While great advances have been made in the detection and analysis of analytes (protein, nucleic acids, etc.) over the past few decades, improvements in sample preparation have been relatively modest, generating a ‘‘bottleneck’’ in the process workflow. We present a new technology, termed Exclusion-based Sample Preparation (ESP), that relies on “excluding” contaminants from analytes of interest bound to magnetic particles by either moving the magnetic particles, liquid or surface. Many of these unique ESP platforms are enabled by the dominance of surface tension over gravity at the microscale. By removing repetitive, dilutive wash and centrifugation steps we can streamLine sample preparation workflows to create non-laborious and cost effective devices.

Here I utilize ESP technology to develop several sample preparation platforms to extract and isolate multiple analytes of interest, such as the protein botulinum neurotoxin Type A for food safety testing and viral HIV RNA for viral load determination. I also exploit an inherent advantage of ESP in that starting sample is never lost or diluted which enables resampling. Using this simple concept we developed an ESP platform to enable multiple analyte interrogation from a single and rare cell population. Using this device, we begin to highlight the potential effectiveness of ESP for biological and clinical applications.

To my parents Don and Debra,

and loving fiancé Aaron

Acknowledgements

I would like to begin by thanking my advisor, David Beebe, for providing the opportunity for me to pursue my graduate studies in the Microtechnology, Medicine, and Biology (MMB) laboratory and for providing me with valuable insights and guidance throughout my graduate school career. I also wish to thank the members of the MMB lab; I would not be where I am without the brainstorming and insight gained from interacting with every one of you. In particular, I would like to thank Scott Berry for your guidance over the years as well as Ben Casavant, Ashleigh Theberge, Erwin Berthier, Rachel O'Connell, Sam Schultz and Peter Thomas whom I have had the chance to work closely with during my graduate career and have greatly benefited from your hard work and insight. I also wish to acknowledge a key collaborator at the University of Wisconsin, Joshua Lang and his lab members Jamie Sperger, Stephanie Thiede and Benjamin Gibbs who enabled me to fulfill my graduate school goal of clinical translational research.

I wish to thank my parents Don and Debra Strotman who have always provided support and guidance in all of my endeavors, and my sibling Katie Strotman all of their support.

I also thank my friends, old and new, for the many laughs and good times.

I owe much of my happiness in graduate school to my wonderful soon to be husband, Aaron DeWitt, who has supported me every day of my career even going so far as to move to Wisconsin with me. During the past few years you have helped me to stay balanced and much, much more.

Table of Contents

List of Figures

List of Tables

Papers

Chapter	Adapted / taken from papers
Chapter 2	"Facile and rapid DNA extraction and purification from food matrices using IFAST (immiscible filtration assisted by surface tension." Lindsay N. Strotman, Guangyun Lin, Scott M. Berry, Eric A Johnson and David J. Beebe, Analyst. 2012
Chapter 3	Manuscript in preparation
Chapter 4	"Nucleic Acid Sample Preparation Using Spontaneous Biphasic Plug Flow." Peter C. Thomas‡, Lindsay N. Strotman‡, Ashleigh B. Theberge, Erwin Berthier, Rachel O'Connell, Jennifer Loeb, Scott M. Berry and David J. Beebe. *Analytical Chemistry,* 2013
Chapter 5	Manuscript in preparation
Chapter 6	"Selective Nucleic Acid Removal via Exclusion (SNARE): Capturing mRNA and DNA from a Single Sample" Lindsay N. Strotman, Rachel O'Connell, Benjamin P. Casavant, Scott M. Berry, Jamie M. Sperger, Joshua M. Lang and David J. Beebe. *Analytical Chemistry* 2013
Chapter 7	"Paired diagnostic and pharmacodynamic analysis of rare non-small cell lung cancer cells enabled by the VerIFAST platform" Benjamin P. Casavant‡, Lindsay N. Strotman‡, Jacob T. Tokar, Stephanie M. Thiede, Anne M. Traynor, J. Scott Ferguson, Joshua M. Lang and David J. Beebe. *Lab on a Chip* 2013
Chapter 8	Manuscript in preparation
Appendix A	Manuscript in preparation

‡Denotes equal contribution

Chapter 1 – Exclusion-Based Sample Preparation

1.1 Background

1.1.1 Need for New Sample Preparation Methods

Technological innovations in analytical techniques have enabled scientists to collect information faster and with greater sensitivity than in the past. But despite these advancements many analytical techniques are still subjected to time-consuming and labor intensive sample preparation methods, resulting in a processing bottleneck[1]. To help resolve this bottleneck and enable high throughput applications, new sample preparation methods are needed.

Sample preparation is often a limiting factor to the sensitivity and specificity of many analytical techniques[2]. These processes are needed to reduce sample complexity, enrich for low abundant analytes and remove contaminants that might mask or interfere with the analysis of the analyte of interest[3]. During the past decade, active research on sample preparation has been increasingly fueled by the pressure to analyze the unprecedented large-scale complex samples in various "-omics"[4]. This has led to the exploration of sample preparation techniques that are fast, easy-to-use and cost effective while also being robust, reproducible and easily scaled for high throughput screenings. As the future progresses, experts have stated that advances in sample preparation methods will be driven by the analysis of small sample volumes and integration with downstream analytical techniques to improve the overall workflow[5]. These needs have greatly paralleled the advantages of microfluidics; including, lower reagent and sample consumption, reduction in analysis times and potential for integration[6], leading to new microfluidic sample preparation devices.

1.1.2 Traditional Sample Preparation Techniques

The most common sample preparation methods for bioanalytes include precipitation (PE), dialysis, filtration, centrifugation, liquid-liquid extraction (LLE) and solid phase extraction (SPE). Other techniques involve more advanced technologies, such as capillary electrophoresis, isoelectric electrophoresis, free flow electrophoresis and gel electrophoresis[3]**.** Of these sample preparation approaches, SPE has become the most popular due to the following advantages: high recovery, effective pre-concentration, the need for less organic solvent (compared to LLE & PE), no foaming in the formation of emulsions, ease of operation and greater possibility of automation as compared to other approaches[1]**.** In SPE, the analyte of interest is retained on a solid phase by interactions with various sorbents while a mobile liquid phase removes undesired compounds before elution of the purified analyte[2] (Figure 1).

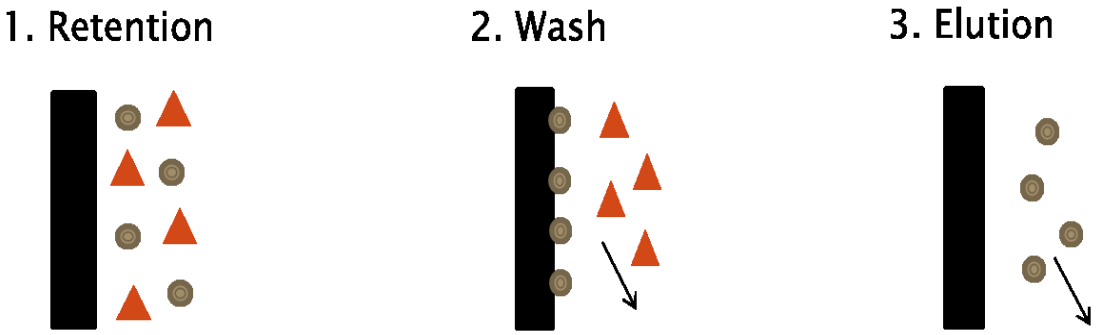

Figure 1-Solid Phase Extraction Method (SPE) 1) Retention of analyte 2) Washing away of contaminants 3) Elution of analyte

Several SPE stationary solid phase supports exist; including, column cartridges, discs and well-plates, pipette tips and microfibers. Several of these embodiments have been developed to be used with vacuum, positive-pressure manifolds and centrifugation for faster, easier and scaled-up liquid handling[1]. In 1976, John Ugelstad introduced monodispersed polystyrene

particles, which were the first mobile solid phase support. The polystyrene particles were later made magnetizable to form paramagnetic particles (PMPs) for SPE applications[7].

In addition to the variety of solid phase supports that exist, a variety of sorbents with different chemical moieties exist to capture analytes of interest. The choice of sorbents depends strongly on the analytes and their physical or chemical properties, such as size, charge, hydrophobicity, binding affinity and biological activity[8]. Sorbents for nucleic acids SPE include hydrogen-binding interaction under chaotropic conditions (i.e., silica), anion exchange carriers and affinity mechanisms[9]. Sorbents for protein SPE include commonly employed chromatographic chemistries, such as ion-exchange (weak-cation exchange "WCX", strong-cation exchange "SCX", weak-anion exchange "WAX", strong-anion exchange "SAX", etc.), affinity (protein G, protein A, streptavidin, etc.) and reverse phase (octadecyl "C18", octyl "C8", metyl "C4", etc.)[10]. Despite the multitude of sorbents that have been developed to facilitate the convenient processing of different types of samples, most still suffer from multiple wash steps or centrifugation steps. While these methods are time consuming and require larger sample volumes, they also expose samples to unnecessary shear forces and complexity when trying to automate for high throughput studies.

1.1.3 Microfluidic Sample Preparation Techniques

There have been several microfluidic devices developed for sample preparation. These devices rely on reducing macroscale procedures such as dialysis, filtration, LLE, various electrophoresis methods and the most popular SPE[11]. Methods to integrate SPE with microfluidics include wall derivatizations, which usually suffer from poor surface-to-volume ratios and bead packed columns, *in-situ* polymerized porous monoliths and pre-formed porous

membranes, which suffer from high backpressure and clogging[6]. To help the fluids move through SPE supports faster, microfluidic disks that use centrifugal forces to transport liquids were developed[12]. Finally, microfluidic devices that magnetically trap PMPs while sample is being washed have been developed but they are sensitive to PMPs being washed away[13]. While the above microfluidic devices have been shown to work they are often complex and difficult to scale-up for automation and laboratory integration limiting their use for high throughput proteomics[2].

1.1.4 Exclusion Based Sample Preparation

To overcome the current challenges associated with sample preparation our lab developed a suite of platforms, following under the umbrella of Exclusion-based Sample Preparation (ESP) technology. In ESP platforms, instead of holding the PMPs stationary and adding/removing liquids as in traditional SPE methods, either the PMPs, liquid or surface can move (Figure 2). This allows one to imagine several platforms with the idea always to "exclude" contaminants away from the analyte bound PMPs.

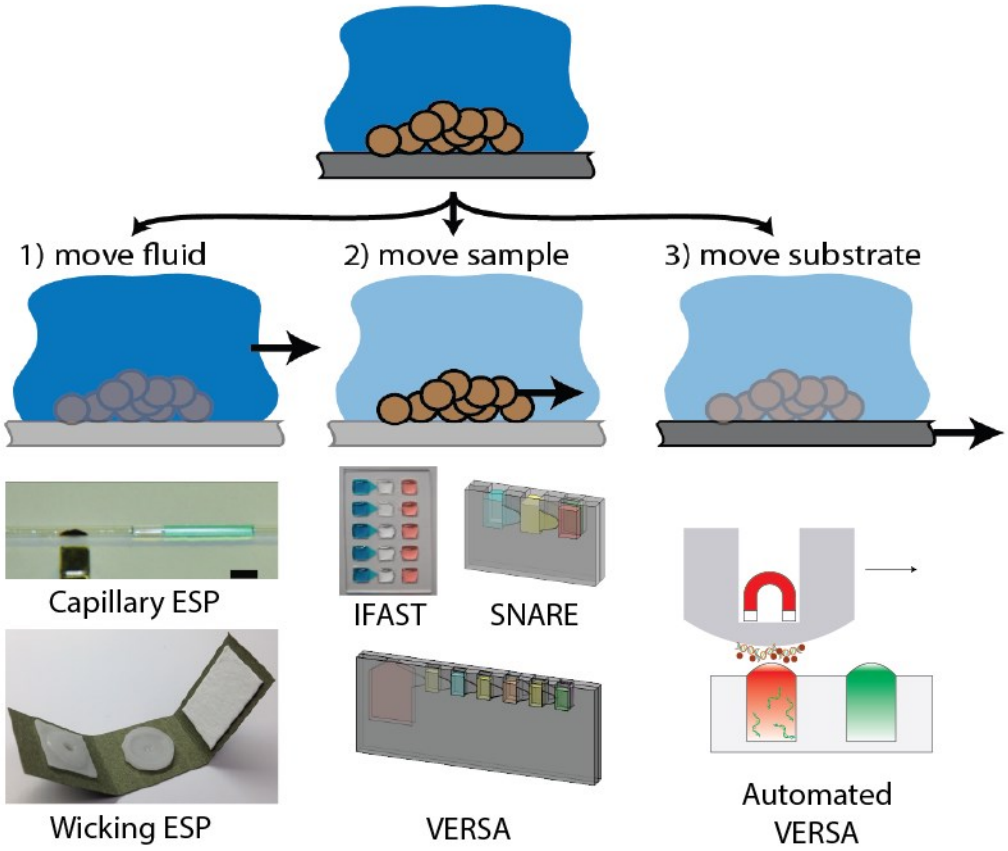

Figure 2-Multiple ESP Methods 1) Move the fluid: capillary and wicking ESP 2) Move sample: IFAST (Immiscible Phase Filtration Assisted by Surface Tension), SNARE (Selective Nucleic Acid Removal via Exclusion) and VERSA (Vertical Exclusion-based Rare Sample Analysis) 3) Move substrate: Automated VERSA. Modified figure courtesy of Benjamin Casavant.

The majority of ESP methods introduced here are enabled by the dominance of surface tension at the microscale[14]. Surface tension is the cohesive force that holds liquid molecules together on a surface and resists forces that would otherwise separate it, including gravity, shear or other forces imposed on a fluid surface. Dominance of surface tension is predicted by the Bond number, which is proportional to the buoyancy force divided by the surface tension force; therefore being characterized by density (ρ), length (L) and fluid surface tension (γ). If the Bond

number is less than one, surface tension is more influential than gravity. The Bond number is defined as:

$$B = \frac{\rho g L^2}{\gamma}$$

The dominance of surface tension at the microscale, allows us to create stable air/liquid interfaces[15, 16] such that PMPs can be moved through these stable interfaces via magnetic force. For another ESP method that relies on surface tension, the difference in surface tension between two immiscible fluids causes the liquids to self-propel eliminating the need for specialized external equipment for fluid manipulation.

The advantages of ESP over traditional sample preparation methods is further enhanced because a single traverse of the air/liquid interface or fluid removal eliminates contaminants as effectively as multiple traditional wash and centrifugation steps. Thus, a single motion of a magnet is the equivalent of multiple liquid transfer steps, streamLining the entire sample preparation workflow (Figure 3).

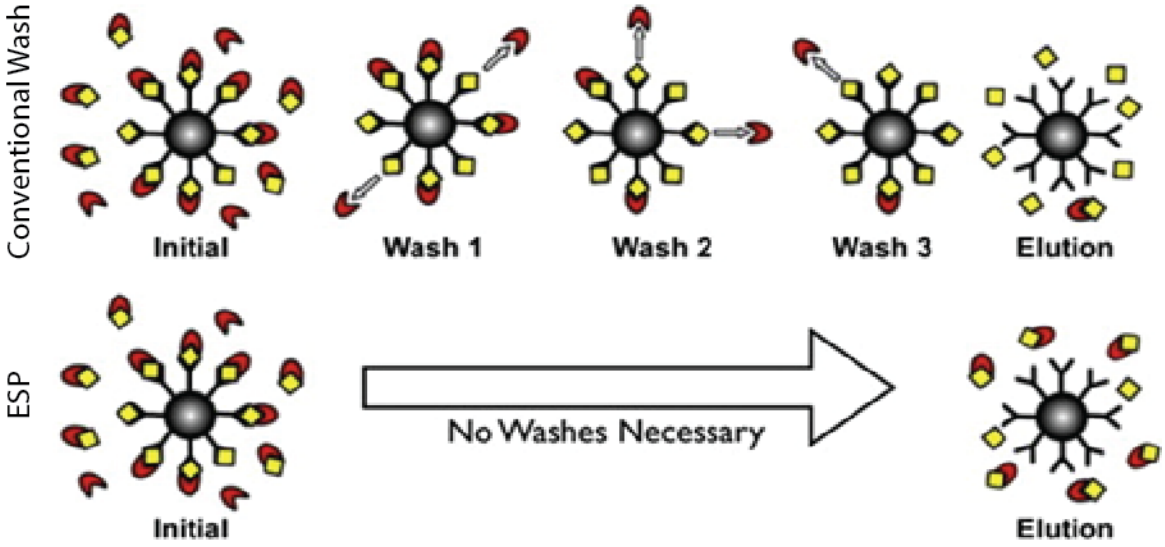

Figure 3-Comparison of ESP and conventional wash methods. Image courtesy of Scott Berry.

Furthermore, as the sample is never discarded or diluted using some ESP platforms the ability to resample multiple analytes from a single rare or precious sample emerges[17]. This allows paired genomic, transcriptomic and proteomic comparison. Due to a shift away from traditional sample preparation methods, ESP significantly simplifies the process workflow, resulting in a cost effective and time efficient platform. Additionally, the simplicity ESP affords, allows for easy manufacturing and automation[18].

Finally, another unique advantage of ESP that we have demonstrated is the ability to isolate protein-protein interactions that are weak (high dissociation constant, K_D) or brief (short half-life of the complex) that would otherwise dissociate during traditional wash methods. This is of high importance as many critical biological processes are mediated through very transient interactions. To prove ESP efficacy in isolating weak protein-protein interaction we used a GFP model system from the Burgess Lab that employs a monoclonal antibody to capture a GFP

molecule tagged with an epitope from RNA polymerase. We manipulated the dissociation constant of this antibody/antigen complex by selectively changing the ammonium sulfate and propylene glycol concentrations in the system buffer. Results showed that ESP could purify GFP (Figure 4A). It was also shown that as the ammonium sulfate concentration increased ESP (reducing K_D) was able to recover more GFP than conventional co-immunoprecipitation processes that utilize harsh washing conditions to remove unbound and non-specific proteins from the target complex (Figure 4B).

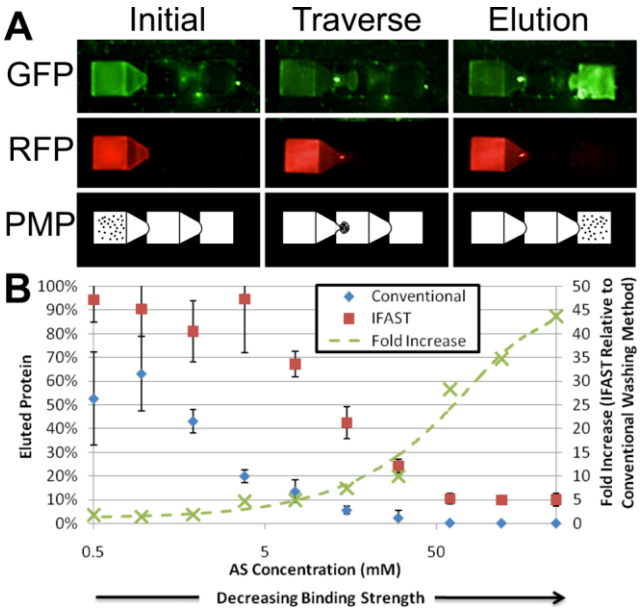

Figure 4- A) Fluorescent images of GFP lysate isolation showing little carryover of RFP. B) Graph depicting protein concentration eluted using conventional washed based PMPs and IFAST methods.

This method was also used by Scott Berry and Emily Chen, using proteins involved in the Wnt signaling pathway to demonstrate its ability to work for clinically relevant, transient protein complexes[19]. This work is further being extended to cell isolation, specifically focused on circulating tumor cells (CTCs) expressing low levels of, epithelial adhesion molecule (EpCAM),

which we use to capture the cells. Using a prostate cancer cell line, PC3 known to have low levels of EpCAM, we were able to show ESP platforms were able to isolate more PC3 cells as compared to traditional wash methods (Figure 5). This is especially important as the literature has shown that actual CTCs express low levels of EpCAM comparable to the PC3 cell line[20].

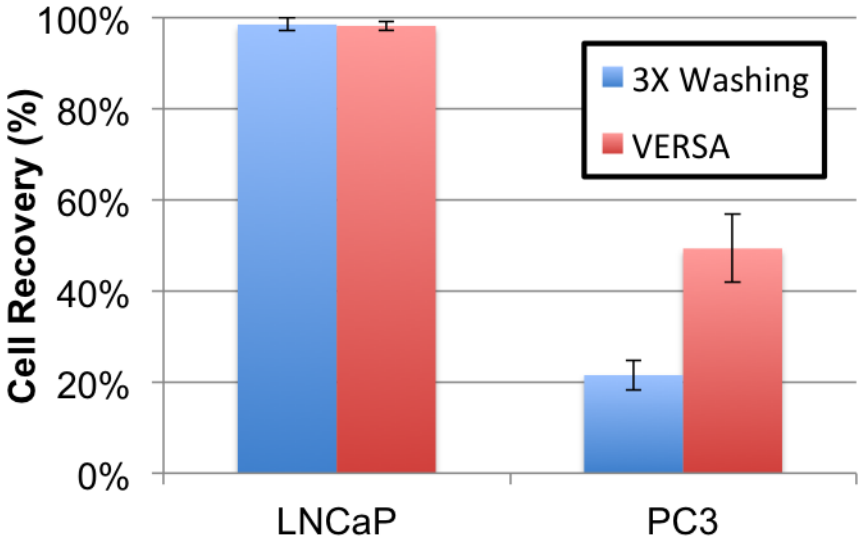

Figure 5-Cell Recovery percentage of two different prostate cancer cell lines either high in EpCAM expression (LNCaPs) or low in EpCAM expression (PC3) isolated using VERSA (i.e., similar to ESP technology IFAST) or wash methods.

While significant advancements and achievements have occurred in the past few decades concerning downstream analytical techniques, upstream sample preparation has largely been ignored. This has led to a current workflow bottleneck in several industries; including biology with the introduction of "onmics", healthcare, agriculture, etc. Due to the inherent advantages of ESP technology, including streamLining of sample preparation workflow, which results in reduced cost and time; as well as, the ability to resample, easily automate and isolate weak

interactions I have intensely explored this subject area for a variety of different downstream assays.

1.2 Methods & Materials

1.2.1 IFAST device fabrication

IFAST devices were fabricated from polydimethylsiloxane (Sylgard 184; Dow Corning) using soft lithography and then pressed onto glass bottoms (No. 1 cover glass; Fisher). The initial IFAST configuration consisted of three wells (volume/well 8.5 µl) connected by two trapezoidal microfluidic channels (Figure 6).

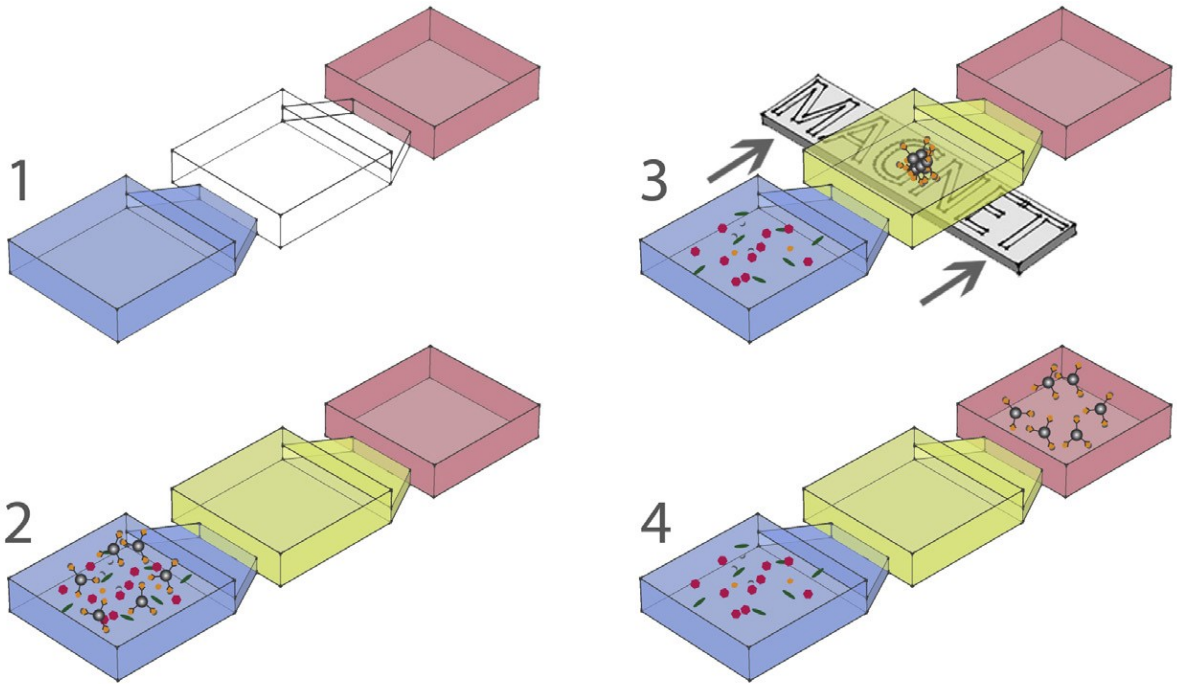

Figure 6-IFAST device operation and configuration. 1) Aqueous sample solution containing PMPs is added to input well (blue) and elution buffer is added to the output well (red) of the three well device. The microfluidic constrictions act as virtual walls, preventing the solution from filling into the middle well. 2) Oil is then added to the middle well (yellow) to establish the immiscible barrier. 3) During operation, a magnet is used to draw PMP-bound antigens through the oil barrier. 4) Protein bound PMPs are then pulled into the output well, completing isolation and purification

1.2.2 Protein expression and preparation of lysates

The plasmid construct containing green fluorescent protein (GFP) with a C-terminal epitope tag consisting of the amino acids PEEKLLRAIFGEKAS (etGFP) and the expression of soluble protein by growth at 26 °C in *Escherichia coli* in the presence of an overexpressed *GroEL* and *GroES* system have been described[21]. To this lysate was added an amount of His6-tagged red fluorescent protein (RFP) that had been produced in *E. coli* and purified on a Ni–NTA column (Qiagen). In this mixture, the initial concentration of RFP was 20 times higher than the concentration of etGFP.

1.2.3 Preparation of PMP for etGFP experiments

A solution containing 15 mg/mL protein G-conjugated PMPs (Dynabeads Protein G; Invitrogen) and 0.031 mg/mL of polyol-responsive mAb 8RB13 in phosphate-buffered saline (PBS) containing 0.01% Tween 20 (PBST) was prepared and incubated for 30 min at room temperature to allow mAb attachment to the PMPs. The beads were then washed twice with 100 μl of PBST.

1.2.4 IFAST operation and characterization

MAb-labeled PMPs were resuspended in PBS (15 mg/mL PMP concentration), and 2% (by volume) bacterial lysate was added. Following a 10-min incubation of the bacterial lysate with mAb-PMPs at room temperature with rotation, the etGFP was purified using both conventional PMP-based purification and IFAST.

Conventional PMP-based purification was done according to the manufacturer's protocol (Invitrogen immunoprecipitation kit). Briefly, a magnetic stand (DynaMag-2; Invitrogen) was utilized to aggregate PMPs from 100 μl of PMP/bacterial lysate solution onto the side of a 1.5-mL microcentrifuge tube. After removal of the supernatant, 200 μl of wash buffer (Invitrogen IP

kit) was added and the PMP aggregate was resuspended via agitation with a micropipette. This wash process was repeated for a total of four washes before the protein was eluted with elution buffer (50 mM Tris–HCl and 0.1 mM EDTA (pH 7.9) containing 750 mM ammonium sulfate (AS) and 40% propylene glycol).

For IFAST purification, 8.5 µl of bacterial lysate, 8.5 µL of olive oil (Unilever), and 8.5 µl of elution buffer were added. A magnetic bar (BX041; K&J Magnetics) was then placed under the input well and used to draw the PMP aggregate through the oil and into the elution buffer at a rate of approximately 1–2 mm/s (total traverse time ≈3–4 s). Once in the elution buffer, PMPs were given 2 min for elution before the eluent was collected via pipette for analysis.

1.2.5 Varying binding conditions

To demonstrate the ability of IFAST to isolate weakly bound protein, lysate containing epitope-tagged etGFP protein (1% by volume, approximately 12 µg/mL etGFP) was mixed with mAb-labeled PMPs in a variety of solutions containing 20% propylene glycol and 0 to 250 mM AS and incubated for 30 min at room temperature to allow protein binding. Previous work[21] demonstrated that the strength of the mAb 8RB13/epitope tag interaction could be weakened by increasing AS concentration, such that weakly bound complexes could be artificially generated in a predictable and repeatable manner. Immunoprecipitation of etGFP was performed using both IFAST and washing-based protocols as previously described, except that the washing and binding solutions were replaced by AS buffers (50 mM Tris–HCl and 0.1 mM EDTA, pH 7.9) containing 0 to 250 mM AS and 20% propylene glycol. As before, elution was

performed in a solution containing 750 mM AS and 40% propylene glycol and the etGFP recovered was quantified.

1.2.6 Quantification of etGFP and RFP

To quantify the etGFP (λ_{ex} 490 nm and λ_{em} 509 nm) and RFP (λ_{ex} 563 nm and λ_{em} 582 nm), in the various steps of the IP (bacterial lysates, depleted lysates, washing steps where applicable, and eluted materials), solutions were loaded into well plates (384 or 1536 wells) and imaged using a fluorescence scanner (Typhoon Trio; GE) and quantified with ImageQuant software. Well plates were used to prevent evaporation during the scanning process, which took approximately 15 min, as the IFAST devices are not sealed. A two-tailed, unpaired Student *t* test was used to determine significance. Representative IFAST samples were fluorescently imaged during purification (Fotodyne Luminary).

1.2.7 Cell Culture

The LNCaP and PC3 prostate cancer cell lines (ATCC, USA) were cultured in Corning Cellgro® RPMI 1640 Medium (VWR, USA) containing 10 % fetal bovine serum, 1 % Pen-Strep, 1 % Sodium-Pyruvate and 1 % α-MEM. All cells were cultured at 37 °C and maintained under 5 % CO_2 in polystyrene flasks until confluent. Cells were released using a 0.05 % trypsin/EDTA solution and collected via centrifugation.

1.2.8 Cell Isolation and Quantification

M-280 streptavidin coupled PMPs (Dynabeads®, Life Technologies, USA) at a concentration of 250 µg per a reaction were used for all experiments. The PMPs were washed twice and resuspended in 0.01% Tween-20 in phosphate buffered solution (PBS). 0.4 µg/mL of epithelial cell adhesion molecule (EpCAM, R&D Systems, USA) biotinylated were added to the solution.

The PMPs and antibodies were mixed for 30 minutes at RT followed by three washes and resuspension in 0.1 % BSA in PBS. EpCAM bound PMPs were mixed with 1,000 cells stained with 2 mM calcein AM (Life Technologies, USA) in a 1.5-mL microcentrifuge for 30 minutes at 4 °C on a tumbler. Purification was performed as described above using either the IFAST method with an input of 50 μL or the conventional wash method (3x's). Cells were then imaged in the input well at 492 nm using a fluorescent microscope (Olympus IX70). Cells were analyzed and counted using ImageJ.

1.3 Conclusion

While ESP in an inclusive name for several different sample preparation platforms, I want to highlight the ones explored here. First, we present a platform termed IFAST (Immiscible Filtration assisted by Surface Tension) for specific sample preparation applications. IFAST operates on the principle of immiscible phase filtration, which was pioneered by our lab[22, 23] and others[24-27]. IFAST technology differs by taking advantage of surface tension dominating gravity at the microscale to enable "side-by-side" loading of the immiscible phases with no mixing. Therefore, any analyte bound to paramagnetic beads (PMPs) through various chemical moieties can be purified by a translocation through the immiscible phase by a handheld permanent magnet. First, we demonstrate its ability to isolate DNA from the bacterium *C. botulinum* and then botulinum neurotoxin Type A protein. We then introduce a new ESP platform termed, capillary IFAST that uses the differences in surface tension between two immiscible fluids to propel contaminating sample away. The last ESP method I introduce is wicking ESP, which was designed for low resource settings to extract HIV viral RNA for viral load measurement. Finally, building on the strengths of ESP, we not only integrated isolation and enumeration of CTCs but

also add the ability to perform intracellular histochemistry and sequential mRNA and DNA isolation. Termed the VERSA, we demonstrate how this platform can be used to start designing and accessing prognostic, predictive and pharmacodynamics biomarkers of CTCs. In each of the coming chapters, I will highlight how ESP technology can either enhance or enable a variety of different analytical assays.

1.4 Acknowledgements

I would like to thank Scott Berry for helpful discussions and contributions throughout the years to this chapter, specifically all the work on weak binding for both proteins and cells. Finally, I would also like to thank David Beebe, Richard Burgess and Josh Lang on all the long discussions about weak binding and the potential advantages of ESP methods.

Chapter 2 – Facile and Rapid DNA Extraction and Purification from Food Matrices Using IFAST (Immiscible Filtration Assisted by Surface Tension)

2.1 Introduction

Efficient and reliable DNA extraction and purification is an essential component in downstream sensing and analytical methods. It is a labor intensive and time-consuming process resulting in upstream sample preparation bottlenecks[8]. As recently as the 1990s, DNA extraction and purification required the use of toxic and hazardous chemicals, however the advent of DNA solid phase extraction methods (SPE) drastically changed this paradigm[28]. The majority of commercial kits now available for DNA extraction and purification are SPE-based protocols, which can be generalized as 1) bind DNA to immobilized surface 2) wash or centrifuge away contaminants and 3) elute DNA. While these SPE-based methods are faster than previously established methods, they still require a significant amount of hands-on work time due to the multiple wash or centrifugation steps required for contaminant removal. While some larger labs have robotic instrumentation for automated sample preparation, the high cost and large footprint are prohibitive to most.

As the popularity of highly specific and sensitive DNA-based assays increases for point-of-care applications (i.e., medical diagnostics, environmental monitoring and food safety testing), new DNA sample preparation methods that are easy to perform, cost effective and transportable are needed. To this, researchers have developed miniaturized devices utilizing functionalized surfaces and microparticles to capture DNA and remove contaminants[29]. These microscale SPE devices also have the added advantages of lower reagent consumption, higher

integration potential and increased throughput[22]. Since most of these microscale devices are derivatives of macroscale protocols they still require multiple wash and centrifugation steps, resulting in device complexity. These limitations increase manufacturing complexity and cost leading to lower commercialization potential and reduced user adoption. This report describes how we have overcome these limitations with a technology termed IFAST by demonstrating simplified, rapid and efficient extraction and purification of DNA from food matrices.

The IFAST device operates on the principle of immiscible phase filtration, developed in various embodiments by our group and others for analyte isolation[22-26]. IFAST technology exploits the dominance of surface tension over gravity at the microscale to establish "virtual walls"[15, 16] allowing "side-by-side" loading of these immiscible phases (i.e., oil). The immiscible phase acts as a filter to separate an upstream "dirty" side from a downstream "clean" side, thereby replacing the multiple washes or centrifugation steps required for other DNA SPE-based methods. IFAST doesn't require the use of any external equipment outside of a pipette and magnet. This is in contrast to other microfluidic examples that require multiple electronic, pneumatic, or hydraulic connections to manipulate fluids in complex pathways, greatly increasing complexity and decreasing use outside of a laboratory setting. While the IFAST device has previously been shown to be effective for mRNA isolation and whole cell purification[22, 23], its applicability to DNA extraction and purification has not been reported.

To demonstrate the utility of the IFAST device as an effective DNA sample preparation method, *C. botulinum* DNA was extracted and isolated. *C. botulinum* was used as a representative biowarfare detection application because it produces botulinum neurotoxin, which is the most lethal toxin known (LD_{50} of 1-10 ng/kg)[30] and classified as a potential bioterroristic

threat[31], especially within the food supply chain. The quality of extracted and purified DNA was determined by qPCR and compared with the commercially available SPE Invitrogen ChargeSwitch® kit. We demonstrated that a sample containing *C. botulinum* cells can be processed in the IFAST and is comparable to the ChargeSwitch® method. We also extracted and purified *C. botulinum* DNA from complex food matrices (i.e., milk and orange juice) contaminated by *C. botulinum* to show that IFAST is a robust method for food safety applications. Given the simplicity, cost-effectiveness and portability of IFAST it could serve either as an independent DNA sample preparation method or be easily integrated with previously developed downstream detection technology.

2.2 Materials & Methods

2.2.1 Reagents

ChargeSwitch® kit was purchased from Invitrogen. SYBR® Green PCR Master Mix was purchased from Bio-Rad.

2.2.2 Bacterial Strain and Culture Conditions

The Clostridium botulinum strain ATCC 3502 (Type A) used in this study was from Dr. Eric A. Johnson (E.A.J.) laboratory. Cultures were grown in 10 mL of sterile TPGY media containing (per liter) 50 g Trypticase peptone, 5 g Bacto peptone, 4 g D-glucose, 20 g yeast extract and 1 g cysteine-HCl, pH 7.4 for 24 hours at 37°C under anaerobic conditions.

2.2.3 IFAST Device Fabrication

IFAST devices were fabricated from poly (dimethylsiloxane) (PDMS; Sylgard 184, Dow Corning) using standard soft lithographic techniques. The PDMS mold was attached to glass cover slips. Each IFAST device consists of three wells that are connected in parallel by

microfluidic constrictions (500x250 μm), which act to "pin" aqueous fluids, to enable side-by-side loading of immiscible fluids (See Figure 7). The input size can be increased provided the microfluidic constriction remains in a surface tension dominated range[6].

2.2.4 DNA Extraction using ChargeSwitch® kit

DNA extraction was performed according to ChargeSwitch® manufacturer's directions, as a positive control. Briefly, resuspension buffer and lysosome (5 mg/mL) were added to *C. botulinum* cells in culture media followed by a 10 minute incubation at 37 °C. Next, lysis buffer with proteinase K was added to *C. botulinum* cells followed by a 10 minute incubation at 55 °C. Finally, binding buffer was added to adjust the pH of the solution to less than 6 to enable *C. botulinum* DNA to bind to PMPs 1 μm in size. After binding, two wash steps were performed, followed by elution at pH 8.5. A negative control of culture media with no *C. botulinum* cells was also completed using the same method described above.

2.2.5 DNA Extraction in IFAST Device

All reagents and PMPs used in IFAST operation were from the ChargeSwitch® kit. However, some deviations in the manufacturer's directions concerning lysis of the *C. botulinum* cells were made in terms of lysing on and off IFAST as described below. A negative control of culture media with no *C. botulinum* cells was completed using both methods described below.

2.2.6 Off IFAST Cell Lysis

10^8 *C. botulinum* cells/mL were first lysed according to ChargeSwitch® manufacturer's protocol in an Eppendorf tube before loading on the IFAST device. Then 8.5 μL of *C. botulinum* lysate and PMPs (9 μg) were added to the input well of the IFAST device. The DNA binding capacity range for the PMPs in the IFAST input is 45-90 ng. After that, 8.5 μL of elution buffer was

added to the output well and lastly 8.5 µL of olive oil (Unilever) was added to the middle well. A handheld external magnet was used to draw the PMPs from the input well through the olive oil into the output well. The PMPs and elution buffer were then removed from the output well to perform qPCR.

2.2.7 On IFAST Cell Lysis

10^8 *C. botulinum* cells/mL were lysed on IFAST by combining the cells and lysing reagents (resuspension buffer and lysis buffer) used in the ChargeSwitch® at the same ratio as specified in the manufacturer's protocol to the input well. The loaded IFAST was then placed in an Omnitray (NUNC) with 1x PBS sacrificial drops to prevent evaporation and incubated for 30 minutes at 25 °C. Afterwards, PMPs and binding buffer were added following a 5 minute time period to allow DNA binding. IFAST was operated as described above. Binding buffer was added to adjust the pH of the input solution to allow *C. botulinum* DNA to bind to the PMPs since binding is charge dependent.

2.2.8 PCR Amplification

The primers used in this study included a BoNT/A specific forward primer: 5'-AGCAAACTTTAATGGTCAAAATACAG-3' and a reverse primer: 5'-TCTTGAGCACGAAGATAATGGAAC-3'which were used to amplify part of the BoNT/A binding domain. For each qPCR sample, 1 µL of purified *C. botulinum* DNA was mixed with 12.5 µL of SYBR® Green PCR Master Mix, 10.5 µL nuclease free water and 0.5 µL of both BoNT/A forward and reverse primers at a 5 µM final concentration. The reaction was run using a thermal cycler (MyiQ Thermal Cycler, Bio-Rad). The hot start was completed at 95 °C (denature) for 3 minutes, followed by 45 cycles consisting of 95 °C (denature) for 15 second, 55

°C (annealing) for 30 second, and 72°C (extension) for 1 min and 45 seconds. This was followed by a cycle of 95 °C for 1 min, 55 °C at 1 min, and 55 °C at 10 s to determine melt curves. Detection was established by observing the threshold cycles and melt curves of qPCR. The amplified qPCR products were also visualized on a 1 % agarose gel and sequenced at UW-Madison DNA-sequencing facility. The sequencing results were analyzed using Vector NTI Suite program (Invitrogen) to confirm the correct gene (BoNT/A) was amplified.

2.2.9 Detection of C. botulinum in Food Matrices

10^8 *C. botulinum* cells/mL were spiked in whole milk (Kemps) and orange juice (Tropicana). DNA purification and qPCR detection was then carried out as described above using both the ChargeSwitch® and Off IFAST lysis method.

2.2.10 IFAST Sensitivity Study

C. botulinum cells were counted using a hemocytometer and cells were pelletized. The cells were then resuspended in TPGY media to obtain approximately 10^8 cells/mL. Next, 1 to 10 serial dilutions were performed to obtain approximately 1 cell/mL. DNA purification and qPCR detection was performed as described above using both ChargeSwitch® and Off IFAST Lysis methods. Purification efficiency was determined from the sensitivity curve using the following equation. $Efficiency = 10^{-1/slope} - 1$.

2.3 Results

The IFAST device isolated DNA from *C. botulinum* cells in culture broth and in complex food matrices as effectively as the ChargeSwitch® method (Figure 7). Detection was accomplished by qPCR and measured by determining the threshold cycle (C_t). No C_t values were shown, when a negative control of culture broth with no cells was purified using both IFAST and

ChargeSwitch® methods (Supplementary Figure 11). The amplified qPCR products were confirmed by both agarose gel electrophoresis (See Figure 9b) and DNA sequencing, in which the sequences matched the amplicon.

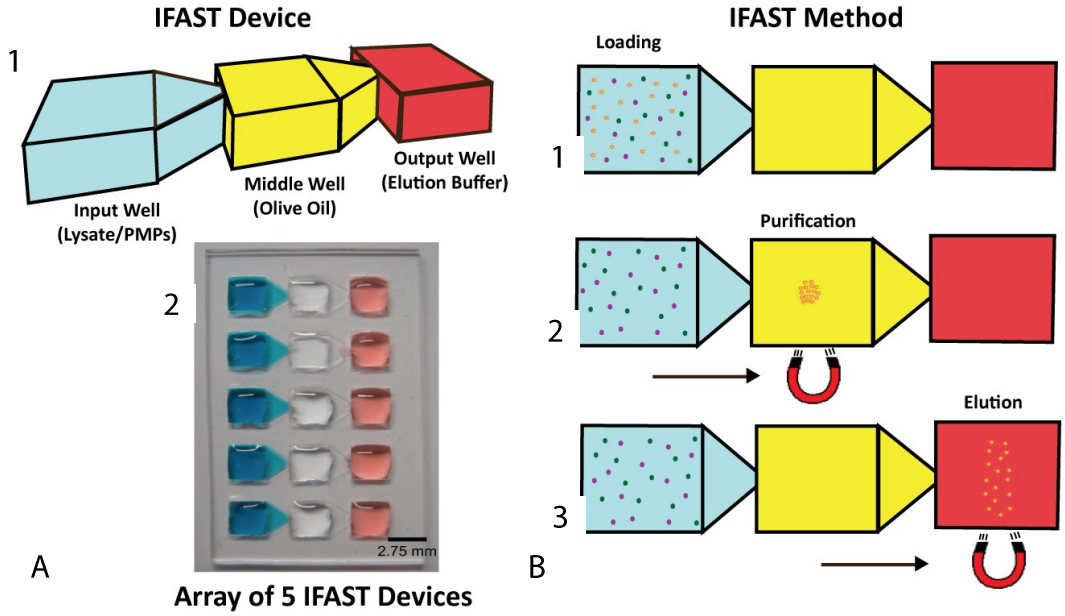

Figure 7-A. IFAST Device. 1) Diagram of IFAST Device. Input Well (Lysate/PMPS), Middle well (Olive Oil) and Output Well (Elution Buffer). 2). Array of 5 IFAST Devices. B. IFAST Method. 1) C. botulinum cells and PMPs are added to the input well containing lysis buffer. After cell lysis C. botulinum DNA binds to PMPs. 2) A handheld magnet draws the C. botulinum DNA bound PMPs through the immiscible phase (olive oil). 3) PMPs are drawn into the elution buffer where C. botulinum DNA dissociates from the PMPs for downstream qPCR detection.

2.3.1 Cell Lysis & Off IFAST

Lysis of *C. botulinum* cells was performed both on and off IFAST device. *C. botulinum* cells lysed off IFAST were prepared according to the ChargeSwitch® manufacturer's protocol. For *C. botulinum* cells lysed on IFAST, the ChargeSwitch® manufacturer's protocol was adjusted to combine all lysing reagents simultaneously, followed by incubation at ambient temperature. On IFAST lysing simplified the off IFAST method by reducing the number of processing steps.

Once DNA was purified by IFAST from the *C. botulinum* cells, the DNA was ready for detection by qPCR. Results showed that off IFAST had a statistically ($p<0.03$) higher C_t value as compared to on IFAST when an n=6 sample were compared (See Figure 8).

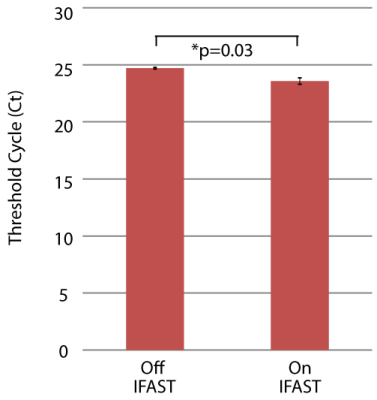

Figure 8-Threshold cycle (C_t) of *C. botulinum* cells lysed on the IFAST device compared to cells lysed off IFAST (n=6).

2.3.2 Detection of *C. botulinum* in Food Matrices

C. botulinum cells spiked into whole milk and orange juice were detected by qPCR following DNA purification by either the ChargeSwitch® or off IFAST methods (See Figure 9). Results showed that both ChargeSwitch® and IFAST methods were able to detect *C. botulinum* DNA in complex food matrices. In addition, the qPCR products were also sequenced to confirm they were correct and not false positives. Results also showed that the C_t values for the IFAST method were lower for all spiked samples (n=6) as compared to the ChargeSwitch® method (See Figure 9A). Further calculations using the $2^{\Delta n}$ method showed that IFAST purified 3.07±0.52 times more product than the ChargeSwitch® method (Supplementary Figure 12). Agarose gel electrophoresis and DNA sequencing analysis confirmed that the correct qPCR product (480 bp) was amplified (See Figure 9B). In addition, melt curves of food matrices with and without *C.*

botulinum cells from this experiment are shown in Supplementary Figure 13.

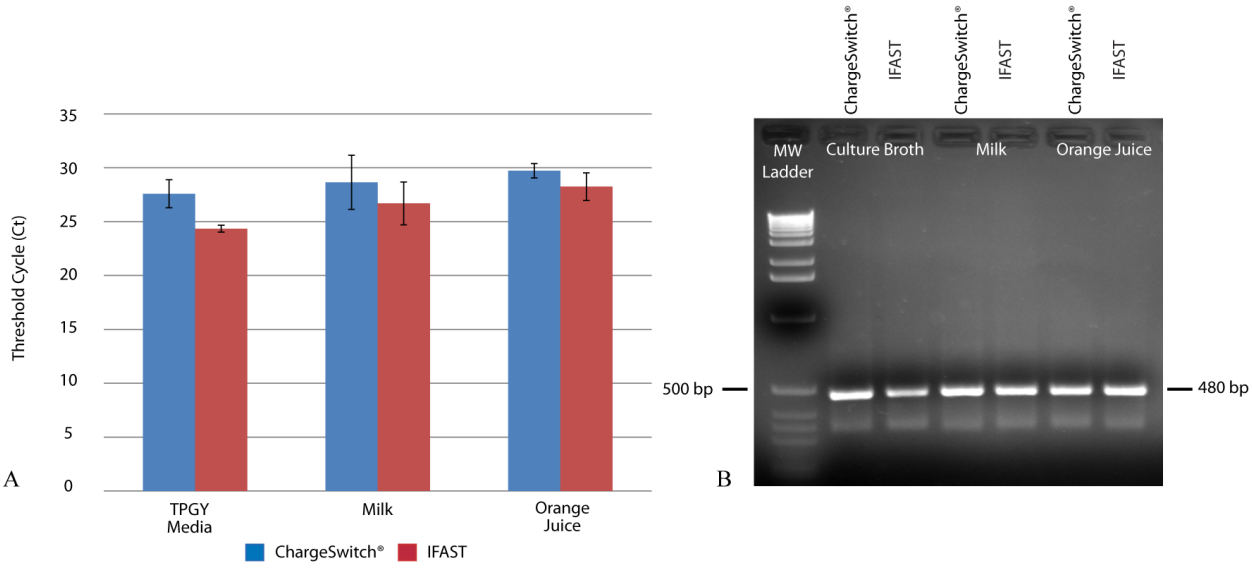

Figure 9-A)Threshold cycle (C_t) comparison among the template DNA samples isolated from *C. botulinum* cells spiked in food samples (n=6). B) Agarose gel electrophoresis of amplified type A toxin fragment (480 bp) from DNA samples isolated from *C. botulinum* cells spiked in culture broth, whole milk and orange Juice.

2.3.3 IFAST Sensitivity Study

Sensitivity experiments were performed for both the ChargeSwitch® and IFAST method by performing 10-fold serial dilutions of *C. botulinum* cells spiked into culture broth from 10^8 cells/mL to 1 cell/mL. This experiment was repeated three times for both methods and the C_t values averaged. The qPCR baseline of fluorescent signal intensity was manually set at the same value for each experiment to reduce sample-to-sample error. For both methods the sensitivity limit was determined by the presence of a C_t value. Negative controls showed a null C_t value as well as the non-template controls. The sensitivity limit was found to be 10^4 *C. botulinum* cells/mL (85 cells per an IFAST reaction) for both methods with lower dilutions having a very high C_t value (>40) or none at all. These data indicate that both methods have comparable

sensitivity, with the IFAST device demonstrating lower C_t values for each dilution, similar to the data collected for the detection of *C. botulinum* spiked food samples (See Figure 10). The only statistical difference observed between the two methods occurred at dilutions of 10^7 and 10^8 *C. botulinum* cells/mL (See Figure 10). The efficiencies of the assays were found to be 90 % for IFAST and 103 % for the ChargeSwitch® method. These efficiencies fall within the generally acceptable range[32] confirming both sample preparation methods as appropriate for *C. botulinum* detection by qPCR (See Figure 10).

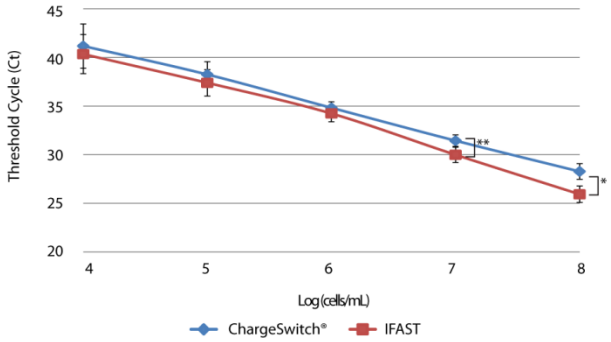

Figure 10-Sensitivity curve for detection of C. botulinum cells spiked in culture broth. *p-value=0.0007 for 10^8 *C. botulinum* cells/mL ** p-value=0.0106 for 10^8 *C. botulinum* cells/mL

2.4 Discussion

IFAST is a novel DNA sample preparation method that can isolate and purify DNA from *C. botulinum* contaminated samples more simply and rapidly as compared to the commercially available ChargeSwitch® method. While the ChargeSwitch® method relies on multiple washes to purify the DNA-bound PMPs, IFAST relies on a single traverse of DNA-bound PMPs through an immiscible phase by a handheld external magnet (See Figure 8). In this manuscript, olive oil was used as the immiscible phase due its interfacial energy with the aqueous phase, however other oils can be used[23]. The total hands on-time per a sample, which includes IFAST device

loading and operation, is 2-3 minutes as compared to the 10-15 minutes referenced in the ChargeSwitch® manual. The time efficiency is even greater when the IFAST device is arrayed to process multiple samples simultaneously, since the only increase in time comes from additional sample loading. This is unlike the ChargeSwitch® method, where each sample must be processed through multiple steps individually. While the sample preparation time savings may seem insignificant when considering the 2 hour qPCR DNA amplification and detection it greatly reduces hands-on working time as well as process complexity. Also, while several others have presented high throughput microfluidic systems to reduce the qPCR time they neglect to address the time spent on sample preparation thereby negating their time saving benefit. The simplification of processing results in the consumption of fewer materials including pipette tips, tubes, etc., which decreases cost. Cost is further reduced by the lower reagent volumes required to operate the IFAST device. Through these combined advantages, the IFAST method represents a simplistic, rapid and cost effective approach for the DNA detection assays, such as the detection of *C. botulinum* DNA as compared to the ChargeSwitch® method.

In order to further streamLine DNA sample preparation for IFAST, DNA was isolated from *C. botulinum* cells on the IFAST device, which has not previously been shown in other IFAST applications. This reduction in processing steps of the IFAST method allows the sample to be added directly to the input well, reducing the need for further material consumption. Further developments will enable preloading of the IFAST device, making it easier for the operator to use and handle. Final results demonstrated that lysing cells on IFAST as compared to off IFAST resulted in a lower C_t value, indicating DNA purification efficiency was higher (See Figure 8). This is likely due to fewer transfer steps between *C. botulinum* cell lysis and *C.*

botulinum DNA purification for on IFAST lysis.

The IFAST method was optimized to satisfy the need for a fast, easy to use and transportable method to extract and purify DNA. The simplicity of the IFAST device makes it amenable to field testing applications for detection of contaminated food matrices. To evaluate IFAST's capability in such an environment, DNA was extracted and purified from *C. botulinum* cells spiked into whole milk and orange juice. These liquid foods were chosen because they are potential targets for intentional BoNT contamination[33]. Milk's high protein and calcium content can also act as PCR inhibitors, decreasing nucleic acid amplification efficiency[34, 35]. As shown in Figure 10, IFAST was able to purify DNA from food matrices spiked with *C. botulinum* cells similar to the ChargeSwitch® method. These data show that IFAST is able to purify 3.07±0.52 times more product as compared to the ChargeSwitch® method. This could be due to the rapid purification of *C. botulinum* DNA by IFAST leaving less time for degradation or loss. The IFAST method also does not require use of a pipette once DNA is bound to PMPs eliminating the possibility of a pipette shearing DNA off the PMPs during the wash steps or accidently aspirating DNA-bound PMPs between wash steps. Finally, C_t values could be lower for the IFAST device because it is better at removing background contaminants as compared to the ChargeSwitch® method.

2.5 Conclusion

IFAST is a novel DNA extraction and purification method with sensitivity comparable to the commercially available ChargeSwitch® method. It has several advantages over the ChargeSwitch® method, including being rapid and easy to use, cost effective and transportable with the ability to purify smaller sample sizes in parallel. Also the simplicity of IFAST means no

complicated external equipment is needed for operation making it amenable to use in resource-limited settings and easy to integrate with existing microfluidic detection and analytical techniques. For example, IFAST could be integrated with previously developed devices that perform qPCR on chip[36-38]. While extraction and purification of DNA was shown from *C. botulinum* cells it is expected that this basic protocol could be used as a DNA sample preparation for a variety of pathogens to be used in medical diagnostics, environmental monitoring and food safety testing assays.

2.6 Supplementary

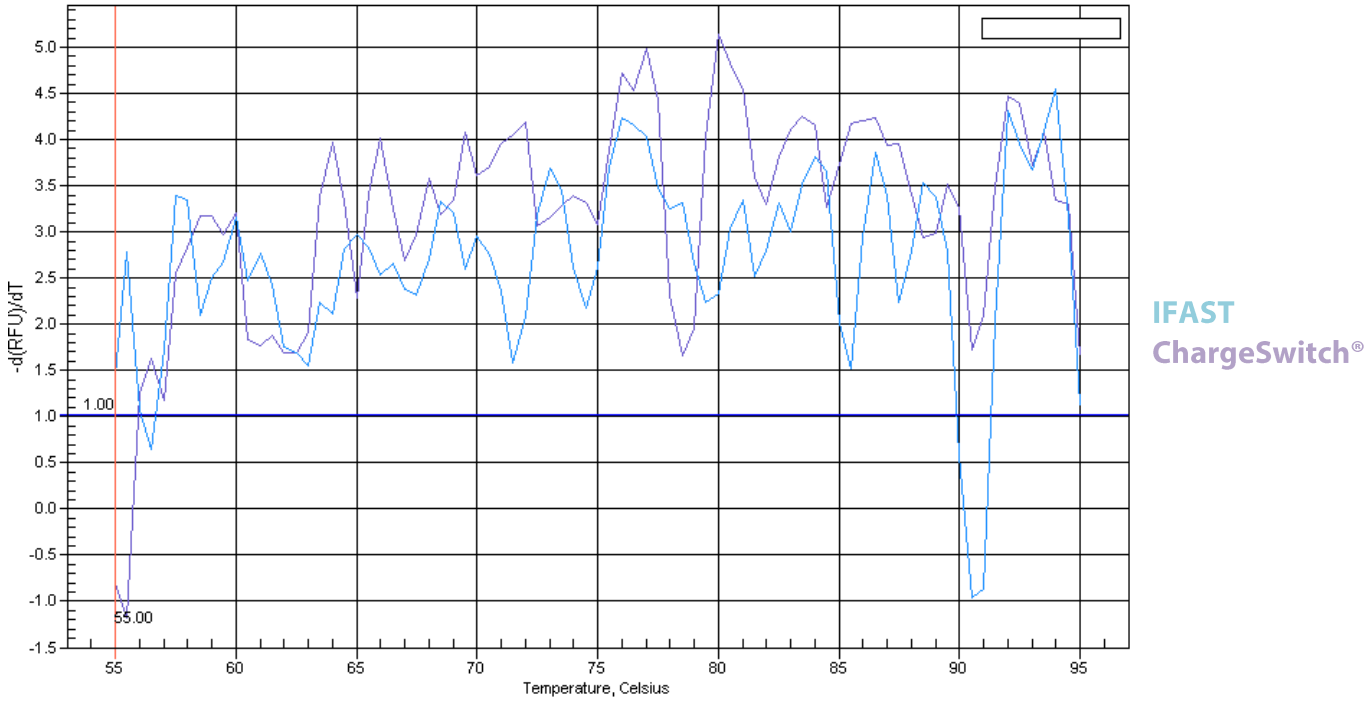

Figure 11- Melt curves of DNA purification from culture broth without *C. botulinum* cells using the IFAST and ChargeSwitch® methods. No amplification was seen.

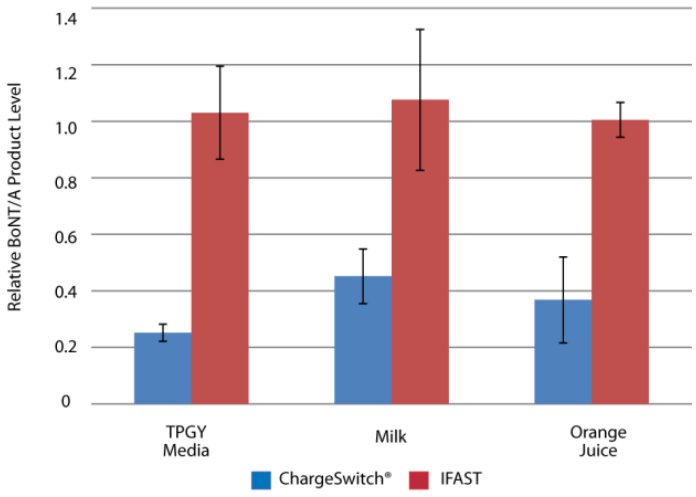

Figure 12- Relative *BoNT/A* product level was determined by the following equation. $\boldsymbol{Relative\ Product = 2^{C_t\ IFAST\ average - C_t\ IFAST\ or\ ChargeSwtich®}}$ The relative products were averaged and graphed. On average IFAST produces 3.07±0.52 more *BoNT/A* product.

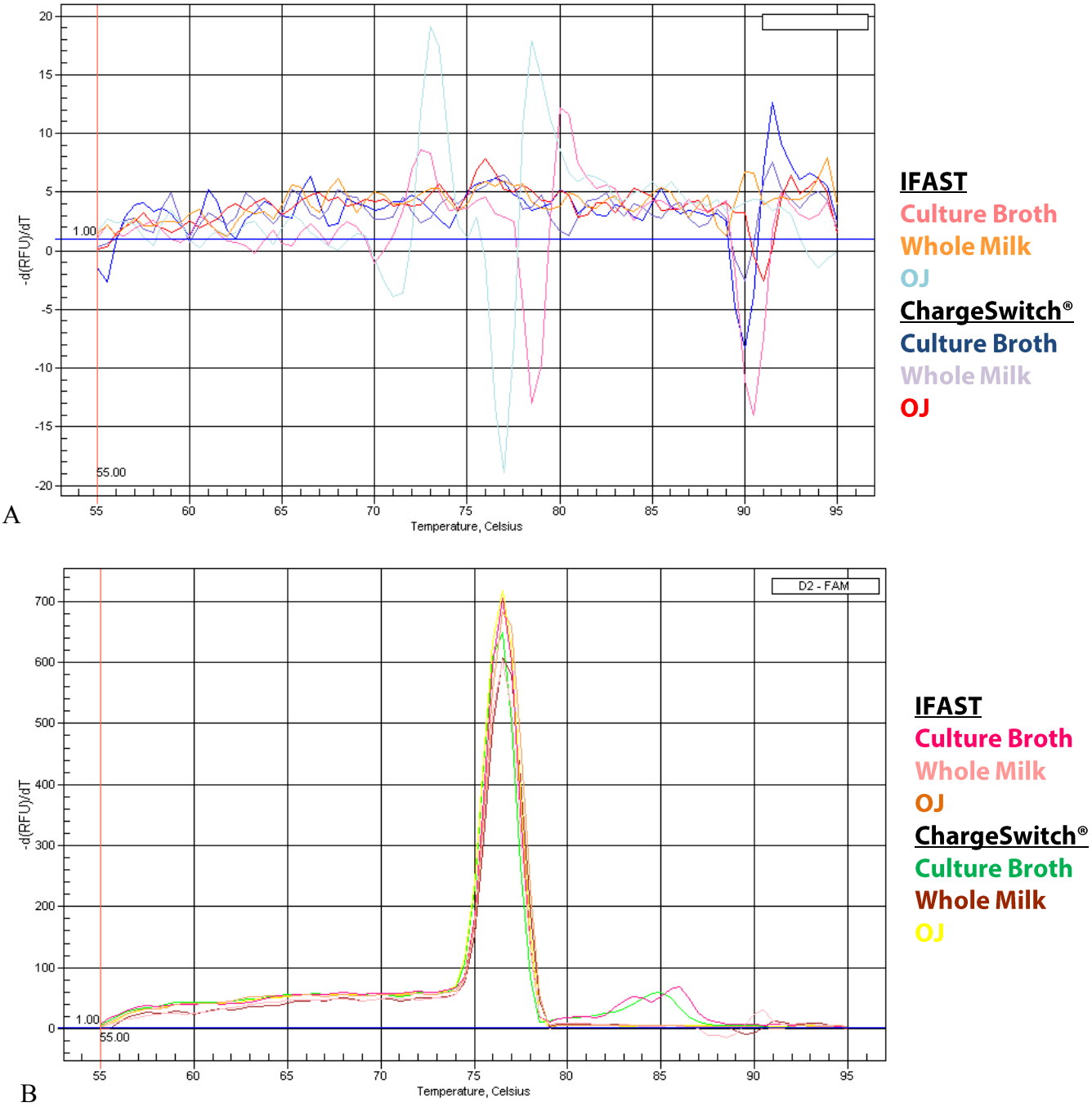

Figure 13-A) Melt curves of DNA purification from culture broth, whole milk and orange juice without *C. botulinum* cells using the IFAST and ChargeSwitch® methods. No amplification was seen. B) Melt curves of DNA purification from culture broth, whole milk and orange juice

spiked with 10^8 *C. botulinum* cells/mL using the IFAST and ChargeSwitch® methods. Amplification was seen.

2.7 Acknowledgments

This material is based upon work partially supported by the U.S. Department of Homeland Security under Grant Award Number 2010-ST-061-FD0001 through a grant awarded by the National Center for Food Protection and Defense at the University of Minnesota. The views and conclusions contained in this document are those of the authors and should not be interpreted as necessarily representing the official policies, either expressed or implied, of the U.S. Department of Homeland Security or the National Center for Food Protection and Defense. This study is also supported by National Science Foundation Graduate Research Fellowship DGE-0718123. Authors would like to acknowledge Mr. Mark J. Jacobson for his assistance of the experiments.

Chapter 3 – Development of an Exclusion Based Colorimetric ELISA Device for Botulinum Neurotoxin Type A Detection

3.1 Introduction

Clostridium botulinum produces botulinum neurotoxin (BoNT), which is the most lethal toxin known with an LD_{50} of 1-10 ng/kg[30]. BoNT is a significant bioterrorism threat especially in the food supply chain. This has led the Centers for Disease Control and Prevention to classify it as a Class A biothreat agent[39]. BoNT is classified into 7 antigenically distinct toxin serotypes (A-G), with each composed of a 100 kDa heavy chain and a 50 kDa light chain[40]. BoNT is taken up at the host's neuromuscular junctions, where the heavy chain binds and translocates across the synaptic membrane and the light chain cleaves proteins associated with acetylcholine vesicle docking and fusion to presynaptic membranes. This leads to rapid flaccid paralysis, which ultimately leads to death through respiratory musculature failure[41].

Currently, the gold standard for BoNT detection is the mouse lethality bioassay, which can detect as little as 10 pg of toxin[42]. However, it has several drawbacks, including ethical concerns over the sacrifice of animals, expense, time to results (>2 days) and the requirement of heavily trained personnel to operate. In addition, further immunological testing still needs to be performed to determine the specific BoNT serotype[43]. Therefore, a number of analytical assays to detect BoNT have been developed, including cell based assays, immunoassays, assays based on enzymatic activity of the toxin's light chain and PCR based assays[43-47]. However, in the event of a BoNT contamination incident, most assays would not be able to be deployed outside of the lab to provide a rapid detection response[48].

The majority of BoNT detection assays have been based on enzyme-linked immunosorbent assays (ELISA) with varying sensitivity limits[49]. Traditionally, ELISA's capture an analyte through an antibody recognition, which are then labeled through a detection antibody conjugated to molecules capable of generating a readout (radioactive label, fluorescent label and color forming enzyme). These assays are typically performed in a 96 well plates and require multiple wash buffers to ensure unbound material and nonspecific interacting molecules are eliminated. These steps are not only laborious but also require trained personnel and specialized equipment, limiting these assays to a laboratory setting. These limitations have led to the development of lateral flow assays, which are also based on an antibody-antigen complex for detection with all fluid manipulations operated by capillary action. While these assays can serve as a rapid, simple and low cost assessment for potential BoNT contamination they have poor sensitivity requiring further specific testing[48, 50].

To overcome complexity of traditional ELISA's and sensitivity limits of lateral flow assays, our lab has developed a technology to simplify and expedite the process[51]. This technology relies on the principle of surface tension dominating gravity to pin fluids allowing side-by-side loading of immiscible phases without density driven stratification[22]. This phenomenon allows us to form discrete compartments of various reagents required in an ELISA. Therefore, paramagnetic particles (PMPs) coated with a capture antibody can bind an analyte of interest to be transferred with a simple magnet through each reagent well, thus eliminating time consuming wash steps and sources of variation (residual wash buffers, dissociation of antibody-analyte complex, etc.). While other groups have used separated droplets or reservoirs surrounded

by immiscible fluids to compartmentalize, extension to streamLining ELISA's has been limited[52].

In this manuscript, we extend previously developed technology to create a BoNT/A colorimetric detection assay[51]. While the basic principle of immiscible phase filtration was used, significant design modifications were completed. These design changes include using a vertical embodiment[53] to hold larger volumes and prevent evaporation, as well as pinning the oil in connection wells to allow mixing on device. Using this device we were able to detect BoNT/A down to 5 pg/mL in PBS, which is two orders of magnitude lower than the lowest sensitivity reported by a lateral flow assay. We also show that the device can detect BoNT within complex food matrices with higher sensitivity than seen with current lateral flow assays. While this device was shown to work with BoNT it could be used to detect a variety of pathogens. Finally, the enclosed nature of the device and simplicity of the method allows this assay to be used outside of the lab.

3.2 Materials & Methods

3.2.1 Device Fabrication

The device was manufactured from 2 mm thick polystyrene (PS, Goodfellow, UK) using a CNC mill (PCNC770, Tormach, USA). The device consists of a through hole hexagon input well 10 mm x 13 mm with a 3 mm opening followed by four through hole wells, 3 mm x 5 mm connected by trapezoids tapering from 2 mm to 0.8 mm with a depth of 0.3 mm (See Figure 14A). Pressure sensitive adhesive (MicroAmp, Applied Biosystems, USA) was applied to the front and back of the device as walls to contain the fluids.

3.2.2 Paramagnetic Particle (PMP) Preparation

For each reaction, 50 μg of streptavidin-M280 (Dynabeads Invitrogen, US) PMPs were washed with 10 μL PBST (0.01 % Tween 20) and resuspended in 10 μL PBST containing 200 ng of biotinylated anti-BoNT/A. Following a 30 minute incubation at room temperature on a vortexor the PMPs were washed with 10 μL PBST and resuspended in a 5 % goat serum solution (Gibco, US). After an additional 30 minute incubation at room temperature on a vortexor the PMPs were washed and resuspended in 10 μL PBST for further use.

3.2.3 Device Operation

To operate, the trapezoid adjacent to the input well was filled with 6 μL of silicon oil (Fisher, USA). The PMPs with supernatant removed were mixed with 200 μL of sample solution and added directly to the input well. Next, the first wash well was filled with 30 μL of wash/binding buffer (PBST containing 1% BSA) before being placed on a tumbler at room temperature for two hours (See Figure 14B Step 1). During the two hour incubation, the secondary antibody labeling solution was prepared, in which 1:2,500 μL HRP-Streptavidin in wash buffer was mixed with 100 ng biotinylated anti-BoNT/A. After incubation, the remaining trapezoid connections were filled with 6 μL of silicon oil followed by additional wells with 30 μL of secondary antibody labeling solution, wash buffer and ABTS (2,2'-Azinobis [3-ethylbenzothiazoline-6-sulfonic acid]-diammonium salt) substrate (Thermo Scientific, US). To transfer the PMPS through the oil trapezoids into the different solution wells, a simple handheld permanent magnet (B333-N52 K&J Magnetics) was used. During transfer, BoNT/A bound PMPs were guided using a magnet along the side of the device through a wash buffer to the secondary antibody labeling solution (see Figure 14B Step 2), for a 1 minute incubation. Next, the BoNT/A bound PMPs were again

transferred using the same mechanism through another wash solution before final transfer to the ABTS well, in which the enzymatic reaction color development occurred within 4 minutes (See Figure 14B Step 3). Finally, the color enzymatic reaction solution, not containing PMPs, was transferred to a 384 microtiter plate and absorbance read at 405 nm by SpectraMax Plus 384-well Absorbance Microplate Reader (Molecular Devices).

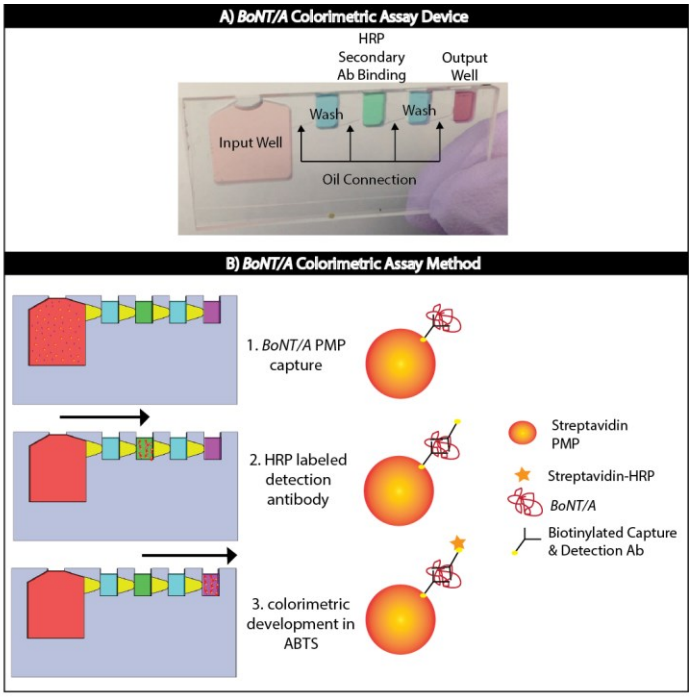

Figure 14-A) Picture of BoNT/A colorimetric ELISA device B) Schematic of BoNT/A colorimetric ELISA method. 1. BoNT/A binds to streptavidin PMPs functionalized with biotinylated anti-BoNT/A antibody in input well. 2. A magnet transfers BoNT/A bound PMPs to secondary antibody labeling well for 1 minute incubation. 3. The same magnet transfers the BoNT/A bound PMPs now attached to a HRP labeled secondary antibody to the output well containing ABTS substrate. Here the enzymatic color development occurs for 4 minutes before absorbance intensity is determined by a spectrophotometer.

3.2.4 Optimized BoNT/A Capture Time, PMP Concentration & Secondary Antibody Binding Time

For all optimization assays, the input sample was 10 ng of BoNT/A diluted in 200 µL wash buffer. For optimized BoNT/A capture time, the input sample and anti-BoNT/A PMPs were incubated on a tumbler for either 30 minutes, 1 hour or 2 hours (n=3). Each assay was then performed as described above. For optimized PMP concentration, the input sample was mixed with 75, 50, 25 or 12.5 µg anti-BoNT/A functionalized PMPs (n=3). Anti-BoNT/A streptavidin PMPs were prepared as described above and were diluted to appropriate concentration after goat serum incubation. For optimized secondary antibody binding time, the assay was performed as described above, however the secondary antibody binding incubation times were adjusted to 1, 7.5 and 15 minutes (n=3).

3.2.5 Validation of Mixing

All devices were loaded with 10 ng BoNT/A in 200 µL wash buffer. Devices were either placed on tumbler or left sitting horizontally for two hours (n=3 for each condition). Each assay was then performed as described above.

3.2.6 BoNT/A Assay Limit of Detection

A 1:10 serial dilution of 50 ng/mL BoNT/A in wash buffer was completed until concentration reached 0.005 ng/mL (n=6 for each condition). Each assay was then performed as described above.

3.2.7 BoNT/A Assay Food Limit of Detection

Orange juice (Tropicana) was centrifuged for 5 minutes at 3000 rpm to remove all pulp. A 1:10 serial dilution of 50 ng/mL BoNT/A in centrifuged orange juice was completed until the

concentration reached 0.005 ng/mL. The dilutions were repeated for 2 % milk (Dean) without centrifugation. The BoNT/A spiked dilutions were added to the input well and the assay completed as described above.

3.3 Results

3.3.1 BoNT/A Assay Optimization

Figure 15 shows various parameters used to optimize the assay including, concentration of PMPs, BoNT/A capture time and secondary antibody labeling solution incubation time. In figure 15A, four different concentrations of PMPs were tested to determine which concentration resulted in the highest absorbance intensity as compared to background. Results show that 12.5 and 25 µg of PMPs (n=3) resulted in an absorbance intensity range lower than 50 and 75 µg of PMPs. Using a student t-test no statistical difference was seen for 50 and 75 µg ($p>0.23$), therefore 50 µg was used for all subsequent experiments. In figure 15B, 3 different capture times (n=4) were tested to determine the minimal time needed for BoNT/A capture that would result in the highest absorbance intensity range. For 30 and 60 minutes incubation time no statistical difference was observed ($p>0.31$), however at 120 minutes the absorbance intensity range was 2-fold higher. Finally, figure 15C shows different secondary antibody labeling solution incubation times (n=4) tested to determine what would result in the highest absorbance intensity range as compared to background. Results show that as time increased, the absorbance intensity for each secondary antibody labeling solution also increased. However, at time 7.5 minutes, the dotted line, which represents the background absorbance intensity had an average higher than the 10 ng BoNT/A spiked sample. At 15 minutes, the background absorbance intensity was lower than the

BoNT/A spiked sample but the absorbance intensity range was lower as compared to 1 minute incubation time.

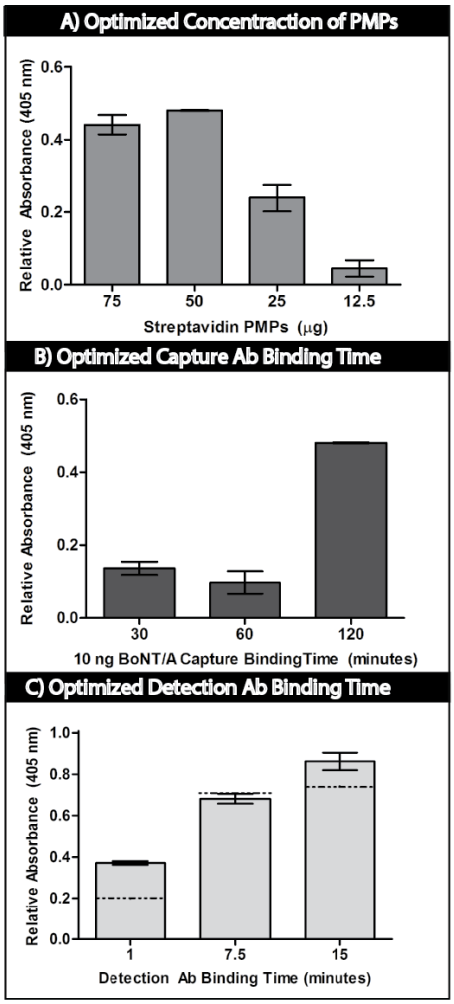

Figure 15-Optimization of BoNT/A colorimetric ELISA assay parameters A) Optimized concentration of PMPs using 10 ng of spiked BoNT/A in wash/binding buffer B) Optimized BoNT/A capture binding time using 10 ng of spiked BoNT/A in wash/binding buffer C) Optimized secondary antibody labeling solution incubation time using 10 ng spiked BoNT/A in wash/binding buffer. Black dotted line represents background signal not subtracted.

3.3.2 Mixing vs. No Mixing In Device

Figure 16 shows the absorbance intensity values for mixing 10 ng BoNT/A and PMPs versus not mixing in BoNT/A colorimetric ELISA device. For this experiment, 10 ng BoNT/A

spiked in wash/binding buffer was incubated for 2 hours with mixing or no mixing in device (n=3). The experiment was repeated with no spiked BoNT/A in PBS for background subtraction. Figure 16a depicts the method of mixing within the device, which included using lab tape to secure them to a tumbler. The other devices were left sitting horizontally on the bench top. Results showed (Figure 16B) that mixing in the device significantly ($P<0.0395$) increased absorbance intensity as compared to not mixing in the device.

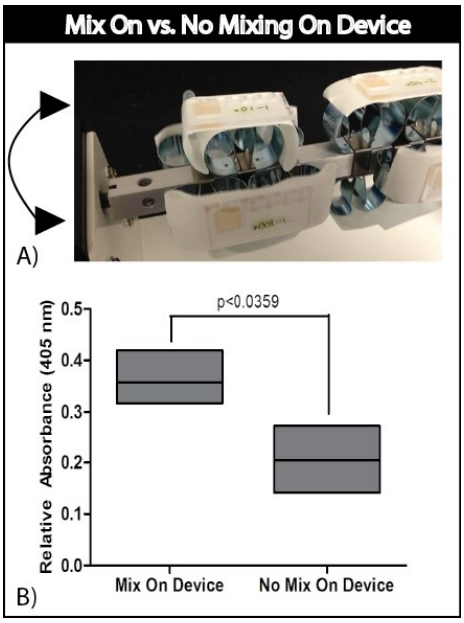

Figure 16-A) BoNT/A colorimetric ELISA device mixing on tumbler. Arrow represents movement direction of tumbler B) Mixing in the device resulted in a higher relative absorbance versus not mixing in the device ($p<0.0359$)

3.3.3 BoNT/A Assay Limit of Detection

A standard curve with background subtracted was performed to determine the sensitivity detection of BoNT/A in wash/binding buffer. The BoNT/A colorimetric ELISA assay was completed for six samples for each dilution, 50 ng to 0.005 ng of BoNT/A per a mL (Figure 17). Following assay completion, results showed that the limit of detection (LOD) was 5 pg/mL.

LOD was quantified using Clinical and Laboratory Standards Institute (CLSI) standard EP17 assuming Gaussian distribution as shown below.

$$LOD = ((Mean_{Blank} + 1.645(SD_{Blank})) + 1.645(SD_{Low\ Sample\ Concentration}))$$

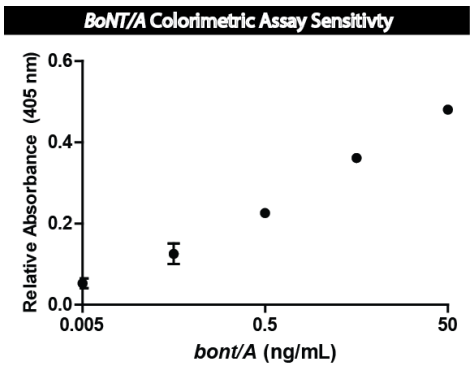

Figure 17-Sensitivity curve of BoNT/A colorimetric ELISA showing LOD of 5 pg/mL

3.3.4 BoNT/A Assay Food Limit of Detection

BoNT/A LOD from different complex food matrices (i.e., orange juice, milk) was determined as described above. Table 1 shows the LOD for milk as 5 ng/mL and orange juice as 50 ng/mL. Milk's limit of detection was 1,000 fold higher and orange juice's 10,000 fold higher than BoNT/A spiked in PBS.

Table 1: Limit of detection of BoNT/A in wash/binding buffer, 2 % Milk and Orange Juice

Matrix	*BoNT/A* Sensitivity (ng/mL)
Phosphate Buffered Saline (PBS)	0.005
2 % Milk	5
Orange Juice (OJ)	50

3.4 Discussion

Here we present a device that uses immiscible phases to compartmentalize ELISA reagents to perform a BoNT/A colorimetric ELISA detection assay. This phenomena is characterized by the dimensionless bond number, in which Bo<1 surface tension dominates and Bo>1 gravity dominates. Therefore, the dimensions of the connection ports were designed to

have a sufficiently low bond number, in order to achieve pinning and stable interfaces between immiscible fluids. While our lab has previously developed an arrayed fluorescent ELISA platform using PSA detection as proof of concept, its 2-D planar configuration, open wells, smaller volumes and need of florescent reader/microscope were better designed for high throughput laboratory settings. To create a more portable and enclosed device, the previous platform was converted to a vertical orientation. While this device still relies on the same physics, its axis is inverted turning the wells and connecting channels perpendicular[53]. This device also allowed us to use larger aqueous volumes without increasing surface area contact to air, helping to prevent evaporation. The self-contained nature of the device also potentially simplifies packaging of reagents. Finally, the use of a colorimetric assay was chosen as it absorbs light in the visible range, making a quick, non quantifiable detection by eye possible. To operate, BoNT/A is bound to PMPs functionalized to anti-BoNT/A antibody within the input of the device. A simple handheld magnet is then used to transfer the BoNT/A bound PMPs through different compartments containing various ELISA reagents, including secondary antibody labeling solution, wash solutions and ABTS substrate. Once color develops, the absorbance intensity of the sample is read by a spectrophotometer at 405 nm (Figure 14).

Several parameters were optimized to increase the BoNT/A colorimetric ELISA assay sensitivity and specificity. The optimized concentration of PMPs was determined to be 50 μg as it resulted in a higher absorbance intensity range as compared to lower PMP concentrations and was more cost effective. Also a higher PMP concentration did not result in a statistically significant higher absorbance intensity range ($p>0.238$). Next, the optimized BoNT/A binding time to PMPs in the input well was determined to be 2 hours. Less time resulted in lower assay

absorbance intensity ranges, which would result in decreased assay limit of detection. Finally, incubation time of the PMPs in secondary antibody labeling solution was determined to be 1 minute. Increasing time resulted in a higher background (dotted line) that decreased the absorbance intensity range for the BoNT/A containing sample. This was probably a result of using biotinylated anti-BoNT/A antibody as the secondary antibody since it could bind to open streptavidin sites on the PMPs. Steps were taken to mitigate this non-specific binding, including pre-incubating the secondary antibody with an access of HRP-streptavidin to block all biotinylated sites and using goat serum during PMP preparation to prevent further nonspecific binding. Overall high background is problematic with colorimetric assays. While there is a wide range of different HRP substrates available, we chose ABTS substrate for color development as other enzymatic reaction substrates (TMB and TMB-Ultra) resulted in too fast of color development. This prevented us from establishing a linear relationship to BoNT/A concentration and made it difficult to perform the assay.

Another benefit of the vertical design is that each well's opening dimensions were designed to allow pinning of aqueous fluids. However, due to the low surface tension of oil it would not pin at the well's opening and would creep along the edges of the device if trying to seal. To overcome this problem, we prefilled the trapezoid wells with oil before adding aqueous reagents. This is unlike previous embodiments were oil would not pin due to the dimensions and volumes of the wells. Therefore, by decreasing these parameters we can achieve a significantly low bond number and thus oil pinning. Once device filling is complete and the oil wells are totally encompassed by aqueous reagents, it can be rotated without leakage allowing mixing within the device (See Figure 16). While not mixing in the device still resulted in detection of 10

ng BoNT/A, the absorbance intensity was not as high as mixing in the device. This was most likely a cause of the PMPs settling out over time. While a tumbler may not be amenable to the field, due to size and complication, gentle agitation would most likely overcome this problem since the PMPs stay suspended for more than 10 minutes. Finally, the ability to directly load the sample into the device without the need of any other tubes or pipettes also helps to further simplify and streamLine the BoNT/A colorimetric ELISA detection assay.

Following optimization, a LOD study was completed by spiking various concentrations of BoNT/A within wash/binding buffer. LOD of BoNT/A colorimetric ELISA device assay was determined to be 5 pg/mL based on CLSI standards as compared to 200 pg/mL of lateral flow assays[48]. The BoNT/A colorimetric ELISA device assay is also within the sensitivity range of the gold standard mouse bioassay[43]. Therefore, use of this platform within the field would allow users to detect BoNT/A contamination with higher sensitivity. This is highly important given the public health threat BoNT represents and its lethality. It should be noted that there are already several developed handheld spectrophotometers commercially available that would complete integration to allow in-field BoNT/quantification.

Finally, BoNT/A was spiked into complex food matrices at different concentrations to determine LOD. Orange juice and milk were chosen because they are potential targets for intentional BoNT contamination[33]. The LOD for milk was determined to be 5 ng/mL, which was an order of magnitude better than lateral flow assays[48]. The LOD of orange juice was 50 ng/mL, which was the same LOD as lateral flow assays[48]. However, in our BoNT/A colorimetric ELISA assay the acidic orange juice, which decreases assay sensitivity, was not buffered as in the lateral flow assay.

3.5 Conclusion

Here we present an optimized platform to perform a colorimetric BoNT/A immunoassay. The device uses immiscible phase filtration to compartmentalize all ELISA reagents, eliminating the multiple wash steps used in traditional immunoassays. These advantages greatly simplify the assay, increasing ease of use and reducing reagent and consumption use. While we have previously shown a fluorimetric immunoassay using immiscible phase filtration, additional features including a vertical design, oil pinning and use of a colorimetric design helping to create a more portable immunoassay for testing outside of a traditional laboratory. Finally, we show the colorimetric BoNT/A immunoassay device has a LOD of 5 pg/mL, which is higher than the standard mouse bioassay and an order of magnitude lower than the lateral flow assays. While this manuscript details the development of a BoNT/A colorimetric immunoassay the platform could easily be adapted for other pathogenic detection assays.

3.6 Acknowledgements

This material is based upon work partially supported by the U.S. Department of Homeland Security under Grant Award Number 2010-ST-061-FD0001 through a grant awarded by the National Center for Food Protection and Defense at the University of Minnesota. The views and conclusions contained in this document are those of the authors and should not be interpreted as necessarily representing the official policies, either expressed or implied, of the U.S. Department of Homeland Security or the National Center for Food Protection and Defense. This study is also supported by National Science Foundation Graduate Research Fellowship DGE-0718123.

Chapter 4 – Nucleic Acid Sample Preparation using Spontaneous Biphasic Plug Flow

4.1 Introduction

Nucleic acid (NA) testing provides a rapid and sensitive way of monitoring and diagnosing a wide range of diseases. Currently approved by the US Food and Drug Administration (FDA) are NA tests that are used to diagnose tuberculosis, chlamydia, gonorrhea, and human immunodeficiency virus (HIV). For viral diseases, NA tests based on polymerase chain reaction (PCR) offer faster disease confirmation prior to seroconversion as well as important quantitative information (e.g., viral load) not available from antibody-based diagnostics. While these PCR based tests provide sensitive quantitative measurements, the reliability of PCR results is heavily dependent on the quality of the nucleic acid template and the presence of inhibitors[54]. As such, effective sample preparation procedures are critical to ensure reliable amplification and accurate test results.

Sample preparation begins with disruption of the cell or virus membrane by chemical or mechanical methods. The majority of commercially available kits employ solid phase extraction (SPE), which utilize functionalized surfaces or silica coated particles (i.e., paramagnetic particles, PMPs) to capture NA. This is followed by extensive and repetitive washing or centrifugation steps to ensure removal of contaminants and inhibitors.[55] These procedures are time consuming, laborious and costly, making NA extraction especially difficult to perform in rural clinics and low resource settings. As such, sample preparation and PCR are usually performed in a centralized laboratory with specialized instruments and skilled technicians. As a

result, implementation of NA testing remains difficult and the impact of these tests is limited in these regions.

To address these issues, a number of research groups have focused on developing microfluidic based diagnostic devices with sample preparation technologies that minimize complex equipment and infrastructure requirements. In particular, paper-based microfluidic devices have received substantial interest due to their inherent low cost, ease of fabrication and simplicity of operation.[56-61] In contrast to lateral flow assays, these devices were prepared by patterning paper with different hydrophobic materials to create confined geometry and channels to facilitate multi-analyte detection.[57, 59] Other groups have combined papers with different properties together to facilitate sample filtration and detection.[58] While a few paper based systems have demonstrated applications for NA testing,[62, 63] the method is predominately used for protein and small molecule detection that are present in blood or serum which do not require complicated sample preparation method to extract.

Other microfluidic NA tests have focused on using immiscible phases to facilitate sample preparation.[64-67] Specifically, Shen et al. performed qPCR to quantify HIV/HCV viral load using the slipchip system and Bordelon et al. performed RNA extraction using a moving magnet that pulls PMPs across air and liquid interfaces. In addition, Sur et al. performed NA purification in a single pass through a liquid wax filtration device. Our group demonstrated the use of "pinned" immiscible fluids to purify nucleic acids.[64] By moving PMPs with captured nucleic acids across oil/aqueous interfaces, a purified sample is achieved in a single step without repetitive washing.

Here, we describe a sample preparation method that utilizes the ability to generate spontaneous biphasic plug flow in capillaries for NA purification. First introduced by Marangoni

and later explained by Bico et al., immiscible fluids connected inside a capillary generate a spontaneous motion without external force.[68-70] Pompano and colleagues took advantage of this phenomenon to control initiation and rate of fluid flow in microfluidic channels on SlipChip.[19] To purify NA, we rely on an imbalance of surface tensions between two immiscible fluids developed inside a capillary tube to spontaneously displace the aqueous phase contaminants from the NA bound solid phase. To operate, lysed sample containing PMPs functionalized to bind NA are introduced to the glass capillary via capillary filling. A magnet then holds the PMPs stationary as an immiscible oil is introduced to spontaneously "displace" the cell debris and contaminants by leveraging an asymmetry between the fluids. Finally, an elution buffer is introduced to release the NA's bound to the PMPs. This method improves assay efficiency by reducing the number of wash steps and eliminates the need for complicated external equipment, potentially making NA testing more accessible in resource limited regions.

4.2 Materials and Methods

4.2.1 Capillary Operation

First, a 10 μL of lysed sample (cell lysate, viral particles in serum or whole blood) with NA capturing PMPs was introduced into a glass capillary tube via capillary action (Figure 18, Step 1). A magnet was held parallel to the capillary to immobilize the beads to the capillary wall surface (Figure 18, Step 2). Next, 10 μL of FC-40 oil containing 1 % PFO was drawn into the capillary connecting the two fluids (Figure 18, Step 3). Once the plug of oil was filled, the juxtaposition of immiscible phases (oil and aqueous lysate) created an asymmetry in the overall surface tension-generated forces. This imbalance generated an overall force that spontaneously moved the fluid plugs towards the end of the capillary where they were removed via a wicking

pad (Figure 18, Step 4). Finally, the magnet was removed and 10 µL of elution buffer (EB) was pulled into the tube to re-suspend the PMPs (Figure 18, Step 5). After 5 minutes, the eluted NA was collected from the capillary using a single pipetting step for downstream detection via RT-qPCR.

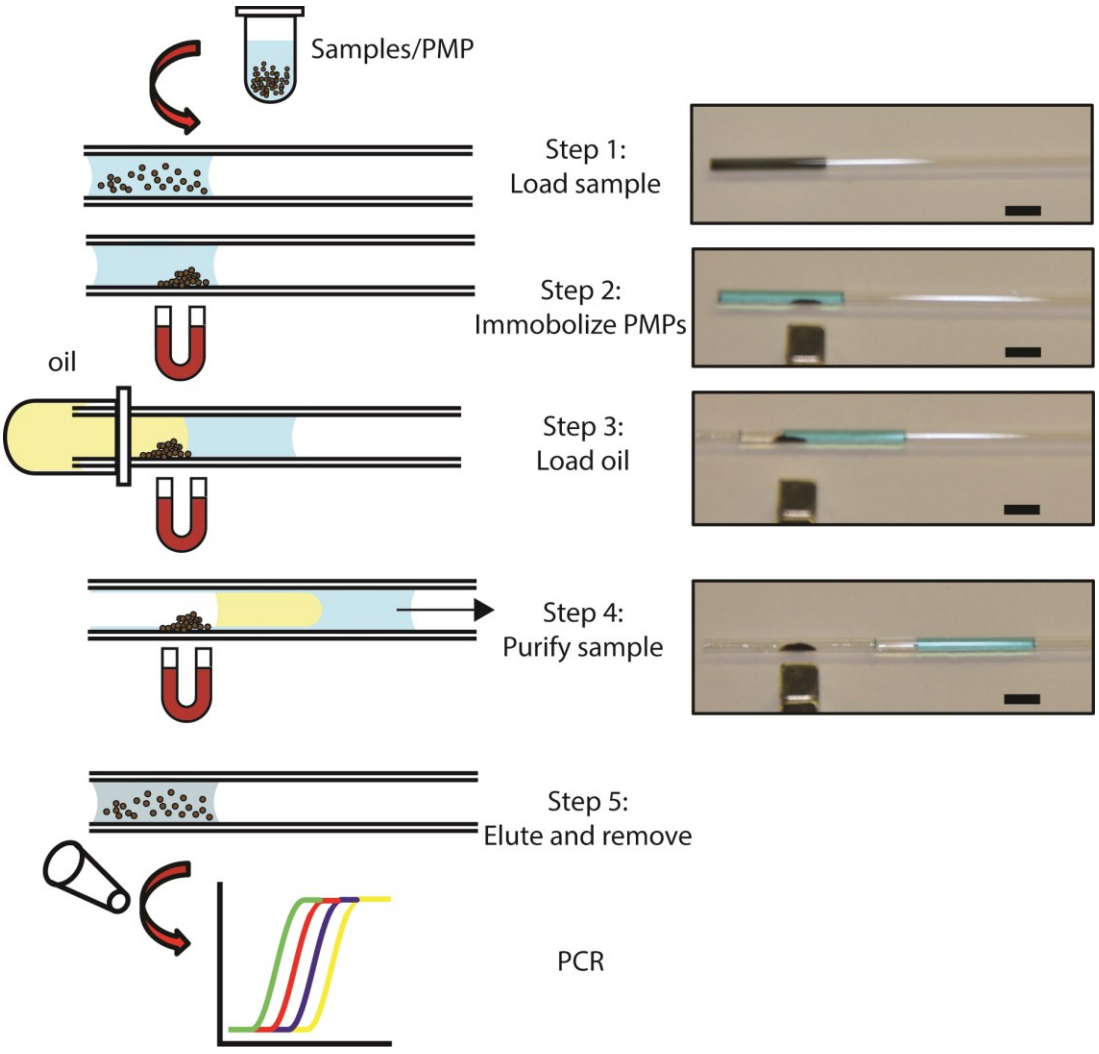

Figure 18-Capillary based nucleic acid purification device. Sample with lysis buffer and PMP was pulled into a tube via capillary forces (Step 1). PMPs with captured nucleic acids were immobilized on the tube surface with a magnet (Step 2). Oil passively pulled into the tube by capillary action (Step 3) creates a surface tension asymmetry between the two phases displacing the entire fluid from one end of the capillary to the other (Step 4). This results in exclusion of PMPs from the uncaptured components of the lysate and purification of the captured nucleic acids (Step 4). Captured nucleic acids were then eluted from PMPs for downstream analysis

(Step 5). Pictures on left correspond to each of the steps shown in the schematic. In these images, the aqueous phase is colored with blue dye for visualization. Scale bar is 5 mm.

4.2.2 Residual Sample Characterization

2% (v/v) red fluorescent protein (RFP) in PBS with varying concentration of Triton-X 100 was used to characterize the amount of residual sample on untreated or bovine serum albumin (BSA) treated capillary walls. BSA treated capillaries were prepared by immersing the glass capillary tubes (0.81 mm ID, Fisher Scientific, Pittsburgh PA) in 3% (w/v) BSA in PBS overnight and drying under N_2 to remove any remaining solution prior to experiments. To characterize sample deposition on capillary walls, 10 μL of RFP solution was first drawn into the capillary followed by the addition of 10 μL FC-40 with 1 % 1*H*,1*H*,2*H*,2*H*-perfluoro-1-octanol (PFO, Sigma Aldrich, St. Louis, MO) to facilitate liquid displacement. Fluorescent images of the capillary before and after the solution traveled across the capillary were captured using a fluorescence microscope (Olympus IX70, Center Valley, PA). NIH Image J software was used to determine the amount of residual RFP on the wall surface.

4.2.3 Cellular mRNA Purification and Amplification

Breast cancer epithelial cells (MCF-7) were cultured in Dulbecco's Modified Eagle Medium (DMEM; Mediatech, Herndon, VA) containing 10 % fetal bovine serum (FBS) and 1 % Pen-Strep at 37°C, and maintained under 5 % CO_2 in polystyrene flasks until confluent. Cells were released using a 0.25% trypsin/EDTA solution and collected via centrifugation. 10^6 cells were pelleted and lysed in 1x RIPA buffer (Millipore, Billerica, MA) for 1 minute with constant mixing followed by serial dilution with RIPA buffer. For each purification, 10 μL of the lysate was mixed with 15 μg mRNA Dynabeads Oligo(dT) PMPs (Life Technologies, Carlsbad, CA)

for 5 minutes at room temperature. The standard wash protocol from Dynabeads® mRNA Direct™ Kit (Life Technologies) was compared to the capillary purification method. Briefly, after lysis and mixing, the supernatant was removed and the PMPs were sequentially washed with the buffers provided by the manufacturer. Nuclease free (NF) water was used to elute the nucleic acids from PMPs and collected for downstream analysis. For capillary based purification, the device was operated as previously described using fluorinated oil FC-40 containing 1 % PFO instead of the buffers.

Isolated mRNA was reverse transcribed using the High Capacity RNA to cDNA Reverse Transcription kit (ABI, Foster City, CA) at 37°C for 60 minutes followed by 95°C for 5 minutes. 20 µl qPCR reactions were setup by mixing, 4 µL of cDNA template with SYBR® Green PCR Master Mix (Bio-Rad, Hercules, CA) and NF water along with forward (5'-GACAATGGCAGCATCTACAAC-3') and reverse (3'-GCAGACAGACACTGGCAAC-5') primers for human ribosomal protein P0 to achieve a final primer concentration of 5 µM. The reaction was amplified at 95°C for 15 seconds (denaturing) followed by 60°C for 1 minute (annealing) for 45 cycles using a MyiQ thermal cycler (Bio-Rad). Data were analyzed using software provided by the manufacturer to determine threshold cycle values (Ct) that correspond to gene expression levels.

4.2.4 HIV Viral Like Particles (VLPs) Production

HIV viral like particles expressing p24 capsid protein were produced by transfecting HEK293T cells with Gag-Pol-Vif and Rev plasmids (generous gift from Dr. Nate Sherer). $4x10^6$ cells were plated onto a 100 mm cell culture dish one day prior to transfection. Cells were cultured in DMEM supplemented with 4.5 g/L D-Glucose, L-Glutamine (Life Technologies), and 10% FBS

and maintained under humidified air with 5% CO_2 (v/v) at 37 °C. Transfection medium was prepared by mixing 30 µl of FuGENE®6 Transfection Reagent (Promega, Fitchburg, WI) with 7.5 µg of p24 Gag-Pol-Vif expression plasmid and 2.5 µg of pRev expression plasmid; the mixture was added to the cells. Cells were incubated for 4 days with medium being changed every 24 hr. On days 3 and 4, culture medium was collected and filtered through a 0.2 µm filter (Nalgene, Rochester, NY). The filtered medium was centrifuged for 2 hours at 21,000 x g at 4°C through a 20% sucrose gradient (Sigma Aldrich). The supernatant was discarded and the pellet containing the HIV VLPs was resuspended in 1x PBS containing 10 % FBS. VLPs were stored at -80°C until use in an isolation experiment.

4.2.5 VLP Spike-in Experiment

HIV VLPs were spiked into either fetal bovine serum or human heparinized blood (Valley Biomedical, Winchester, VA) to simulate clinical samples. Nucleic acids from VLPs were purified using the MagAttract Viral M48 RNA kit (Qiagen, Germantown, MD). Lysis, elution buffers, and PMPs were used from the MagAttract kit. Briefly, heparinized blood that was tested negative for HIV was mixed with MLF lysis buffer at a 1:2 ratio. 10 µL of VLP stock solution at a concentration of 140000 copies/µL was spiked into the mixture. From there 4, 1:10 dilutions were performed using the initial 1:2 heparinized blood and MLF lysis buffer solution to keep the buffer to sample ratio consistent. At the lowest concentration, a total of 14 copies of viral RNA were extracted in each procedure. For each reaction, 10 µL of each dilution was added to 1 µL MagAttract Suspension F PMPs. Each sample was incubated for 5 minutes at room temperature. Purification was executed as described above using FC 40 oil containing 1 % PFO instead of wash buffers.

Isolated RNA from VLPs was reverse transcribed as previously described. For qPCR amplification, 4 µL cDNA template was mixed with 10 µL of TaqMan® Gene Expression Master Mix (ABI), 5 µL NF water and 1 µL each of the p24 primers and 0.5 ul of probe (forward 5'-GGCCAGGAATTTTCTTCAGA-3', reverse 5'-TTGTCTCTTCCCCAAACCTGA-3', probe 5'-ACCAGAGCCAACAGCCCCACCAGA-3'). The reaction was amplified for 40 cycles (denaturing at 95°C for 15 sec followed by annealing at 60°C for 1 minute) using the Roche LightCycler 480.

To quantify the amount of extracted viral RNA, a standard curve was generated by amplifying known copy numbers of p24 Gag-Pol-Vif and pREV expression plasmids to determine the corresponding threshold cycle values.

4.2.6 RNA Quantification

RNA samples were quantified using the QuantiFluor RNA Dye System (Promega). Following the manufacturer's protocol, a standard curve was first prepared in order to determine the RNA samples. Briefly, 1.2 Kb RNA Standards (provided by the manufacturer) were serially diluted (0 ng/mL to 250 ng/mL) in TE buffer and mixed with the QuantiFluor RNA Dye at a 1:1 ratio. Mixtures were incubated in the dark for 5 minutes, and 2 µL was added to a Nanodrop (Thermo Fisher Scientific, Waltham, MA). Samples were illuminated at 450 nm and intensity captured at 540 nm. Extracted RNA were diluted and mixed with the Quantifluor Dye at a 1:1 ratio allowing for the concentration to be calculated from the standard curve.

4.3 Results and Discussion

The extraction and purification of NA is a ubiquitous technique performed in both research and clinical laboratories. Current methods utilizing PMPs and other SPE methods

require multiple wash steps with specialized buffers to sufficiently remove any contaminants or inhibitors from the sample. To overcome these obstacles, we have developed a simple method that utilizes spontaneous biphasic plug flow inside a capillary to effectively separate aqueous contaminants from captured nucleic acids on paramagnetic particles (PMPs) without external application of force or equipment. In contrast to conventional methods which involve repeated pipetting of fluids through the capture beads, with our method, the entire purification was completed passively by capitalizing on capillary action and surface tension.

To operate the system, there are two distinct processes that need to occur. First, both phases must fill the tube by capillary action from a reservoir of liquid (Figure 19a). Second, an imbalance in the overall forces generated by surface tension must exist between the immiscible fluids (Figure 19b). To fill the oil behind the aqueous phase, the pressure drop induced by oil-aqueous interface must be smaller than the pressure drop generated by the aqueous-air interface. Using the Young-Laplace equation, the following equation was derived which characterized this phenomenon,

$$\gamma_{SV} - \gamma_{SL} > \gamma_{12} \qquad (1)$$

where γ_{SV} is the surface tension between glass and air, $\gamma_{SL}$is the surface tension between glass and aqueous phase liquid, and γ_{12} is the interfacial tension between the immiscible phases. Only when the interfacial tension γ_{12} is lower than the differences of glass-air and glass-liquid surface tension ($\gamma_{SV} - \gamma_{SL}$) will both fluids fill the capillary (Fig 19a, also see Supplementary Section Table 2 for empirical data and derivation of the equation).

To induce fluid displacement of the combined liquids (aqueous, oil), asymmetry of the forces generated by surface tension between the advancing and receding interfaces must occur (Figure 19b). This spontaneous plug-flow phenomenon creates a forward displacement of fluids was first observed by Marangoni and later explained by Bico[68-70] which is described as:

$$\gamma_1 - \gamma_{12} - \gamma_2 > 0 \qquad (2)$$

where γ_1 is the surface tension of the aqueous phase, $\gamma_2$is the surface tension of oil, and γ_{12} is the interfacial tension between the fluids. The generation of fluid motion in our system does not require any external forces (i.e., pressure) and is solely dependent on the force imbalance created by surface tension. When the forces generated by surface tension are balanced, the fluids remain stationary (Figure 19b, second condition pictured).

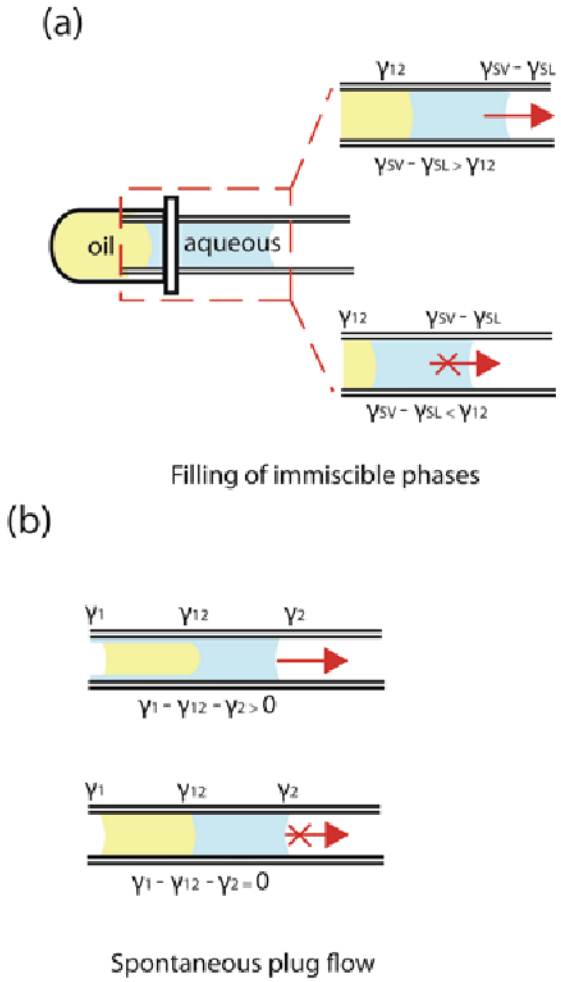

Figure 19-Characterization of the driving force behind fluid displacement in capillary. To fill the capillary with both oil and aqueous phase, the interfacial tension between the two fluids ($\boldsymbol{\gamma_{12}}$) has to be less than the energy required to wet the capillary ($\boldsymbol{\gamma_{SV} - \gamma_{SL}}$), otherwise it will not be energetically favorable for both fluids to be pulled in the capillary (a). Once filling has occurred, the force to displace the fluids within the capillary is the result of an imbalance in the surface tension (b). When surface tensions are balanced, the fluids remain stationary. $\boldsymbol{\gamma_1}$and $\boldsymbol{\gamma_2}$ are the surface tension of aqueous and oil phase, $\boldsymbol{\gamma_{SV}}$and $\boldsymbol{\gamma_{SL}}$are the surface tension of glass in air and glass in liquid, respectively.

We first examined the ability of the current technique to displace aqueous contaminants. Previous studies have shown that the aqueous phase acts as a lubricant, leaving behind a thin film on the capillary walls.[70] RFP was added to the aqueous phase to visualize and determine the

amount of residual sample in the capillary after purification. In untreated glass capillaries, a layer of residual RFP solution was observed after the displacement of the liquid (Figure 20a). After repeated washes with PBS, residual RFP remained unchanged indicating that the protein had adsorbed onto the wall surface. To reduce the effects of non-specific adsorption, capillaries were pre-treated with BSA; thus resulting in decreased RFP intensity (Figure 20a). In untreated capillaries, approximately 25% of the RFP remained within the capillary due to protein adsorption on the wall surface. BSA treated capillaries minimized this effect with less than 3% residual RFP after purification; indicating that protein absorption was further eliminated (Figure 20b). Additionally, increasing the surfactant concentration (Triton-X 100) in the aqueous phase did not affect the overall quantity of residual RFP within the capillary, a potentially useful feature for applications requiring higher aqueous surfactant concentrations especially during lysis step.

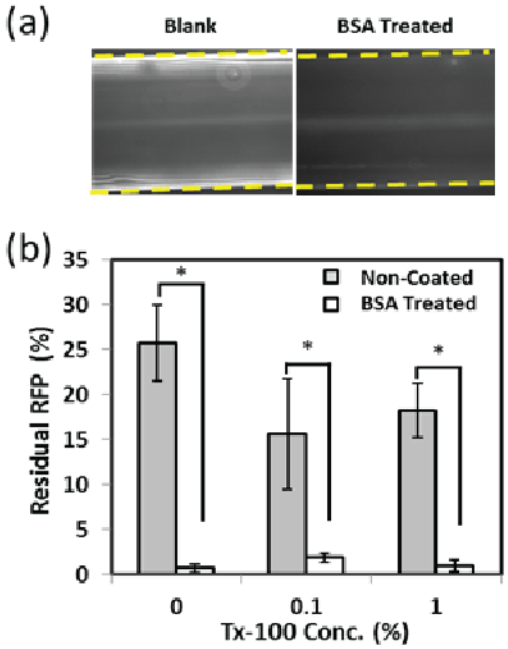

Figure 20-Characterization of residual sample on capillary walls during purification. Red fluorescent protein (RFP) spiked into PBS was used as a model system to quantify the amount of residual sample after the purification step. In both untreated and BSA treated capillaries, RFP was observed on the surface after liquid had traveled across the capillary, with less residual RFP observed in the BSA capillary (a). Dashed lines demonstrate the outer edges of the capillary. Untreated capillaries showed higher residual RFP signal compared to those that were pre-treated with BSA (b). Two tailed t-tests were performed to compare BSA treated and non-treated samples (* indicates $p < 0.05$).

Non-specific adsorption of molecules onto glass surfaces have been extensively studied and attributed to electrostatic interactions. In the context of our current system, minimizing the adsorption onto capillary walls with BSA treatment allowed the quantification of residual fluid after purification. In addition, this method could also serve to reduce potential sample loss of nucleic acids adsorbed on glass surfaces, a commonly used method to capture NA. As such, all experiments from this point were performed using BSA treated glass capillary tubes.

The utility of the current technique to extract NA was examined using different biological samples. First, mRNA from a breast cancer epithelial cell lysate (MCF-7) was extracted and purified. Expression levels of ribosomal protein P0 were amplified and compared to those obtained using the Invitrogen mRNA Direct kit method. The amount of mRNA recovered, as determined by threshold cycle, from both methods showed no statistical difference across the different cell concentrations using the two-tailed Student's *t*-test (Figure 21). Furthermore, the efficiencies of PCR were calculated to be 99 % and 110 % for capillary purification and the commercial kit, both within the acceptable range for PCR assays.[71] In addition, the current method successfully purified mRNA from samples containing a single cell (10 μL input sample at 100 cell/mL), and the threshold cycle agreed with those obtained using the commercial kit

(data not shown). These results show the ability of the current technique to effectively purify mRNA across a range of cell numbers.

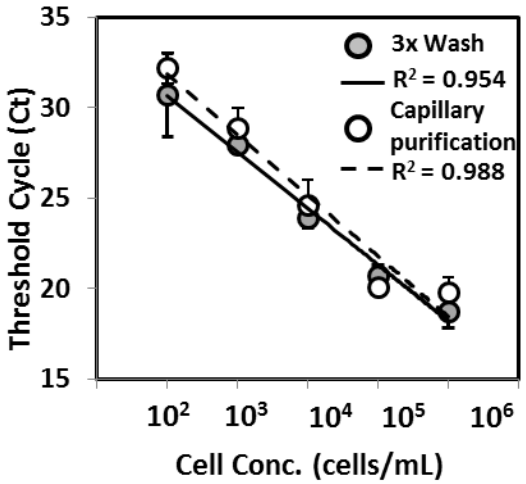

Figure 21-Nucleic acid extraction and purification from cell lysate. RNA from MCF-7 cell lysate was purified using capillary and conventional washing methods. Amplification of ribosomal protein P0 demonstrated similar threshold cycle values between the two purification methods. A linear response was observed across the different cell concentration with both techniques as shown by the R^2 values. Data and error bars represent the mean and the standard deviation of the triplicate experiment.

NA purification kits typically require multiple washing and mixing steps to separate and dilute aqueous contaminants. Depending on the SPE provided from the manufacturer, different equilibration conditions from wash buffers as well as vigorous washing can remove PMPs or bound samples, reducing the overall yield. We compared the amount of extracted viral RNA using the current capillary purification method with from the Qiagen MagAttract Viral RNA kit. The beads provided from this kit are silica coated PMPs and bind to RNA through electrostatic interaction in the presence of chaotropic salts. To demonstrate relevance for clinical testing, HIV viral-like particles (VLP), each containing two copies of viral RNA, were spiked into fetal bovine serum. HIV viral-like particles were prepared by transfecting HEK293T cells and the

particles contain only the specific genetic material that was included during production without the envelope proteins required for viral infection. The sample was lysed and split in half to be purified using our capillary method and the conventional kit-based method. Higher concentrations of viral RNA were consistently extracted with the capillary purification method compared to the protocol from the kit (Figure 22). The multiple buffers in the purification kit require the user to pipette repeatedly creating high shear, thus potentially resulting in sample loss during the wash and transfer processes. In comparison, the capillary method completes purification in a single step without repeated sample mixing thus improving the overall yield of extracted RNA by 5 fold. While this potential sample loss could be due to multiple transfer and pipette steps it could also be a dilutive effect from the wash buffers in comparison to the capillary based exclusion method.

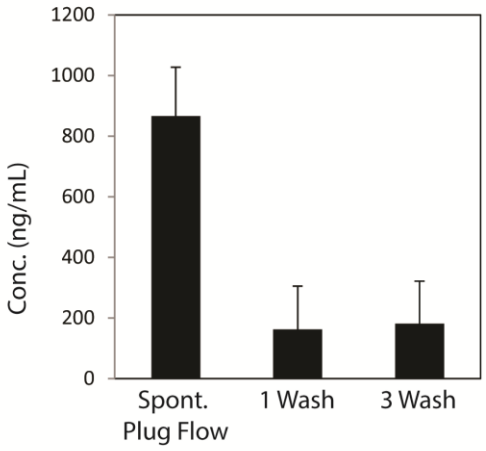

Figure 22-Extraction of viral RNA from fetal bovine serum. HIV viral like particles were spiked into fetal bovine serum. Sample was divided into two aliquots and extracted using MagAttract PMPs. Samples were purified using either the capillary or 1 or 3 conventional wash steps. Extracted RNA was quantified using the fluorescent Nanodrop method. Higher concentrations of RNA were consistently extracted using the capillary method compared to the manufacturer's method. No statistical differences was seen between 1 or 3 wash steps using a Student's t-test ($p>0.29$).

Next, we examined the ability to purify NA from complex human samples. Commercially available viral load tests require blood samples to be centrifuged to first separate the plasma from whole blood prior to analysis. To determine the impact of sample background on the purified sample, we tested the current method to extract viral RNA from human blood. VLPs were spiked into commercially available HIV negative heparinized whole blood. Viral RNA was extracted as previously described, and RT-qPCR performed looking at p24 capsid protein expression to quantify the amount of captured viral RNA. The resulting threshold cycle showed a linear response across the ranges of viral copy numbers and a limit of detection was determined to be approximately 4200 copies/mL (based on the total blood volume) (Figure 23). At this current copy number, a total of 14 copies of viral RNA are in each sample and the data demonstrate consistent extraction and purification. Even in the presence of heparin, which is a known inhibitor of PCR reaction,[54] the sample was successfully processed, indicating that the capillary method is a reliable method to extract nucleic acids from complex samples.

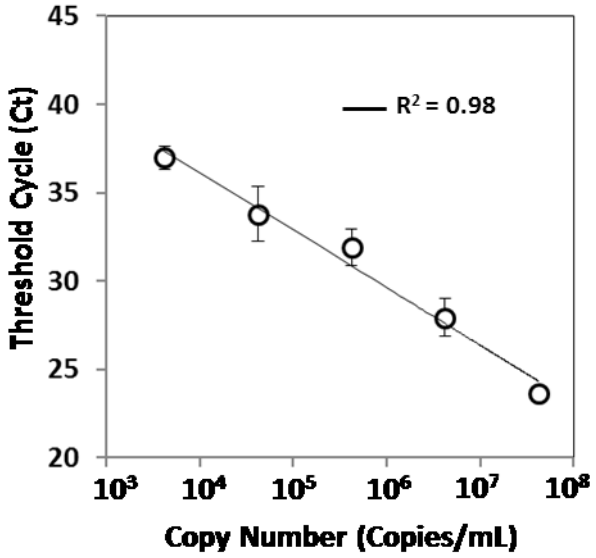

Figure 23-Purification of viral RNA from human blood. HIV viral like particles were spiked into heparinized human whole blood. RNA was extracted and purified using capillary method and RT-qPCR was performed to amplify the p24 capsid protein from the samples. A linear response was observed across the range of viral copy number (shown by R^2 value), and a limit of detection of 4200 copies/mL was obtained using the current method which corresponds to 14 copies per extraction. Data represent the mean and the standard deviation of three to six experiments.

4.4 Conclusion

We have developed a nucleic acid sample preparation method based on surface tension imbalance generated by immiscible phases inside capillary tubes. By filling the capillary with oil and aqueous sample, asymmetry of surface forces creates a spontaneous plug flow which separates contaminants and inhibitors in the aqueous phase from the NA bound PMPs. This method allows the user to achieve sample purification through the simple procedure of filling the capillary with immiscible fluids, thereby greatly reducing the number of pipetting and dilutive steps associated with conventional extraction methods. The overall approach provides a potential solution to address the issues of complicated extraction methods commonly associated with NA testing that limit its use outside of the lab.

4.5 Supplemental

4.5.1 Derivation of Capillary Filling of Biphasic Plug

We mathematically derive the condition for capillary filling of the biphasic plug. Capillary filling of the first phase is described by the pressure differences that occurs across the interface using the Young-Laplace equation,

$$\Delta P_1 = \frac{\gamma_1 \cos\theta_1}{R}$$

where, ΔP_1 is the pressure difference between first phase (aqueous) and the atmosphere, γ_1 is the surface tension, θ_1 is the contact angle between the first phase and glass capillary and R is the radius of the glass capillary.

Using Young-Laplace for phase 2 (oil) capillary filling, we assume that a thin film develops from the first phase but is negligible in height; therefore the radius of curvature of the second phase can be assumed to be a perfect sphere equal to that of the glass capillary ($\theta = 0$).

$$\Delta P_2 = \frac{\gamma_{12}}{R}$$

where ΔP_2 is the pressure difference between first and second phase, γ_{12} is the interfacial surface tension, and R is the radius of the glass capillary.

For the 2nd phase to fill the capillary, the following condition will need to occur where

$$\Delta P_1 > \Delta P_2$$

Substituting Young's equation into left side of the above equation, we derive the following expression,

$$\gamma_{SV} - \gamma_{SL} > \gamma_{12}$$

γ_{SV} is the surface tension between first phase and atmosphere and γ_{SL} is the surface tension between first phase and glass capillary. Therefore, capillary filling of the biphasic plug only occurs when the above condition is met.

Table 2: With the capillary tube set horizontally, 10 µL of a first phase was pulled into the capillary, followed by 10 µL of a second immiscible phase, as indicated in the table above. The capillary tube was visualized to determine if the immiscible phases were displaced (indicated as pulled vs. no pull). Of the cases tested it was determined that if $\boldsymbol{\gamma_{SV} - \gamma_{SL}}$ was lower than $\boldsymbol{\gamma_{12}}$, no pulling was seen, consistent with the model shown in Figure 19.

First Phase	**Second Phase**	γ_{12} **(mN/m)**	$\gamma_{SV} - \gamma_{SL}$ **(mN/m)**	**Experimental Observation (Fill vs. No Fill**
0 % Triton X-100 in DI Water	FC 40	35.58	28.31	No Fill
0.01 % Triton X-100 in DI Water	FC 40	10.55	13.35	Fills Slowly
0.1 % Triton X-100 in DI Water	FC 40	2.78	12.23	Fill
1 % Triton X-100 in DI Water	FC 40	2.88	11.86	Fill
0 % Triton X-100 in DI Water	FC 40 1 % PFO	7.33	28.31	Fill
0.01 % Triton X-100 in DI Water	FC 40 1 % PFO	3.09	13.35	Fill
0.1 % Triton X-100 in DI Water	FC 40 1 % PFO	0.38	12.23	Fill
1 % Triton X-100 in DI Water	FC 40 1 % PFO	0.40	11.86	Fill

4.6 Acknowledgements

This work was supported by a grant from the Bill & Melinda Gates Foundation through the Grand Challenges in Global Health initiative, NIH Grant #5R33CA137673 and NSF GRFP *DGE-0718123*. ABT was supported by the UW-Madison Molecular and Environmental Toxicology Center, NIH grant T32ES007015. David J. Beebe holds equity in Bellbrook Labs, LLC and Ratio, Inc. We would like to thank Dr. Nathan Sherer for all his help and guidance on the production of HIV viral-like particles.

Chapter 5 – Wicking Exclusion Based Sample Preparation in Low Resource Settings for Viral Load Determination

5.1 Introduction

Diagnostics are commonly used to diagnose the cause of symptoms in patients, to monitor treatment efficacy, and to screen for potential diseases[72]. Therefore, diagnostics are of high importance in the healthcare system and help guide decision making clinically. One class of diagnostic assays is the highly specific nucleic acid testing (NAT) assays[73]. Unfortunately, NATs are mainly available in advanced healthcare facilities and not low resource settings due to limited availability of laboratory infrastructure, skilled personnel and cost burdens[74]. This has led to an explosion in the creation of several point-of-care (POC) diagnostics that are rapid, simple and inexpensive thus overcoming the limitations of resource limited settings[75]. But while several NAT POC diagnostics have been developed for downstream detection a lack of upstream sample preparation methods have been shown, limiting their accessibility[75]. These methods are needed to reduce sample complexity, enrich for low abundant analytes and remove contaminants that might mask or interfere with the detection of the analyte of interest[3].

Currently in low resource setting, the dried blood spot (DBS) is the predominant method to preserve blood-based biomarkers. While DBS can be accomplished in remote settings there are several limitations, including achieving quantitative results and an error prone complicated workflow[76]. To overcome challenges associated with DBS and conventional techniques, microfluidic technologies have emerged with evident advantages for POC. These advantages include portable methods, reduced reagent consumption, integratable nature, etc[77]. A majority of microfluidics sample preparation platforms rely on solid phase extraction (SPE), which

incorporates a functionalized surface or immobilized magnetic particles and flow networks to wash and elute[11]. Increasingly, within the microfluidic community a large focus on paper microfluidics has arisen as they are low-cost, lightweight and disposable[78]. However, even in paper microfluidics, sample preparation methods have been few as they are limited in volume and still require significant processing once they reach a laboratory setting[29, 79-84].

Other limitations to NAT accessibility in low resource settings include equipment availability due to expense, power requirement and in some cases need of trained personnel to operate[73]. Another limitation is the lack of a reliable cold chain needed to transport and stabilize samples for further processing in advanced laboratories[74]. Without the cold chain partial or full degradation of nucleic acids due to endogenous proteases and nucleases can lead to false negatives. Finally, an important consideration for point of care sample preparation devices is the proper disposal of medical waste accumulated during sample collection and processing. This consideration stems from the fact that most sample preparation devices are single use, in order to limit cross-contamination. However, the devices are often fabricated from plastics making them difficult to expose of when only landfills and low temperature incinerators are available[85].

Recently, our lab has introduced a suite of technologies known as exclusion-based sample preparation (ESP)[17-19, 22, 23, 47, 53, 86, 87] for a variety of applications. In ESP, any analyte of interest is bound to magnetic beads and either the PMPs, surface or fluid moves, in order to remove contaminants from a sample. The main advantages include streamLining of workflow through elimination of harsh wash or centrifugation steps. Here, we leverage the wicking properties of paper and previous development of wax devices within our lab to create a new technology for POC sample preparation that is self-contained and portable. Specifically, we

analyze the wicking ESP device for viral load quantification, which remains cost prohibitive for much of the developing world but is critical for proper management of anti-retroviral therapy (ART).

5.2 Materials and Methods

5.2.1 Device & Magnetic Stand Fabrication

The wicking ESP device consists of three components connected by double sided tape (OfficeMax) to a piece of laminated cardboard (OfficeMax), named the input well, wicking pad and output well (Figure 24A & 24B). The first component, the input well, was fabricated from wax and holds a liquid volume of 100-300 µL with a center indent of 500 µm for paramagnetic particles (PMPs) to gather. To fabricate this device, techniques described by, Berry et. al. 2014 accepted, were utilized. Briefly, a negative mold was machined from a plate of aluminum (MetalsDepot, alloy 6061). Glass petri dishes were then filled with wax shavings (Sasol Wax, B7347) before being melted at 115 °C on a hot plate. The aluminum mold was then pressed into the molten wax. The petri dish was then removed from the hotplate and placed into a larger petri dish partially filled with room temperature water. When finished the wax disk was removed from the petri dish and excess wax removed before removing imprinted device. The second component, the wicking pad was simply cut from nitrocellulose paper (Fisher Scientific). The third component, the output well, was also fabricated from wax using the same technique as mentioned previously. The output well consists of a raised edge with a center cutout holding 10 µL volume that mated to the input well. Separately, from the wicking ESP device a magnetic stand was fabricated by CNC milling (PCNC770, Tormach, USA) compartments into polycarbonate to hold the magnets (B333-N52 K&J Magnetics).

5.2.2 Device Operation for Nucleic Acid Extraction

To operate wicking ESP device, the device is set on top of the magnetic stand with the indention aligning with the magnet. 100-300 µL sample containing PMPs and lysis buffer is then loaded into the input well slowly with PMPs gathering towards the indent (Figure 24C). The side of the device containing the wicking pad is then pressed over the input well for 10 seconds and removed (Figure 24D & 24E). Next, 10 µL elution buffer was added to the output well, which was then folded to mate with the input well. The magnetic stand was removed from bottom and placed on top causing the nucleic acid (NA) bound PMPs to transfer to the output well (Figure 24F). The output well can then be covered with qPCR tape for storage and further transportation.

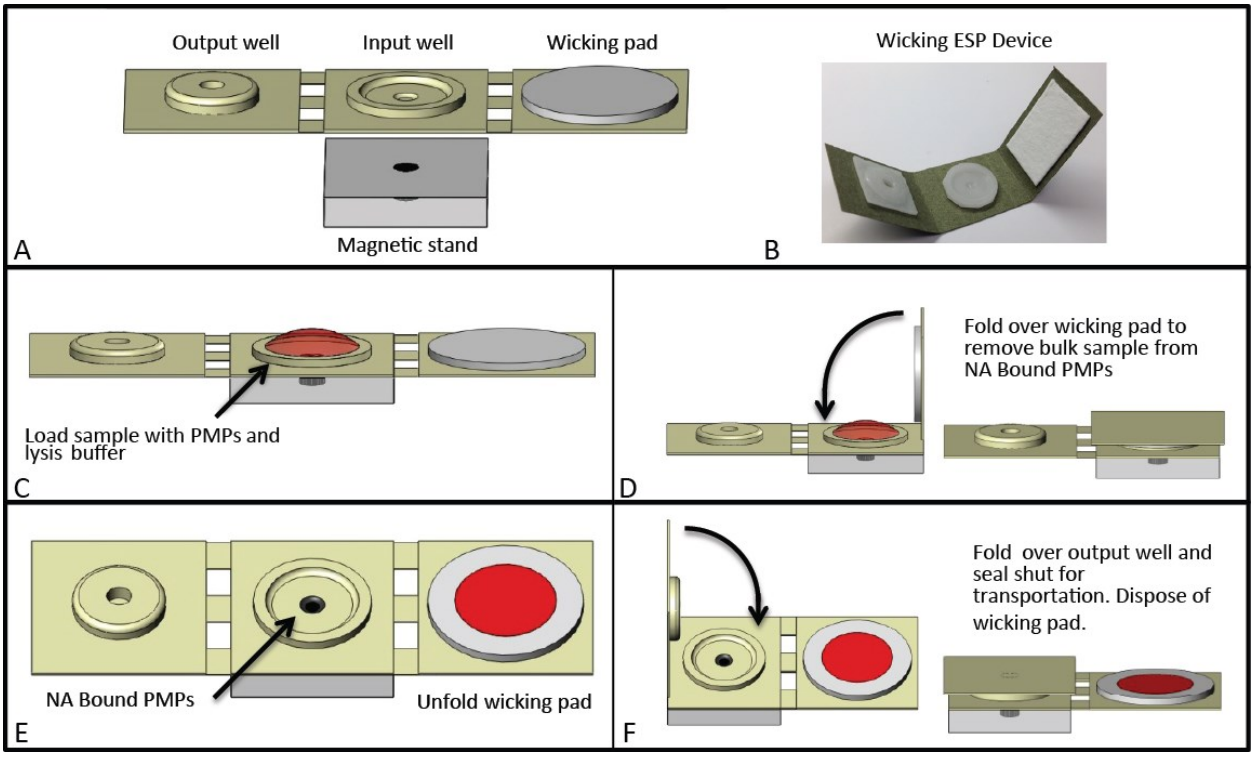

Figure 24-A) Wicking ESP device cartoon with compartments labeled B) Actual wicking ESP device C) Loading of wicking ESP device with sample lysis buffer & PMPs D) Removal of contaminants using wicking pad E) Unfolding of wicking ESP device F) Mating of output well to input well to jump PMPs into elution buffer

5.2.3 Background Contamination

Background contamination was quantified by measuring acridine orange fluorescence with an Invitrogen Qubit 2.0 Fluorimeter using blue light excitation. 5 µL was removed from the elution well following wicking ESP device operation and added to 195µL nuclease-free H_2O in a Qubit ultra-clear assay tube (Q32853, Life Technologies). Sample fluorescence readings were compared to a previously constructed standard curve and percent carryover was determined.

5.2.4 HIV Viral Like Particles (VLPs) Production

HIV viral like particles (VLPs) expressing p24 capsid protein were produced by transfecting HEK293T cells with Gag-Pol-Vif and Rev plasmids (generous gift from Dr. Nate Sherer). $4x10^6$ cells were plated onto a 100 mm cell culture dish one day prior to transfection. Cells were cultured in DMEM supplemented with 4.5 g/L D-Glucose, L-Glutamine (Life Technologies), and 10% FBS and maintained under humidified air with 5% CO_2 (v/v) at 37 °C. Transfection medium was prepared by mixing 30 µl of FuGENE®6 Transfection Reagent (Promega, Fitchburg, WI) with 7.5 µg of p24 Gag-Pol-Vif expression plasmid and 2.5 µg of pRev expression plasmid; the mixture was added to the cells. Cells were incubated for 4 days with medium being changed every 24 hr. On days 3 and 4, culture medium was collected and filtered through a 0.2 µm filter (Nalgene, Rochester, NY). The filtered medium was centrifuged for 2 hours at 21,000 x g at 4°C through a 20% sucrose gradient (Sigma Aldrich). The supernatant was discarded and the pellet containing the HIV VLPs was resuspended in 1x PBS containing 10 % FBS. VLPs were stored at -80°C until use in an isolation experiment.

5.2.5 HIV Purification Standard Wash vs. Wicking ESP

HIV VLPs were spiked into fetal bovine serum (FBS) to simulate clinical samples. NA from VLPs were purified using the MagAttract Viral M48 RNA kit (Qiagen, Germantown, MD). Lysis, elution buffers, and PMPs were used from the MagAttract kit. Briefly, 100,000 VLP per a sample were spiked into 100 µL FBS and a 1:10 serial dilution performed to reach a concentration of 10 VLP per a sample. The sample was then mixed with 200 µL MLF lysis buffer containing 1 µL MagAttract Suspension F PMPs and incubated for 5 minutes at room temperature. Samples were then processed using the wicking ESP device as described previously. Experiment was repeated 3 separate times.

5.2.6 RT-qPCR Detection of VLPs

Isolated RNA from VLPs was reverse transcribed (High Capacity cDNA Master Mix, Life Technologies) using a thermal cycler (Techne TC-412) according to manufacturer's directions. For qPCR amplification, 4 µL cDNA template was mixed with 10 µL of TaqMan® Gene Expression Master Mix (ABI), 5 µL NF water and 1 µL each of the p24 primers and 0.5 ul of probe (forward 5'-GGCCAGGAATTTTCTTCAGA-3', reverse 5'-TTGTCTCTTCCCCAAACCTGA-3', probe 5'-ACCAGAGCCAACAGCCCCACCAGA-3'). The reaction was amplified for 40 cycles (denaturing at 95^{o}C for 15 sec followed by annealing at 60°C for 1 minute) using the Roche LightCycler 480. To quantify the amount of extracted viral RNA, a standard curve was generated by amplifying known copy numbers of p24 Gag-Pol-Vif and pREV expression plasmids to determine the corresponding threshold cycle values.

5.2.7 Sample Degradation to Simulate Shipping

Viral RNA is susceptible to degradation via ribonucleases; therefore, methods to reduce degradation (e.g., continuous cold chain, Dried Blood Spot (DBS)) are typically required when transporting HIV plasma samples from the point-of-collection to the testing lab. To simulate these real-world conditions, we stored VLP samples spiked into FBS at 4°C, 21°C (simulate RT) and 37°C for 72 hours and then purified RNA via ESP wicking device and detected viral RNA via RT-qPCR as previously described. Separately, using the same mock sample we purified RNA via wicking ESP device and stored elution at 4°C, 21°C and 37°C for 72 hours before converting samples to cDNA. Finally, using the same mock sample we purified RNA via wicking ESP device and immediately converted sample to cDNA, which was stored at -20 C until all samples were ready for detection using RT-qPCR. The purpose of this experiment was to determine the effects of unreliable/unpredictable shipping practices (where the sample is exposed to cold and warm temperatures for extended periods of time) on the quality of the measurement either undergoing or not wicking ESP as compared to a sample processed immediately using wicking ESP device.

5.3 Results and Discussion

5.3.1 Wicking ESP Device

Operation of the wicking ESP device is shown in Figure 24. Briefly, sample is mixed with lysis buffer and PMPs to bind NA and added to the input well. A magnet placed underneath the input well causes the PMPs to gather in the center indentation. The wicking pad is then folded over the input well for 10 seconds to remove contaminants. The wicking pad is then unfolded and removed. Finally, the output well containing elution buffer is folded to mate with

the input well. The magnet is transferred to the back of the output well to move the NA bound PMPs into this well. The output well can then be sealed with tape and transported.

The entire NA extraction procedure can be completed within a minute and is non-laborious requiring minimal training to operate. As the process and methodology is low-tech, manufacturing of the wicking ESP devices is cost-effective and amenable to low resource settings. Cost is extremely important as most of the developing world cannot accurately monitor viral load, which is essential to the proper management of ART. While sample preparation does not allow for a complete sample to answer we anticipate significant reduction in complexity and cost of viral load testing. Additionally, all the materials used in the fabrication of the device can be destroyed with low temperature incineration (~400 °C) allowing proper elimination without exposure to toxic chemicals that are emitted during the burning of plastics. The hydrophobic nature of wax also benefits wicking ESP device as it wants to repel the water helping to facilitate aqueous contamination removal.

5.3.2 Background Contamination

In sample preparation of NA's one of the main concerns is carryover of contaminants that might interfere with downstream assays, such as qPCR. In previous research, using an alternate wax ESP device, termed IFAST, carryover was determined to be less than 2 % (Berry et. al. 2014 accepted). Here, using a wicking ESP device we demonstrated similar results. Four separate buffers representing different potential input test matrices were tested. All matrices showed sample contamination on average of 1.6±0.2% (Figure 25). No statistical difference was seen between any matrices. However, when either lysis buffer only or lysis buffer and serum were used the carryover trend was slightly less.

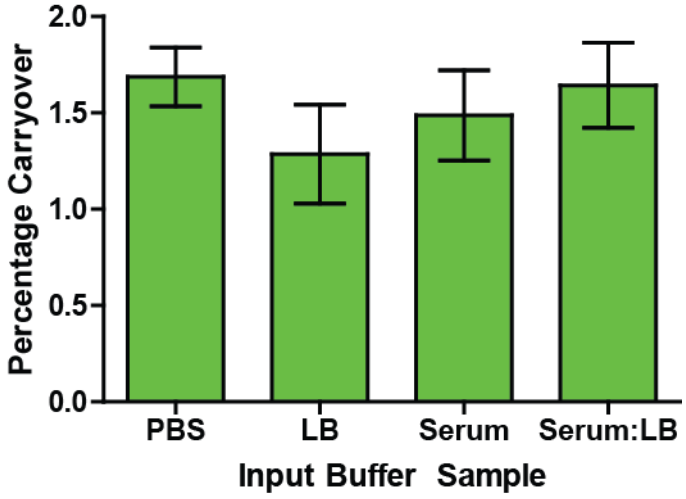

Figure 25-Carryover of contaminants in different sample matrices

5.3.3 Sensitivity of Wicking ESP vs. Standard Wash Methods

Next, we wanted to test the sensitivity of the wicking ESP device, as well as how it compared to a standard wash method. Results showed that both wicking ESP and wash methods had a sensitivity of 100 VLPs/mL (Figure 26). Wicking ESP device also demonstrated lower Ct values for all the different concentrations of VLP's. On average, the Ct values demonstrated by wicking ESP device were an order of magnitude lower as compared to wash methods. This means wicking ESP device was either superior in extracting more DNA or was more effective at removing contaminates. In addition to the added sensitivity benefit, the advantages of eliminating additional buffers, pipette tips, transfer steps etc. make the wicking ESP device a more attractive method for low resource settings.

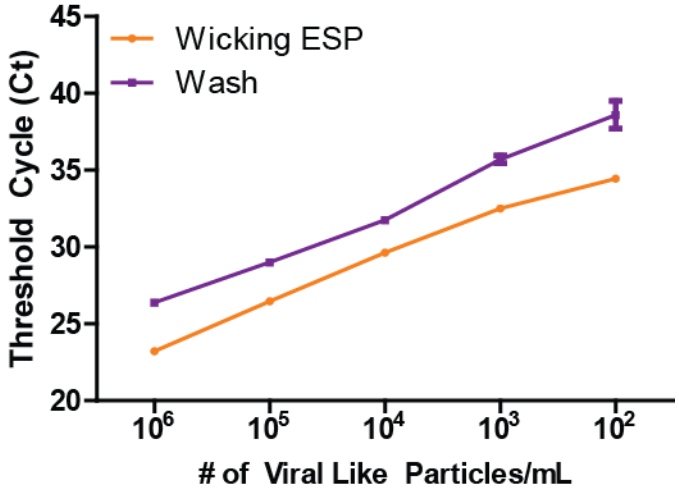

Figure 26-Sensitivity of wicking ESP versus standard wash methods across different VLP dilutions in FBS

5.3.4 Sample Degradation of Wicking ESP Processed vs. Unprocessed

As wicking ESP device was designed for sample preparation in a low resource setting, the ability to transport the sample effectively without degradation for downstream detection was of paramount importance. Samples processed at 72 hours, stored at either 4, 21 or 37 °C, exhibited a lower and more stabilized Ct value as compared to samples left unprocessed (Figure 27). All samples were normalized to samples processed immediately. At each temperature there was a statistically significant difference between the unprocessed and processed (Figure 27).

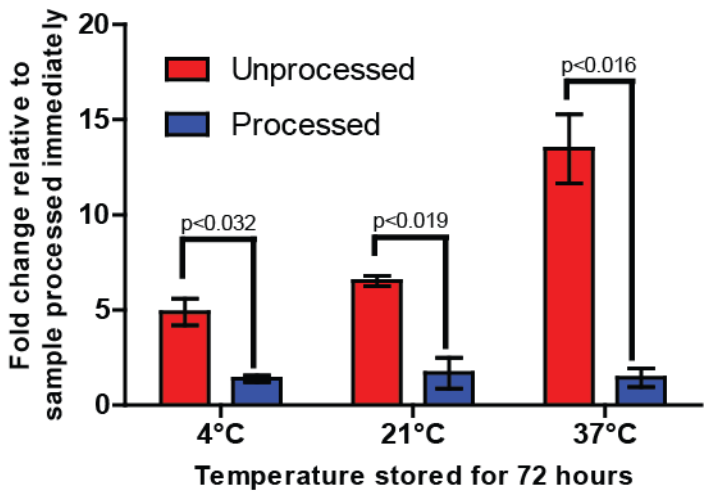

Figure 27 - Sample degradation of processed vs. unprocessed samples after 72 hours at different temperatures as normalized to a sample processed immediately using wicking ESP device. A significant difference was seen at every temperature between unprocessed and processed.

5.4 Conclusion

The wicking ESP device overcomes several challenges associated with current point of care sample preparation devices. As the wicking ESP device only consists of nitrocellulose paper and wax it is inexpensive to fabricate and easy to dispose of. We have also shown it has comparable or better sensitivity than current laborious and time consuming wash methods. Finally, we showed sample preparation in the field helps stabilize the sample better than no processing for up to a week as compared to a sample processed and analyzed right away. These advantages combined show wicking ESP device to be an attractive method for sample preparation in low resource settings.

5.5 Acknowledgements

I would like to specifically thank Chandresh Singh for all his help in designing, fabricating and testing the devices. This work was supported by a grant from the Bill & Melinda

Gates Foundation through the Grand Challenges in Global Health initiative, NIH Grant #5R33CA137673 and NSF GRFP *DGE-0718123*.

Chapter 6 – Selective Nucleic Acid Removal via Exclusion (SNARE): Capturing mRNA and DNA from a single sample

6.1 Introduction

Biological complexity emerges from different organizational levels in highly regulated and coordinated processes, involving the path from gene (DNA) to gene product (RNA). Full understanding of these links is beginning to unlock the secrets of cell differentiation, development, aging and pathological conditions. But for a more complete picture, techniques that allow for integrated RNA and DNA extraction within the same biological sample will be essential[88]. For example, recent studies using paired genomic and transcriptomic analysis in cancer have begun to identify driver genes that could possibly serve as potential therapeutic intervention candidates or be involved in the mechanisms of disease progression[89-91]. These methods are also increasingly important as many biological samples are difficult to obtain, valuable and of limited size, leading to the need to extract as much information as possible from a small amount of material[92]. In addition, simultaneous RNA and DNA extraction helps reduce potential errors and variation in data due to experimental differences and sample loss. While techniques exist for the extraction of RNA and DNA from the same sample, they are often not capable of rare cell analysis due to sample damage and loss during processing. To overcome these obstacles, we present a simple and rapid method for the extraction and purification of mRNA and DNA from a single sample.

Until recently, the traditional approach to analyzing RNA and DNA from the same sample was to split the sample. But even when sample size was not limited, researchers feared losing data or introducing error, especially when trying to correlate genomic changes with gene

expression changes[88]. These traditional techniques for simultaneous nucleic acid (NA) purification include cesium chloride step-gradient ultracentrifugation[93] or a phase separation guanidinium thiocyanate-phenol-chloroform procedure[94]. While several variations of the guanudinium-based technique now exist (Trizol, TriFAST or Tri-Reagent) they are time consuming, labor intensive, require use of hazardous reagents and require relatively large sample sizes (>1000 cells)[95]. Alternatives to the phase separation guanidinium-based methods include spin column technologies[95, 96], which are faster and avoid the use of toxic reagents. These are now commercially manufactured by Qiagen, GE Healthcare, Macherey-Nagel, Norgen Biotek and Serva[92]. Of these manufacturers, only Qiagen's DNA/RNA Allprep Micro kit is recommended for small sample sizes. However, the Qiagen kit requires an increased number of processing steps, such as centrifugation and must use carrier RNA if fewer than 100 cells are used. Klein and colleagues also used olgio$(dt)_{25}$ Dynabeads® to purify mRNA and collected all the wash buffers to precipitate out the DNA[97]. While the technique showed single cell sensitivity, it was laborious and took over 24 hours to complete. Additionally, several RNA and DNA microfluidic purification devices have been developed that promise to reduce laboratory time, human interaction, and reagent and equipment costs[98]. While a few microfluidic devices have been developed to purify RNA or DNA interchangeably[99, 100], to our knowledge none have been developed to purify RNA and DNA simultaneously from a single sample in a cost-effective and time-efficient way.

Another area of emerging interest for simultaneous mRNA and DNA purification is rare cells, however current methods for lower sample sizes are limited due to sample loss, poor reproducibility and incompatibility with whole genome and transcriptomic amplification

methods[101]. These rare cells are important in a range of clinical and biological spheres, including the characterization of circulating tumor cells (CTCs) for disease prognosis and personalized treatment[102-104]; circulating fetal cells for prenatal diagnosis[105]; T-cells for immune monitoring[106, 107]; and stem cells for analysis of biochemical and developmental processes[108]. High importance is placed on these rare cells as they can be captured from blood replacing painful and expensive biopsies and permitting more frequent testing. While numerous publications have described methods for rare cell capture, the main end point has been enumeration with little focus on molecular interrogation of these cells due to lack of tools. Such analysis could allow us to predict therapeutic benefit and select optimal treatment strategies on a per-patient basis.

Here we present a microfluidic device termed Selective Nucleic Acid Removal via Exclusion (SNARE), which has been designed to overcome limitations of current technology. SNARE builds on previous work that exploited the dominance of surface tension over gravity at the microscale to establish "virtual walls" between immiscible and aqueous phases. These virtual walls were used to separate the complex upstream from the downstream solution for purification of mRNA, DNA or cells[22, 23, 47]. Specifically in the previous work, we described the physical principles of using immiscible phase for mRNA extraction[22]. Additionally, we demonstrated purification of specific cell populations[23, 53] and DNA extraction for detection of botulism neurotoxin from complex food matrices[47]. To operate, any analyte bound to paramagnetic particles (PMPs) is translocated across the immiscible phases using a simple handheld magnet. One unique advantage conferred by this system is the ability to resample the original input material as it is never lost by aspiration, transfer, dilutive or centrifugation based processes, an important advantage when dealing with rare biological samples. This non-destructive sampling

method allows repeated interrogation of the original input material by the sequential addition of paramagnetic particles (PMPs) of varying chemistries and different lysis/binding buffers to the input well to isolate mRNA and DNA from the same sample. Overall, SNARE requires less time, labor, resources and laboratory equipment than current methods with the potential for high throughput automation and robotic processing.

In this manuscript, we demonstrate that SNARE technology is able to extract and purify mRNA and DNA from a single sample. To benchmark SNARE, we utilize the only commercially available spin column technology recommended for DNA and RNA extraction from low cell numbers. We demonstrate the sensitivity of SNARE to perform low cell number (<10) extraction of both mRNA and DNA by qPCR. We further show that purified mRNA and DNA is suitable for Sanger sequencing from the same cell population. Finally, we use SNARE to isolate mRNA and DNA from CTCs, a rare cell population. The ease of use and sensitivity of SNARE make it a unique technique for purification of mRNA and DNA from a single, rare sample.

6.2 Materials and Methods

6.2.1 SNARE fabrication

SNARE was manufactured from 2 mm thick polystyrene (PS, Goodfellow, UK) using a CNC mill (PCNC770, Tormach, USA). The complete device was 19 x 27 mm, in order to increase ergonomic handling. The input and middle well consisted of two through holes, 3 mm in width and 5 mm in height. The mRNA and DNA output well has the same dimensions as the input well with a 1.5 mm depth. Each well was connected by a trapezoid with a height ranging from 2 mm down to 0.8 mm and was milled to a depth of 0.3 mm (See Figure 28). The back was mirrored

based on the front piece. The front and back were solvent bonded using acetonitrile so that the input and middle well had an approximate volume of 40-60 µL and the output well 15-20 µL. Pressure sensitive adhesive film (MicroAmp, Applied Biosystems, USA) was then applied to the front and back of the device as walls to contain the fluids.

6.2.2 Lysis/Binding Buffer Optimization

Three separate lysis/mRNA binding buffers were evaluated to determine which resulted in the highest relative GAPDH signal, signifying better nucleic acid capture. The SNARE protocol was performed as described below, except different lysis/mRNA binding buffers were used including; 1x RIPA buffer (Milipore), LIDS (Life Technologies, USA) and a less stringent Modified LIDS buffer. While the Modified LIDS buffer is described in detail in the SNARE Operation section, the only difference from the commercially available LIDS buffer is the replacement of the ionic detergent lithium dodecyl sulfate (LDS) with a nonionic detergent Igepal® CA-630. GAPDH detection by qPCR was performed on both mRNA and DNA. Relative GAPDH signals were determined and a Student's two-tailed t-test performed for comparison of each lysis/mRNA binding buffer with $p<0.05$ considered significant.

6.2.3 SNARE Operation

Operation of SNARE is outlined in Figure 28B. To operate SNARE, 15 µL of nuclease free water was added to both output wells. Next, 10 µL of cells suspended in 1xPBS was added to the input well, followed by 15 µL lysis and mRNA binding buffer, referred to as Modified LIDS, (10 mM Tris-HCL, 500 mM lithium chloride , 1 % Igepal® CA-630 (Sigma-Aldrich, USA), 5 mM ethylenediaminetetraacetic acid (EDTA), 5 mM dithiothreitol, pH 7.5) containing 30 µg olgio$(dt)_{25}$ Dynabeads® (Life Technologies, USA). To complete filling of the device, 40 µL

silicon oil (Fisher, USA) was added to the middle well. After 5 minutes, a permanent magnet (B333-N52 K&J Magnetics) was introduced to the front side of the input well to gather the olgio(dT) PMPs. Next, the magnet was manually pulled across the front until the olgio(dt) PMPs reached the RNA output well. Next, 25 µL of DNA binding buffer (10 mM Tris-HCl, 6 M Guanidinium Thiocyanate (GTC), 0.1 % Igepal® CA-630, pH 7.5) containing 1 µL MagneSil® PMPs (Promega, Madison) was added to the input well. After 5 minutes, the MagneSil® PMPs were transferred across the back side of the device to the DNA output well using the permanent magnet. The elution buffers along with PMPs were collected for further downstream analysis.

6.2.4 Quantitative PCR

The mRNA elution sample containing PMPs was reverse transcribed using a High Capacity cDNA Reverse Transcript kit (ABI, Foster City, CA) according to manufacturer's directions. For GAPDH assays, 4 µL of cDNA template was mixed with 10 µL LightCycler 480® probes master mix (Roche, USA), 1 µL TaqMan® Gene Expression Assay (primers specified in Supplementary Table 5, Life Technologies, USA) and 5 µL nuclease free (NF) water. Each reaction was amplified for 50 cycles (denatured at 95 °C for 15 seconds followed by annealing at 60°C for 1 minute) using a LightCycler® 480 Real Time PCR System (Roche, USA). Relative GAPDH signal levels were quantified and normalized using, $(2^{-(45-C_p)})$.

6.2.5 Cell Culture

Prostate cancer epithelial cells (LNCaPs) were cultured at 37 °C and maintained under 5 % CO_2 in polystyrene flasks in Corning Cellgro® RPMI 1640 Medium (VWR) containing 10 % fetal bovine serum (Gibco®), 1 % Penicillin Streptomycin (Gibco®), 1 % MEM-nonessential amino acids (Gibco®) and 1 % NaPyruvate (Corning Cellgro®) until confluent. Cells were released

using a 0.05% trypsin/EDTA solution and neutralized using media for collection via centrifugation.

6.2.6 SNARE Comparison to Qiagen AllPrep DNA/RNA Microextraction Kit

A 1:10 serial dilution of 100,000 to 100 LNCaP cells/mL in 1x PBS was performed for three seperate experiments. Ten µL of each serial dilution (n=2) was processed using SNARE to equal 1000, 100, 10 and 1 LNCaP per device. Ten µL of the same serial dilutions were added to 65 µL RLT buffer and processed according to Qiagen AllPrep DNA/RNA Micro Kit manufacturer's directions. For all samples containing 100 cells or fewer, carrier RNA was added to the Qiagen samples as recommended in the manufacturer's protocol. A control sample containing no cells was performed with each methodology. GAPDH detection by qPCR was performed for direct comparison of both methods.

6.2.7 Sequencing of the Androgen Receptor from mRNA and genomic DNA

For mRNA purified from 10 LNCaP cells using the SNARE procedure, exon 5 and 6 of the androgen receptor (primers shown in Supplementary Table 4) were amplified by qPCR according to directions above. After amplification, PCR products were purified using the MinElute PCR Purification Kit (Qiagen, USA). The product was cloned using the pGEM®-T Easy Vector System (Promega, Madison).

For DNA purified from 10 LNCaP cells using the SNARE procedure, exon 8 of the androgen receptor (primers shown in Supplementary Table 4) was amplified using Phusion Hot Start II High-Fidelity DNA Polymerase (Thermo Scientific, USA) according to manufacturer's directions. The reaction was completed using Bio-Rad C1000 Thermo Cycler (Bio-Rad, USA) with initial denaturation at 98°C for 30 sec, denature at 98° C for 10 seconds, anneal and extend

at 72° C for 20 seconds, which was repeated for 35 cycles with final extension at 72° C for 10 minutes. Samples were sent to the Wisconsin Biotechnology Center where a Big Dye (Life Technologies, USA) reaction was performed and PCR products directly sequenced (ABI 3730xl). Samples were analyzed using ABI Sequence Scanner Version 1 and nucleotide NCBI blast.

6.2.8 **Patient Data**

Prostate circulating tumor cells defined as EpCAM positive, intact nuclei based on Hoescht, and CD45 negative were collected under a University of Wisconsin IRB-approved protocol and isolated in a method previously described[53]. mRNA and DNA were extracted from the prostate CTCs using the SNARE method. Cycle threshold (C_t) values for AR and GAPDH were determined by qPCR according to directions above (See Supplementary Table 4 & Table 5 for primers & probes).

6.3 Results and Discussion

6.3.1 SNARE Operation

SNARE uses exclusion-based immiscible filtration assisted by surface tension (IFAST)[22] to extract and purify mRNA and DNA from the same sample (Figure 28A). Immiscible phase filtration takes advantage of the ability of aqueous and oil phases to be loaded side-by-side, without stratification, to form virtual walls[16]. This principle is based on the dominance of surface tension over gravity at the microscale, as defined by the dimensionless Bond Number ($B_o<1$)[22]. To operate SNARE, PMPs functionalized with oligo(dt) and a lysis/binding buffer optimized to bind mRNA are added to the input well (Figure 28B, step 1). Following mRNA binding, an external magnet draws the mRNA –bound PMPs through the middle well containing silicon oil

(Figure 28B, step 2) to the front output well (Figure 28B, step 3). Next, silica PMPs and a lysis/binding buffer optimized to bind DNA (Figure 28B, step 4) are added to the input well. Following DNA binding, the DNA- bound silica PMPs are moved through the middle well along the backside of the device (Figure 28B, step 5) to the back output well (Figure 28B, step 6). Samples can then be collected and used for downstream mRNA or DNA assays. It should be noted, in applications where only mRNA or DNA is required one could choose to collect either or.

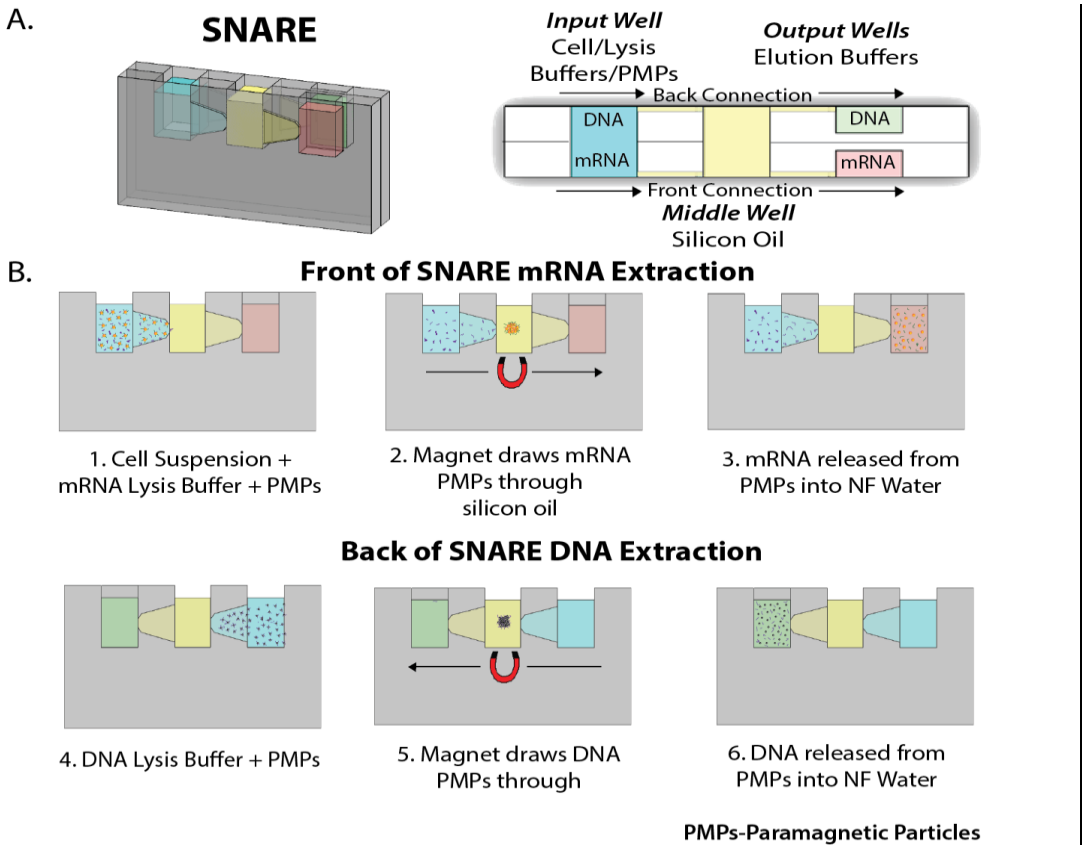

Figure 28-A) (left) Picture of SNARE device with dimensions labeled and (right) top down schematic of SNARE device with wells labeled. Note the two fluid paths. One on the front of the device and one on the back. mRNA extraction occurs along the front and DNA extraction occurs along the back. B) Operation of SNARE for mRNA and DNA extraction and purification from a single sample. Steps 1-3 show front side of SNARE for mRNA isolation. Steps 4-6 show backside of SNARE for DNA isolation. (PMPs: Paramagnetic Particles)

SNARE was designed to simplify purification of mRNA and DNA from a single sample by minimizing work flow and preparation time while maximizing sample recovery for downstream analyses. Figure 29 illustrates a comparison of SNARE to the current methods to isolate RNA and DNA from a single sample. The traditional method is guanidinium thiocyanate-phenol-chloroform commericially known as Trizol, which uses phase separation to extract RNA and DNA. However, Trizol requires several processing steps that are time consuming, laborious and require high reagent and material consumption. Trizol also uses toxic chemicals and is not recommended for small sample sizes. While spin columns are faster than Trizol they still require high reagent and material consumption. In addition, the multiple centrifugation and pipetting steps are still time consuming and can result in sample loss due to dilution and transfer steps. In contrast, the SNARE process takes only 10 minutes to complete reducing time and labor needed. As SNARE only requires the use of a pipette and a handheld magnet to operate, the cost of use is greatly reduced. However, if a large number of samples need to be processed, SNARE has the potential to be easily automated[18]. Lastly, SNARE's simplistic design also helps to lower the cost as it could be manufactured using standard methods.

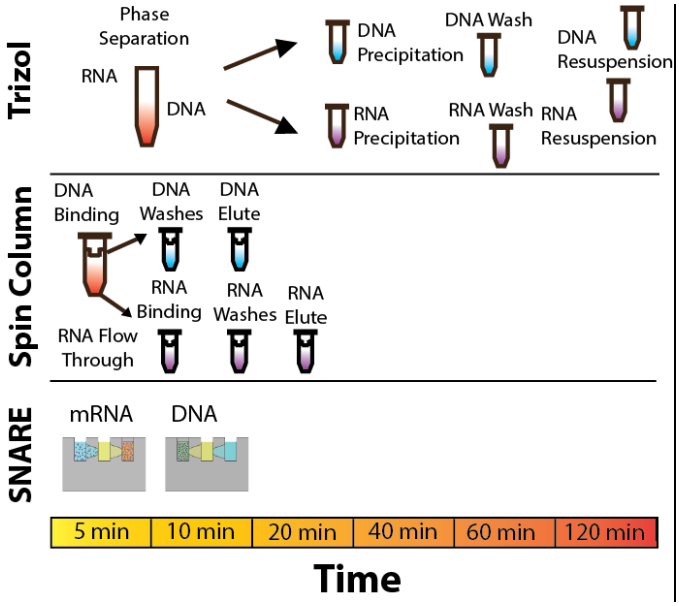

Figure 29-RNA and DNA extraction methods from a single sample, using the traditional Trizol (guanidinium thiocyanate-phenol-chloroform) or Spin Column methods as compared to SNARE

6.3.2 Lysis/Binding Buffer Optimization

For successful NA isolation using SNARE, selection of PMPs with optimized binding chemistries and binding buffers is critical to affect cell lysis and facilitate NA-PMP binding interactions. To achieve maximum RNA and DNA extraction efficiency, three different lysis mRNA binding buffers (RIPA, LIDS, Modified LIDS) were evaluated using SNARE and the relative GAPDH signal was calculated for both mRNA and DNA from 1000 LNCaP cells. LNCaPs were chosen for this study and subsequent analysis as a representative model system for rare prostate cancer CTCs. Relative GAPDH signal was detected by qPCR because traditional methods to determine purity and amount (Agilent Bioanlayzer, absorbance at 260 nm & flourimeter) were not applicable for the limited amount of material isolated from low numbers of cells. GAPDH was also used as it is a commonly used reference gene and is expressed in LNCaPs. There was no difference in mRNA isolation as measured by relative GAPDH signal

between LIDS or Modified LIDS ($p>0.5$) (Figure 30). However, use of either LIDS or Modified LIDS resulted in a higher relative mRNA GAPDH signal as compared to RIPA ($p<0.03$ and $p<0.001$, respectively). The relative increase in GAPDH mRNA signal could be due to the differences in the concentration of salts used in the RIPA (150 mM NaCl) as compared to LIDS and Modified LIDS (500 mM LiCl). Especially as binding is dependent on the poly(A)+ tail of mRNA forming stable hybrids with the functionalized oligo(dT) PMPs under high-salt conditions [109]. The ability to efficiently extract DNA from samples after using these lysis/binding buffers was also tested. We observed higher relative GAPDH DNA signal for RIPA ($p<0.04$) and Modified LIDS ($p<0.001$) compared to LIDS, meaning a greater sensitivity was observed. No statistical difference was seen between RIPA and Modified LIDS ($p>0.8$).

Originally only RIPA and LIDS buffers were tested for mRNA extraction but upon addition of lysis/DNA binding buffer, physical examination revealed clumping between the DNA PMPs using LIDS. We hypothesized this difference was due to the ionic detergent lithium dodecyl sulfate (LDS) used in LIDS binding to the PMPs resulting in competitive binding with DNA. To circumvent this issue, the ionic LDS detergent was replaced with the non-ionic detergent Igepal CA-630 in Modified LIDS to achieve efficiency comparable to RIPA. Therefore, the Modified LIDS allowed us to maintain GAPDH signals that were not statistically different from LIDS without compromising DNA GAPDH signal. For DNA lysis/binding buffers, two different buffers containing either 6 M or 8 M guanidinium thiocyanate (GTC) were tested. While the DNA PMPs use silica for DNA binding they also have the ability to bind RNA under the right conditions (i.e., salt, pH), however the buffer was chosen to limit RNA binding and contamination. No differences were seen between RIPA buffers containing 6 M or 8 M

GTC. However, the 8 M GTC buffer was poorly soluble, making operation difficult due to salt precipitation when the devices were kept on ice. Therefore, the Modified LIDS was selected with 6 M GTC for lysis/DNA binding buffer.

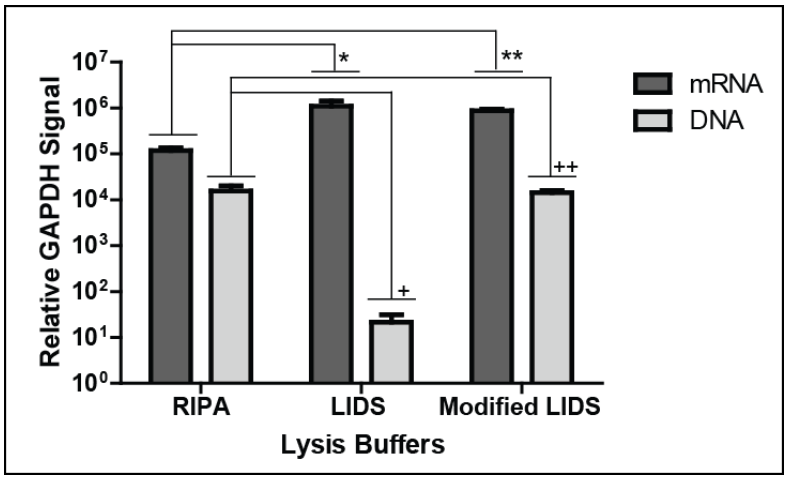

Figure 30 - Relative mRNA and DNA GAPDH signal isolated using SNARE for the comparison of different lysis/mRNA binding buffers. Based on this data, Modified LIDS was recommended for use in SNARE *$p<0.03$, ** $p<0.001$, + $p<0.001$, ++ $p<0.04$ Sample size per a group n=6.

6.3.3 SNARE Comparison to Qiagen AllPrep DNA/RNA Micro Kit

We used a Qiagen Allprep DNA/RNA Micro kit as a benchmark to SNARE as it is the most widely used sensitive commercially available technique. SNARE achieved higher relative mRNA and DNA signal compared to the Qiagen kit, which used carrier RNA since the kit does not purify using a polyadenylated mRNA tail (Figure 31). Using either SNARE or the Qiagen kit for mRNA extraction we were able to detect GAPDH in all of the samples, including sample dilutions containing a single cell (Figure 31A). To assess for possible NA contamination from the device or buffers, a control sample containing no cells was processed and no amplification was seen. Higher variability in mRNA isolation was observed for the Qiagen technique as cell number decreased, with the average coefficient of variance across all cell dilutions being

48.7±15.1 % for Qiagen and 28.9±7.0 % for SNARE. The differences in relative signal could be due to decreased yield through additional fluid transfer steps, fluid shear stresses and partial elution in wash buffers. In Figure 31B, GAPDH DNA signal was detected in 50 % of the single cell dilutions using SNARE. In contrast, no GAPDH DNA signal was observed for the same dilution using the Qiagen kit. While SNARE showed higher DNA sensitivity, the signal was not always positive at a single cell level likely due to stochasticity. We also confirmed the efficiency of the relative mRNA and DNA GAPDH signal using a standard curve (Supplementary Figure 33). In addition to GAPDH, we were also able to detect by qPCR androgen receptor (AR) and prostate serum antigen (PSA) with greater sensitivity as compared to Qiagen (Supplementary Figure 34). Finally, we used SNARE to isolate mRNA and DNA from the same sample using two other cell lines (THP-1: Human acute monocytic leukemia cell line, HMF: Human myocardial fibroblasts) to demonstrate its broad utility (Supplementary Figure 35).

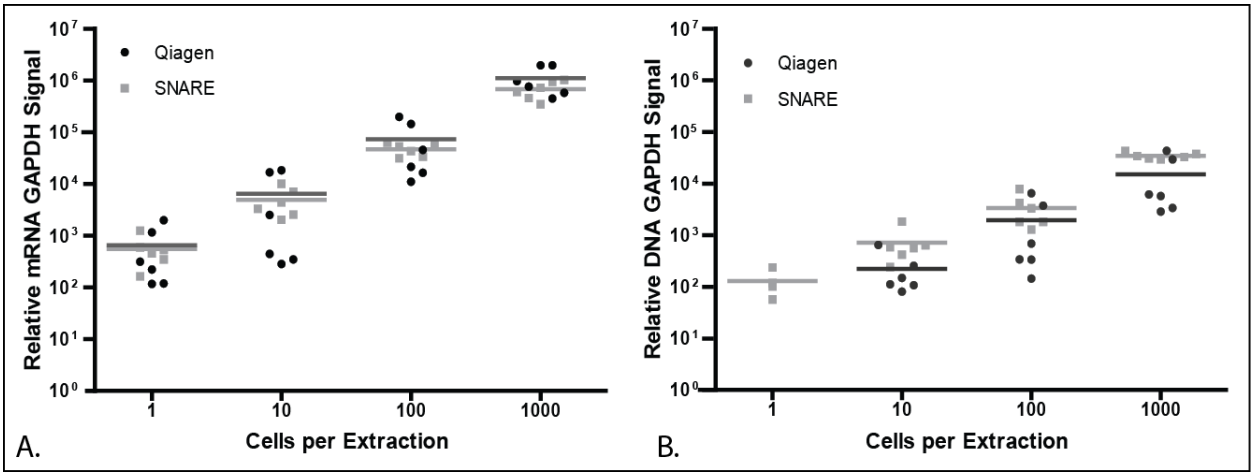

Figure 31 - Comparison of A) relative GAPDH mRNA, and B) GAPDH DNA signal purified from 1000, 100, 10 or 1 LNCaPs using SNARE (grey dots) or Qiagen (black dots). Each dot represents a nucleic acid purification procedure with horizontal lines representing the mean of the individual experiments. Sample size per a group n=6.

6.3.4 SNARE Enables Sequencing of Clinically Relevant Mutations

Deciphering nucleic acid sequences is essential for virtually all branches of biological research especially cancer pathogenesis, which is driven by inherited genetic variation and acquired somatic mutations. Therefore, we demonstrate mRNA and DNA extracted from 10 LNCaPs using SNARE could be used in Sanger sequencing. We specifically sequenced amplified regions of the AR, as it is a major driver of prostate cancer[110] from which the LNCaP cell line was derived. Figure 32A shows that the amplicon of the AR from SNARE-isolated mRNA was correctly amplified. Figure 32B shows that exon 8 of the AR was also correctly amplified from SNARE isolated DNA. A known mutation found in LNCaPs at T887A was also identified, as expected[111]. These data demonstrate the utility of SNARE for Sanger sequencing applications.

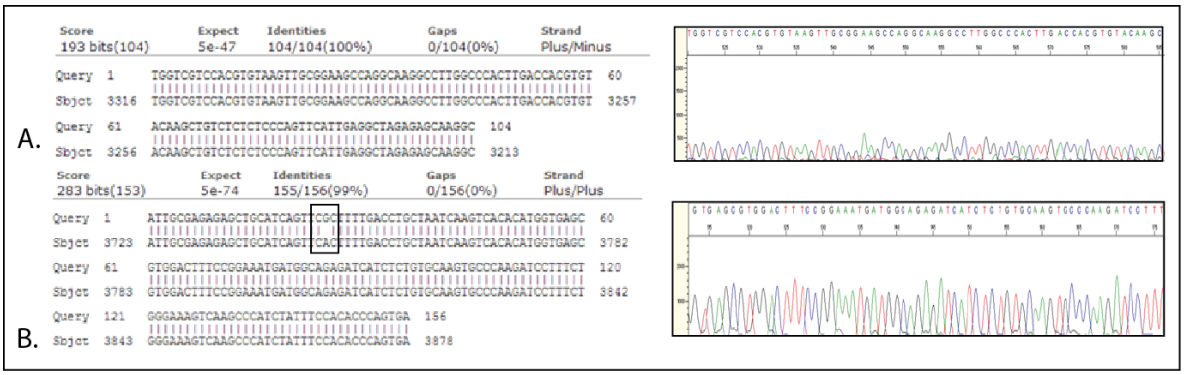

Figure 32 - A) Sequencing chromatogram and alignment of exon 5 and 6 of the AR from mRNA purified from 10 LNCaP cells using the SNARE method. B) Sequencing chromatogram and alignment of exon 8 of the AR from DNA purified from 10 LNCaPs using the SNARE method. The T887A LNCaP mutation was identified (black box).

6.3.5 Patient Data

SNARE was shown to be efficient for extracting mRNA and DNA from LNCaPs serving as a model for rare prostate cancer CTCs. To demonstrate that SNARE can extract both mRNA and DNA from clinical samples for molecular interrogation, we processed CTCs from three patients

with prostate cancer and examined relative GAPDH and AR signal by qPCR. This is a critical step forward as we move from the end point of CTC enumeration to the focus of molecular interrogation[101]. Within these patient samples, we were able to detect GAPDH and AR for both mRNA and DNA (Table 3). When CTCs were present we were able to amplify AR, a CTC specific gene which PBMCs do not express. While future molecular characterization will be dependent on the purity and efficiency of upstream rare cell capture methods, SNARE represents a method for sequential extraction of mRNA and DNA that maximizes the amount of information received from a single rare cell population. Importantly, SNARE is not limited to CTC mRNA and DNA extraction but can be expanded to use with other samples of interest.

Table 3-GAPDH and AR relative mRNA and DNA Threshold Cycle (C_T) from nucleic acids purified using SNARE from CTCs in three different patients diagnosed with prostate cancer

Patient #	CTC #	mRNA Threshold Cycle		DNA Threshold Cycle	
		GAPDH	AR	GAPDH	AR
1	47	30.46	27.06	30.24	35.03
2	7	33.31	38.07	30.35	38.44
3	0	35.52		28.17	34.5

6.4 Conclusions

We have shown SNARE can sequentially isolate both mRNA and DNA from a single sample by using immiscible phase exclusion. This method is advantageous when working with rare cell populations as it eliminates dilutive and centrifugation processes that result in sample loss due to increased fluid manipulation and purification time. In addition, SNARE enhances yield and reduces inter-experimental variability as no splitting of the original sample is needed. And given the increase in paired genomic and transcriptomic studies[89-91] the advantages and need of SNARE are becoming more apparent, especially when analyzing rare cell populations, such as

CTCs. In the future, whole genome and transcriptome amplification may be incorporated into the analysis to further expand the range of molecular assays that can be performed, including microarray analysis and whole genome/transcriptome sequencing applications. SNARE can be further expanded to integrate with other, previously developed microfluidic devices for rare cell isolation and analysis[103]. SNARE's reduction in time, cost and equipment needed make it amenable to widespread adoption for low cell number nucleic acid isolation in both the research lab and for clinical use.

In summary, SNARE was shown to isolate as much or more mRNA and DNA from 1-10 cells as compared to the Qiagen Allprep DNA/RNA micro kit as demonstrated by qPCR. We also demonstrated the mRNA and DNA extracted from a low number of cells could be used as template for Sanger sequencing. Finally, the utility of SNARE to isolate mRNA and DNA from rare cell populations was shown using CTCs as a model. Detection of both relative GAPDH and AR signal was achieved from collected prostate cancer CTCs. While CTCs are just one example of a real world sample, the mRNA and DNA isolated using SNARE could allow for expansion into early disease detection, monitoring of treatment response, selection of targeted therapies and understanding of disease development.

6.5 Supplemental

6.5.1 qPCR Primers

Table 4-Primers and probes used for detection in qPCR of mRNA androgen receptor (AR) and mRNA prostate specific antigen (PSA)

Gene Expression Assay	Forward Primer (5'->3')	Reverse Primer (3'->5')	Probe Sequence (Roche Universal Probe Library)
AR mRNA	gccttgctctctagcctcaa	ggtcgtccacgtgtaagttg	ctgggaga (#14)
PSA mRNA	tccgtgacgtggattggt	cagggttgggaatgcttct	ggaggctg (#75)

Table 5-TaqMan® gene expression assays for detection in qPCR of mRNA glyceraldehyde 3-phosphate dehydrogenase (GAPDH), DNA GAPDH, DNA AR and DNA PSA.

GAPDH mRNA	Hs02758991_g1 (Cat. # 4331182)
AR DNA	Hs04272737_s1 (Cat. # 4351372)
PSA DNA	Hs00377590_s1 (Cat. # 4351372)
GAPDH DNA	Hs9999905_m1 (Cat #. 4331182)

6.5.2 GAPDH mRNA and DNA Standard Curve

Methods & Materials. To estimate the threshold cycle values (C_t) for different LNCaP cell dilutions, we purified mRNA (Dynabeads® mRNA Direct™ Kit, Invitrogen) and DNA (MagaZorb®, Promega) separately from 10^6 LNCaP cells according to manufacturer's directions. Total mRNA and DNA amount was quantified using Qubit® 2.0 Fluorometer (Life Technologies, USA). A standard curve was established for both mRNA and DNA using the GAPDH gene expression assay. It was assumed that a single cell expressed approximately 3 pg mRNA (Dynabeads® mRNA Direct™ Kit) and 6.6 pg of DNA[112]. These values were then used to confirm appropriate C_t values were obtained using the SNARE technique.

Results & Discussion. In Figure 33A & 33B the GAPDH expression for mRNA and DNA is shown for nucleic acids purified from 1000, 100, 10 & 1 LNCaPs using the Qiagen DNA/RNA AllPrep kit and SNARE. Both techniques were graphed along with a standard curve. For both mRNA and DNA the standard curve was established by assuming LNCaPs have 3 pg of mRNA and 6.6 pg of DNA per a cell. Both standard curves show the gene expression values obtained using either Qiagen or SNARE technique are within the correct ranges. Finally, the mRNA standard curve shows lower efficiency but the amount of mRNA can greatly differ between cell types as compared to the DNA.

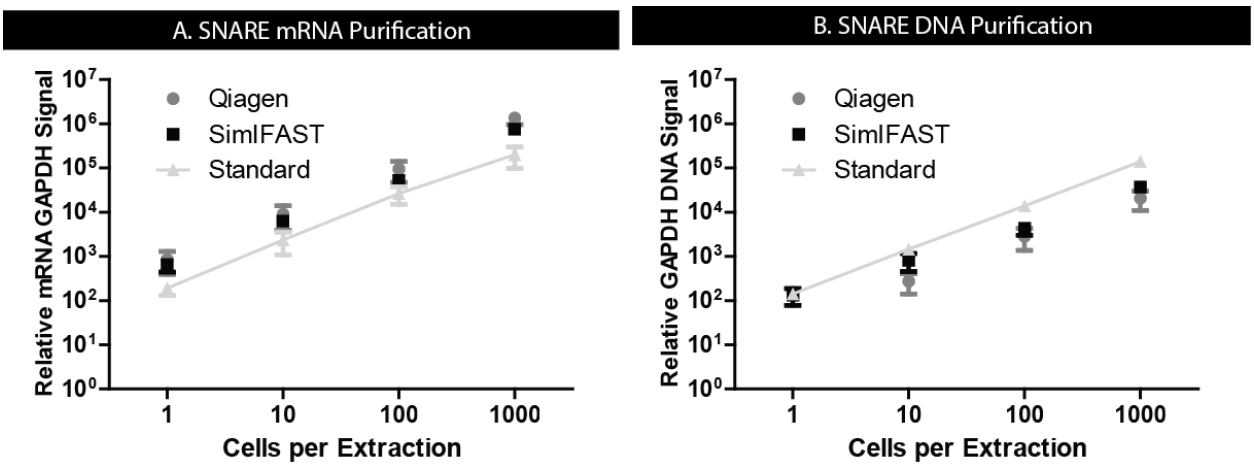

Figure 33-A) GAPDH mRNA Expression of Qiagen vs. SNARE as compared to standard curve of mRNA extracted using Dynabeads® mRNA Direct™ Kit with 1 cell equal to 3 pg/cell B) GAPDH DNA Expression of Qiagen vs. SNARE as compared to standard curve of DNA extracted using MagaZorb® with 1 cell equal to 6.6 pg of DNA/cell

6.5.3 AR & PSA Relative Signal SNARE vs. Qiagen

Methods & Materials. mRNA elution from LNCaPs containing PMPs was reverse transcribed using a High Capacity cDNA Reverse Transcript kit (ABI, Foster City, CA) according to manufacturer's directions. For PSA and AR mRNA gene expression assays, 4 µL of template was mixed with 10 µL LightCycler 480® probes master mix (Roche, USA), 0.3 µM forward and reverse primers, 0.2 µM probes (Universal Probe Library, Roche, USA) and 5.2 µL NF water (Primers and probes specified in Supplementary Table 4 & 5). For all other gene expression assays, 1 µL TaqMan® Gene Expression Assay (Life Technologies, USA) replaced the primers and probes used previously (TaqMan® Gene Expression Assays specified in Supplementary Table 4). Each reaction was amplified as previously described and relative gene signal was quantified and normalized using, $(2^{-(45-C_p)})$.

Results & Discussion. Figure 34A shows both the SNARE and Qiagen method were able to detect AR and PSA using mRNA purified from approximately a single cell by qPCR. However,

SNARE was able to detect AR and PSA in all samples at approximately a single cell, whereas the Qiagen kit could only detect 75 % of the samples. Higher variability in mRNA isolation was also observed for the Qiagen kit as sample size decreased. The differences could be due to sample lost through additional fluid transfer steps, centrifugal forces that result in fluid shear stresses and partial elution in wash buffers. In Figure 34B, using SNARE we show AR signal is reduced to 75 % for 10 cell samples and PSA gene signal to 75 % for 100 cell samples. For the Qiagen kit AR signal was reduced to 50 % for 100 cell samples and PSA gene expression to 50 % for 1000 cell samples. The higher sensitivity seen with that of GAPDH DNA expression could be due to copy number aberrations from aberrant karyotypes in LNCaPs[113], a feature common to cancer cell lines. For AR and PSA, the lower sensitivity could also be due to primer design,

especially for PSA as there are three highly homologous isoforms[114].

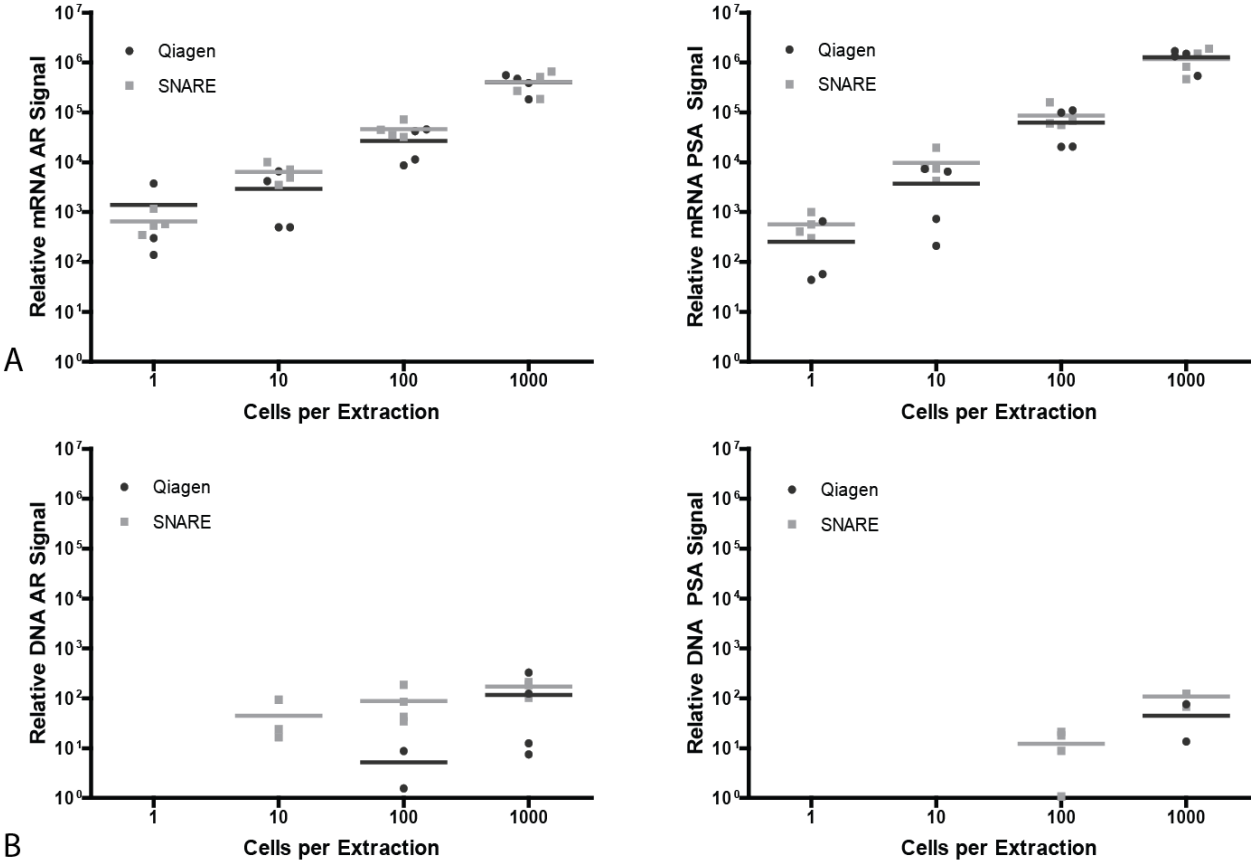

Figure 34-Comparison of A) relative AR and PSA mRNA, and B) AR and PSA DNA signal purified from 1000, 100, 10 or 1 LNCaPs using SNARE (grey dots) or Qiagen (black dots). Each dot represents a nucleic acid purification procedure with horizontal lines representing the mean of the individual experiments. Sample size per a group n=4.

6.5.4SNARE Method Using Two Different Cell Lines

Methods & Materials. Two different cell lines were used to verify mRNA and DNA extraction and purification using SNARE. All cells were cultured at 37 °C and maintained under 5 % CO_2 in polystyrene flasks until confluent. Human myocardio fibroblasts (HMFs) were cultured in Dulbecco's Modified Eagle Medium (DMEM; Mediatech, Herndon, VA) containing 10 % fetal calf serum (FCS) and 1 % Pen-Strep. Human acute monocytic leukemia cell line (THP-1) were

cultured in Corning Cellgro® RPMI 1640 Medium (VWR, USA) containing 10 % fetal bovine serum (FBS) and 1 % Pen-Strep. Cells were released using a 0.05 % trypsin/EDTA solution and collected via centrifugation. A 1:10 serial dilution of 100,000 to 1000 LNCaPs/mL of 1x PBS was performed. 10 µL of each serial dilution (n=2) was processed using SNARE, which correlated to 1000, 100, 10 and 1 LNCaP per a device. 10 µL of each serial dilution was processed using the SNARE method. GAPDH gene expression assays were performed on both mRNA and DNA and delta C_t values calculated.

Results and Discussion. To determine that SNARE could be used for a variety of cells lines, two cell lines of monocyte and fibroblast origin were processed. Both mRNA and DNA were able to be purified from the low cell number population using the SNARE technique. With both cell lines, single cell sensitivity was achieved (See Figure 35). However, for DNA the sensitivity was reduced to 10 cells. The decrease in relative DNA expression sensitivity could be due to the hypothesis that LNCaPS, a cancer cell line, might have more copies of GAPDH due to aberrant chromosome numbers.

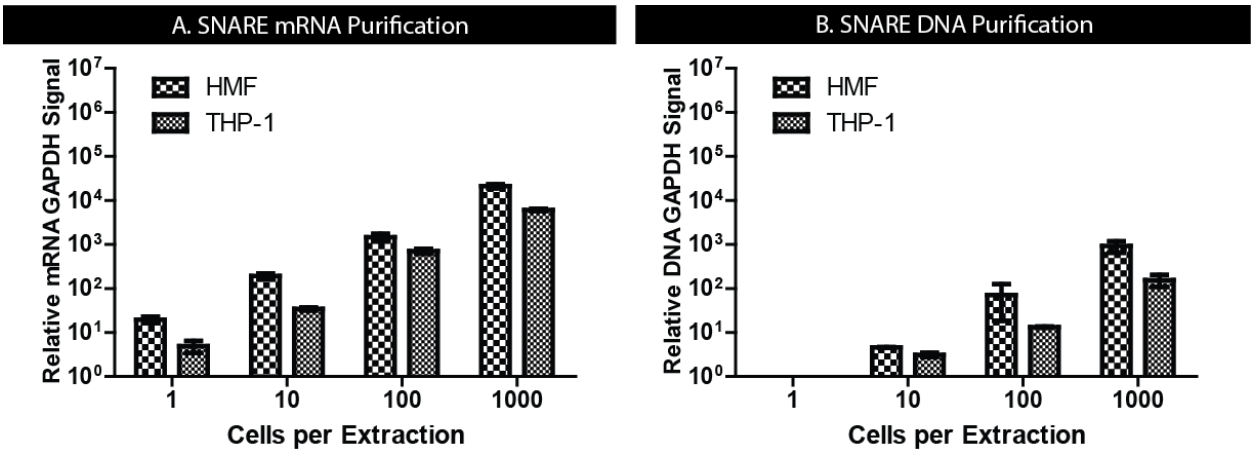

Figure 35-A) Comparison of GAPDH relative mRNA expression purified from 1000, 100, 10 or 1 using the SNARE method for HMF or THP-1 cell lines. B) Comparison of GAPDH relative

DNA expression purified from 1000, 100, 10 or 1 using the SNARE method for HMF or THP-1 cell lines.

6.6 Acknowledgements

The authors are grateful to Ms. Stephanie Thiede for her efforts cloning for sequencing. This work was supported by a grant from the Bill & Melinda Gates Foundation through the Grand Challenges in Global Health initiative, NIH Grant #5R33CA137673, NSF GRFP DGE-0718123 awarded to Lindsay Strotman, DOD grant W81XWH-12-1-0052 and the Prostate Cancer Foundation Young Investigator awarded to Dr. Lang. Scott Berry hold equity in Salus Discovery, LLC. David J. Beebe holds equity in Bellbrook Labs, LLC, Ratio, Inc and Salus Discovery, LLC.

Chapter 7 – Paired Diagnostic and Pharmacodynamic Analysis of Rare Non-Small Cell Lung Cancer Cells Enabled by the VerIFAST

7.1 Introduction

Lung cancer is the leading cause of cancer-related death in the United States and worldwide[115]. Non-small cell lung cancer (NSCLC) represents 88% of lung cancer diagnoses, with small cell lung cancer (SCLC) comprising the remaining 12%. The most frequently diagnosed subtype of NSCLC is adenocarcinoma. Before metastasis occurs and the tumor is < 30mm, the 5-year survival is near 77% (Stage 1A)[116]. When the primary tumor is >30mm or metastasis occurs, that survival rate drops to between 58% and 9% (Stages IB - IV). These clinical observations have led to major research initiatives focused on improving the early diagnosis rate as well as the development of pharmacodynamic biomarkers that enable precision medical care for patients with advanced disease[117]. Recent advances in these areas have involved high content molecular analyses from tumor cells isolated from lung biopsies. For example, Sequist et al performed serial tumor biopsies from patients with advanced NSCLC for paired histologic and genomic analysis[118]. These authors identified unexpected histologic subtypes of lung cancer in serial biopsies that altered therapeutic management and improved patient outcomes. However, broad clinical integration of these approaches is limited due to the nature of these invasive lung biopsies or resections including, but not limited to, hemorrhage, infection, pneumothorax[119]. These complications also occur with significantly higher frequency on lung lesions <4cm in size, as is commonly found in early stage disease[120]. Improving cancer care for patients across all stages of lung cancer will require the development of minimally invasive techniques for tumor sampling and rare cell analysis.

One recent advance for sampling suspicious lung nodules is known as electromagnetic navigation bronchoscopy (ENB)[121]. ENB utilizes advanced hardware and software to guide bronchoscopic tools directly to suspicious lung nodules for the early diagnosis of malignancy. Following nodule visualization, a mini-bronchoalveolar lavage (mBAL) uses 20-50 mL of saline solution to wash cells from the area of the nodule. The collection of mBAL during ENB thus allows sampling of cells in proximity with very small lung nodules in a significantly less invasive manner than fine needle aspirates or core needle biopsies. This method has previously been shown to be diagnostically relevant, as the isolation of tumor cells has revealed insight into the genetics of malignant tumors[122, 123]. However, ENB and mBAL have been limited by standard cytology techniques to identify tumor cells in a complex mBAL specimen that includes leukocytes, stromal and non-malignant epithelial cells. Thus, the relatively low sensitivity and specificity of these assays for rare tumor cells in heterogeneous mBAL samples limits broad utility for diagnostic purposes.

A second method for minimally invasive sampling of tumor cells is through the use of standard blood draws for the capture and analysis of circulating tumor cells (CTCs)[124]. CTCs are a rare population of tumor cells shed into peripheral circulation from primary and metastatic tumor sites that may both contribute to the development of metastatic disease and reflect the heterogeneity that likely exists between various tumor deposits. This hematogenous dissemination of tumor cells has long been recognized as one route by which solid tumors can create secondary metastatic sites – the main cause of patient mortality[125]. CTCs present an alternative method to collect lung cancer cells with a less invasive approach than the mBAL methods, but present a more difficult and heterogeneous population, as lung CTCs can exist at

approximately 5 cells per 10 million peripheral cells[126]. The frequency of CTCs in peripheral blood is also significantly lower in early versus late stage disease. Though the enumeration of CTCs has been linked to prognostic relevance in both NSCLC and SCLC[127-129] their utility can be expanded towards pharmacodynamic and other biologically and clinically relevant endpoints.

Unfortunately, the clinical utility of these minimally invasive techniques is often limited by the small amount of tumor cells recovered for standard cytologic and histopathologic analysis[130]. Thus advancing minimally invasive tumor sampling into clinical utility requires technologic advances that permit high content, cellular analyses on these rare cell populations. With physical characteristic scales enabling high precision relative to macroscale techniques, microfluidics is well positioned to capture and assess these rare cell populations with minimal sample loss. These microfluidic methods include the CTC Herringbone chip[131], the Micro-Hall Detector[132], DEP approaches[133], among others. Emerging studies continue to highlight the need for more sophisticated methods of CTC capture and analysis that go beyond enumeration[103]. However, the ability to use these methods on patient samples other than blood (i.e., bone marrow analysis, urine samples, mBAL) for rare cell capture and analysis has not been fully explored.

We have recently published a technique for the capture and proteomic analysis of rare cells[134]. The VerIFAST platform leverages surface tension at the microscale to pin aqueous and oil fluids in adjacent chambers to create a virtual filter between two aqueous wells[22, 23]. Using paramagnetic particles (PMPs) with attached antibody, specific cell populations can be targeted and isolated from complex backgrounds through a simple traverse of the oil barrier. Further, this platform integrated a microporous membrane into an aqueous chamber, enabling multiple fluid transfers without the need for cell transfer or centrifugation. This integrated platform enabled

removal of PMPs used for capture as well as multi-step molecular assays with essentially no cell loss during processing or analysis. We previously demonstrated the capacity of this platform to perform complex extracellular and intracellular staining for any protein target of interest.

In this report, we further enhance the VerIFAST's capabilities by integrating unique oil-pinning interfaces to enable chip tumbling without disruption of the aqueous-oil interfaces between each well and reduces the footprint of this device. We demonstrate the ability of the enhanced VerIFAST microfluidic platform to integrate with minimally invasive techniques in use for patients with lung cancer: mBAL samples and peripheral blood (CTC) samples. We further develop the base assays used in standard histopathologic assays for diagnostic and pharmacodynamic analysis of these rare lung cancer cells. The thyroid transcription factor-1 (TTF-1) is a diagnostic marker identified in primary lung adenocarcinomas and loss of expression correlates with more aggressive disease[135]. TTF-1 expression was evaluated in mBAL as a diagnostic assay and CTC samples as a confirmatory marker of a malignant cell. We pair TTF-1 analysis with protein analysis and quantification of staining intensity of the epidermal growth factor receptor (EGFR), which, when mutated by an activating deletion or point mutation in the kinase domain of exons 19 or 21, serves a high value therapeutic target in lung cancer[136]. These two targets have been shown to have utility as diagnostic, predictive and pharmacodynamic biomarkers.[137]

7.2 Materials and Methods

7.2.1 Device Fabrication

The device was fabricated via CNC milling (PCNC770, Tormach, USA) from 2 mm thick polystyrene (PS, Goodfellow, UK). The height and widths varied for each well with

differing volume capacities. The input well held 200 µL, whereas subsequent wells consisting of the staining well and sieve well held 30 µL and 50 µL respectively. The wells were connected via a trapezoid that had a 300 mm depth and height that tapered from 2 mm to 0.8 mm with a channel above for oil loading. A second PS layer containing an additional 50 µL well was solvent bonded using acetonitrile (Sigma-Aldrich, USA) to the first PS piece, with the membrane sandwiched between. The sieve well used for paramagnetic particle (PMP) removal and intracellular staining employed an 8 µm microporous membrane (Part PET8025100, Sterlitech, USA). A pressure sensitive adhesive was applied to each side of the device to contain the fluids (MicroAmp, Applied Biosystems, USA).

7.2.2 Paramagnetic Particle Preparation

Streptavidin coupled PMPs from the Dynabeads® FlowComp™ Flexi (Life Technologies, USA) at a concentration of 250 µg per a reaction were used for all experiments. The PMPs were washed twice and resuspended in 0.01% Tween-20 in phosphate buffered solution (PBS). 0.4 µg/mL of epithelial cell adhesion molecule (EpCAM, R&D Systems, USA) biotinylated according to the Dynabeads® FlowComp™ Flexi manufacturer's directions were added to the solution. The PMPs and antibodies were mixed for 30 minutes at RT followed by three washes and resuspension in 0.1 % BSA in PBS.

7.2.3 Cell Culture

The H358 bronchoalvelolar NSCLC cell line and the A549 adenocarcinoma NSCLC cell line (ATCC, USA) were cultured in Corning Cellgro® RPMI 1640 Medium (VWR, USA) containing 10 % fetal bovine serum and 1 % Pen-Strep. All cells were cultured at 37 °C and

maintained under 5 % CO_2 in polystyrene flasks until confluent. Cells were released using a 0.05 % trypsin/EDTA solution and collected via centrifugation.

7.2.4 Immunohistochemistry

All cell lines were stained with epithelial cell adhesion molecule conjugated to PE (EpCAM, 1:10 dilution, Santa Cruz Biotechnology, USA), Hoecsht stain (1:250), epidermal growth factor receptor conjugated to FITC (EGFR, 1:50, Abcam, USA) and transcription termination factor (TTF-1, 1:50, Santa Cruz Biotechnology, USA). Both the TTF-1 and EGFR primary antibody were located throughout the cell. A secondary antibody labeled with AlexaFlour-488 (Life Technology, USA) was used at a dilution of 1:100 for TTF-1. Samples were imaged using a Nikon Eclipse Ti (Nikon) and images were acquired with NIS Elements AR 4.10 software (Nikon). Image processing was completed using Image J, briefly a ROI was created for the EpCAM stain and used as a mask for TTF-1 and EGFR to measure signal intensity. The mean signal intensity was multiplied by the area. If cells clumped the total intensity was divided by the number of nuclei present before multiplication by area.

7.2.5 Device Operation

5 μL silicon oil (Fisher Scientific, USA) was added to the first trapezoid were it pinned via interfacial tension. PMPs and sample supplemented with 2 mM EDTA, 0.001% Tween-20, and 0.1% BSA in PBS was added to the input well. The device containing the sample was mixed on a tumbler for 30 min at 4 °C, in order for the cells to bind to the PMPs. Next, the second trapezoid was filled with silicon oil before the addition of a staining cocktail. The staining cocktail consisted of EpCAM conjugated to PE (1:10 dilution, Santa Cruz Biotechnology, USA), a second EpCAM conjugated to PE (1:100 dilution, Abcam, USA) to further increase EpCAM

signal, Hoescht (1:250) and CD45 conjugated to Alexa Fluor 647 (1:10 dilution, Biolegend, USA). A handheld magnet (K&J Magnetics, USA) transferred the PMPs into the staining well were it was incubated for 30 minutes at 4 °C. Finally, 100 µL PMP release buffer from the Dynabeads® FlowComp™ Flexi kit was added to the sieve well and the same magnet used to transfer the PMPs into this well. The magnet was then used to pull the excess unbound PMPs through the membrane to the back of the sieve well. After 30 minutes at RT in the release buffer to further remove excess PMPs from cells, they were removed. Cells were permeabilized for 30 minutes by the addition of 1 % Tween 20 in PBS to the sieve well. Following permeabilization, a primary antibody, either TTF-1 or EGFR-FITC, was added and incubated overnight at 4 °C in a humidified environment. After 24 hours, the samples were washed 3 times with 0.1 % BSA in PBS. For the TTF-1 samples, a secondary antibody labeled with AlexaFlour-488 was added for 1 hour at RT followed by 5 washes with 0.1 % BSA in PBS. Samples were imaged within device.

7.2.6 Cell Capture Efficiency

For quantification experiments H358 cells were incubated for ten minutes with 2 mM calcein AM (Life Technologies, USA) in serum free RPMI media. The cells were centrifuged and washed once in PBS, then counted with a hemocytometer and re-suspended in PBS. H358 cells were spiked in PBS with 0.1 % BSA and 2 mM EDTA at 10, 100 and 1,000 cells per a device. Cells were captured and processed as described above without additional staining.

7.2.7 Patient Samples

Lung lavage and blood samples were collected from NSCLC patients who had signed their respective Informed Consent documents under two separate University of Wisconsin IRB approved protocols. For sample processing the sample was spilt into two for either EGFR or

TFF-1 staining. Lung lavage samples were centrifuged at 1200 x g for 5 minutes. The resulting cell pellets were fixed (BD Cytofix™, USA) for 30 minutes on ice before being washed once in PBS. Blood samples underwent a standard density centrifugation (Ficoll-Paque, GE, USA) to isolate peripheral mononuclear blood cells (PBMCs), which were then fixed and washed once in PBS. Samples were then processed using the device as described above. Circulating tumor cells (CTCs) and cells of interest in the lung lavage samples were defined as having an intact nucleic, EpCAM positive and CD45 negative. Image processing was completed as described above.

7.3 Results and Discussion

7.3.1 VerIFAST Innovation

The VerIFAST (Figure 36A) utilizes the relative dominance of surface tension over gravity in the microscale to load immiscible phases side by side without density driven stratification, in order to eliminate laborious and time consuming wash and centrifugation steps required by most sample preparation protocols. VerIFAST builds upon a previous platform that was designed to take advantage of settling of non-target cells to help decrease non-specific carryover[134]. This platform was further modified to incorporate a membrane (< 8 μm) in the sieve well, which was used to remove unbound PMPs that might interfere with imagining and enable fluid exchanges for intracellular staining with no direct contact (Figure 36B). Sample transfer to VerIFAST increases the workflow and represents a potential step where sample could be lost. To enable constant mixing and eliminate a transfer step we utilized oil pinning within the VerIFAST (Figure 36A). In the original VerIFAST design, mixing within the device was hindered because the oil would creep into adjacent compartments during device tumbling. Therefore, we took advantage of the low aspect ratio of the trapezoid for device redesign to

enable oil pinning. While most pinning or virtual wall formations have been described using aqueous fluids, little focus has centered on the use of oil[16, 134, 138]. Here, we are able to exploit oil pinning due to the dominance of surface tension in the microscale. Finally, the inputs of each well were also geometrically constrained such that aqueous fluids remained pinned while mixing.

To operate, oil is first pinned within the confines of the trapezoidal regions using a pipette through the respective input channels. Next, the input well, staining well and sieve well were loaded with the assay-specific buffers. Once the sample was in the input well, it was placed on a tumbler and incubated with PMPs to bind cells (EpCAM+) of interest. Following binding, a simple handheld magnet transferred the PMPs along the front side of the devices through the oil-filled trapezoidal region into the staining well that contained a cocktail of antibodies to enable determination of cells of interest in the sieve well. After the second incubation, the cell bound PMPs were transferred again along the front side of the VerIFAST to the sieve well containing release buffer. Once in the well, a brief incubation was needed to help remove cell-bound PMPs that could interfere with imaging. A magnet held on the backside of the device removed the unbound PMPs from the front of the sieve well to the back, while retaining cells in the front side of the sieve well. Using the backside of the sieve well, fluids could be easily added or removed without manipulating the cells, further reducing potential sample loss. This enabled permeabilization and intercellular staining for cell targets including EGFR and TTF-1. Overall, the operational simplicity and minimization of transfer and manipulation steps reduce the chance of loss of the rare sample and decrease laboriousness of the procedure.

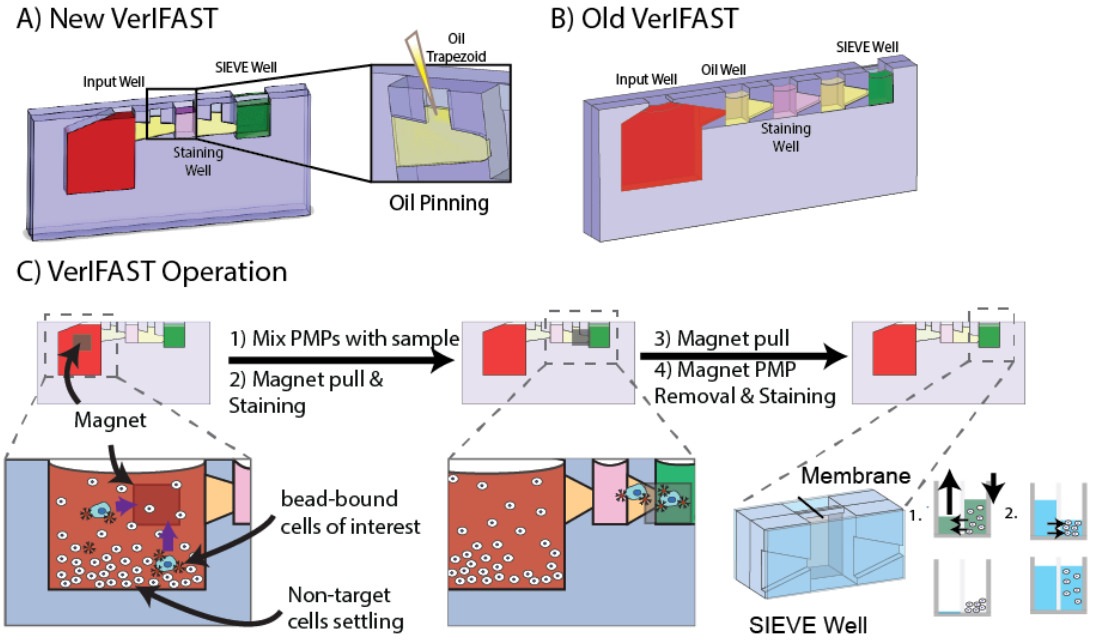

Figure 36-A) VerIFAST Device containing input well for binding cells of interest to PMPs, staining well and sieve well for imagining, intracellular staining and unbound/excess PMP removal. An enlarged view depicts pinning of the oil in trapezoid by surface tension. B) Original VerIFAST containing non-pinning oil wells C) Operation of VerIFAST. Briefly, cells of interest bind to antibody conjugated PMPs in VerIFAST and are transferred to staining and SIEVE well via a handheld permanent magnet. Within the sieve well, unbound PMPs and fluid transfers for intracellular staining are performed without direct perturbing of rare sample.

7.3.2 Integrated Capture and Molecular Analysis Lung Cancer Cells

The VerIFAST utilizes a flexible, antibody-based capture methodology to isolate cells of interest from a heterogeneous population. Given the strength of EpCAM-based capture of lung cancer cells demonstrated by the Veridex platform and others, we evaluated the ability of VerIFAST to capture lung cells targeting this protein. As shown in Figure 37A, the VerIFAST exhibits a capture efficiency of greater than 90% across three varying concentrations of H358 cells (Fig 37A). In order to assess the levels of expression for TTF-1, a molecular marker with diagnostic relevance, and EGFR, contrived cell lines with varying expression of both were used to validate

the assay (Figure 37B). ImageJ was used for quantification, using EpCAM staining to define cellular boundaries, and measuring the fluorescent intensity of the stain interior to EpCAM. For TTF-1, the H358 NSCLC cell line was used for positive expression of TTF-1, with A549 cells demonstrating decreased expression of its protein (Figure 37C). Using this analysis, the two cell populations were statistically different ($n = 5$, $p < 0.05$). The same analysis was applied to EGFR samples (Figure 37D), of which there is variable expression of EGFR between the two cell lines[139]. H358 cells were observed to express significantly higher EGFR than A549 ($n = 5$, $p < 0.005$), allowing the assessment of heterogeneous expression in patient samples.

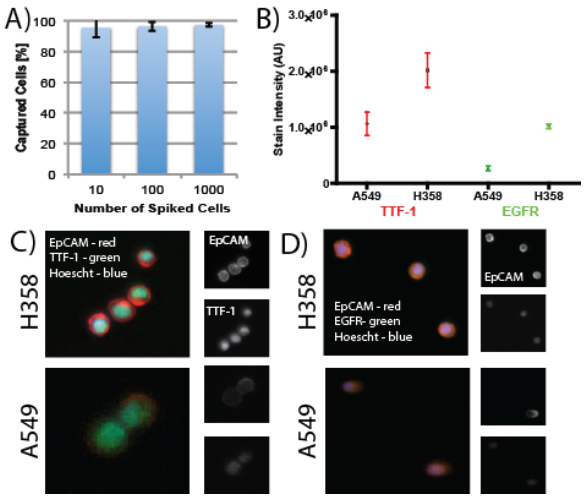

Figure 37-A) Capture efficiency of H358, a lung cancer cell line, using VerIFAST B) Signal intensity of TTF-1 and EGFR staining using two different lung cancer cell lines H358 and A549 C) Images showing staining of TTF-1 in H358 cells and A549 cells. (EpCAM: Red, TTF-1: green & Nuclei: blue) D) Images showing staining of EGFR in H358 cells and A549 cells. (EpCAM: Red, TTF-1: green & Nuclei: blue) Labels same for A549 cells.

7.3.3 TTF-1 and EGFR Expression in Patients Samples

TTF-1 is utilized in standard pathologic analysis to confirm the diagnosis of primary adenocarcinoma of the lung from standard tissue biopsies. Because mBAL samples can be collected in an earlier disease state then CTCs and could also contain benign lung epithelial cells,

molecular assays for TTF-1 on rare cells will be helpful in using these samples for the early diagnosis of primary adenocarcinoma of the lung. Figure 38A shows the average number of cells collected from patients as well as examples of stained cells and clumps of interest that are EpCAM positive, CD45 negative and contain an intact nuclei. In five collected mBAL samples (Figure 38C), the heterogeneity of TTF-1 samples was clear, as the fluorescent intensity of samples could range to nearly 5-fold differences in cellular expression of TTF-1. Interestingly, using H358 and A549 staining as positive and negative controls, respectively, only two mBAL samples displayed full loss of TTF-1 expression (below negative control A549 cells). In one of the samples, however, the expression varied and there was visibly a subset of cells that were below, but not the entire cell population (mBALa). Identical analysis of TTF-1 in CTC samples demonstrated significant heterogeneity across CTCs (Figure 38B) that may reflect the different extent of tumor burden among the patients sampled, as well as possible epithelial-mesenchymal transitions[140] that may characterize components of the metastatic process.

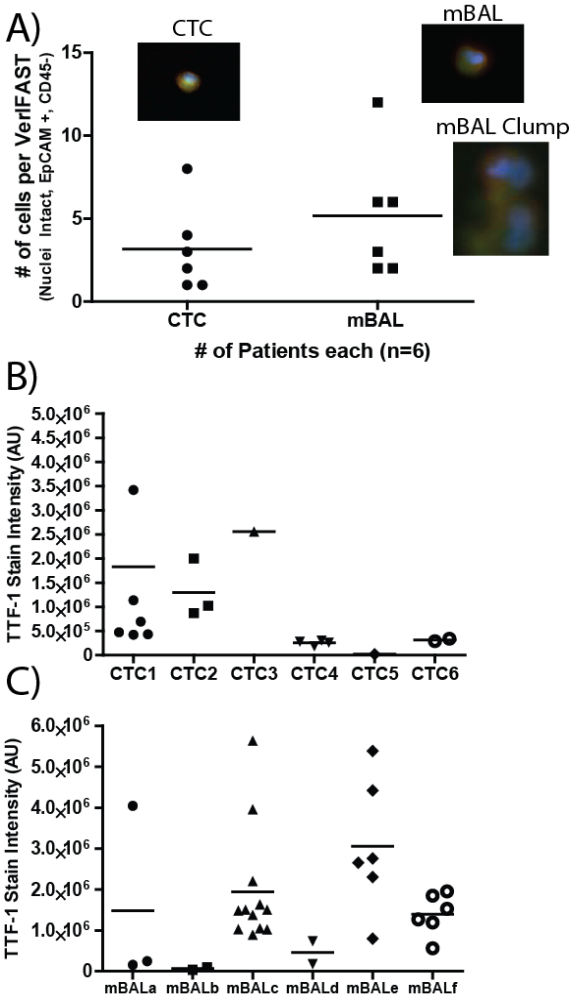

Figure 38-A) Number of cells captured from blood (CTCs) (n=6) or mBALs (n=6) using VerIFAST. Images of a CTC or cell from mBALs. An example of a mBAL lavage cell clump is also given. B) TTF-1 staining intensity of CTCs cells (n=6) C) TTF-1 staining intensity of cells from mBAL samples. (n=6)

Protein expression of EGFR is detected in up to 80% of NSLCC clinical specimens[141] Cetuximab, a chimeric IgG1 monoclonal antibody that inhibits EGFR function, demonstrated clinical efficacy when NSCLC patients were selected by EGFR protein expression[142]. The value of EGFR as a therapeutic target is heightened when activating mutations are present in the kinase domains of exons 19 and 21[143, 144]. Therefore, the ability to perform molecular assays on EGFR in lung cancer cells from patients in the least invasive manner, repeatedly in a longitudinal

manner over the course of their disease, would permit optimal timing and selection of the most individualized EGFR-directed therapies. In Figure 39, we demonstrate the ability of VerIFAST to detect EGFR protein expression in NSCLC patients by obtaining and analyzing clinical specimens without the invasive and potentially risky need for needle aspirate or core biopsies or by obtaining specimens from surgical resections. Signal intensity of EGFR was more consistent among the CTC samples (Figure 39B), compared to more variable EGFR expression in the mBAL samples (Figure 39C). This may be related to the fact that patients who underwent mBAL sampling had a lower disease stage, and therefore a lower tumor burden, compared to patients who underwent CTC sampling.

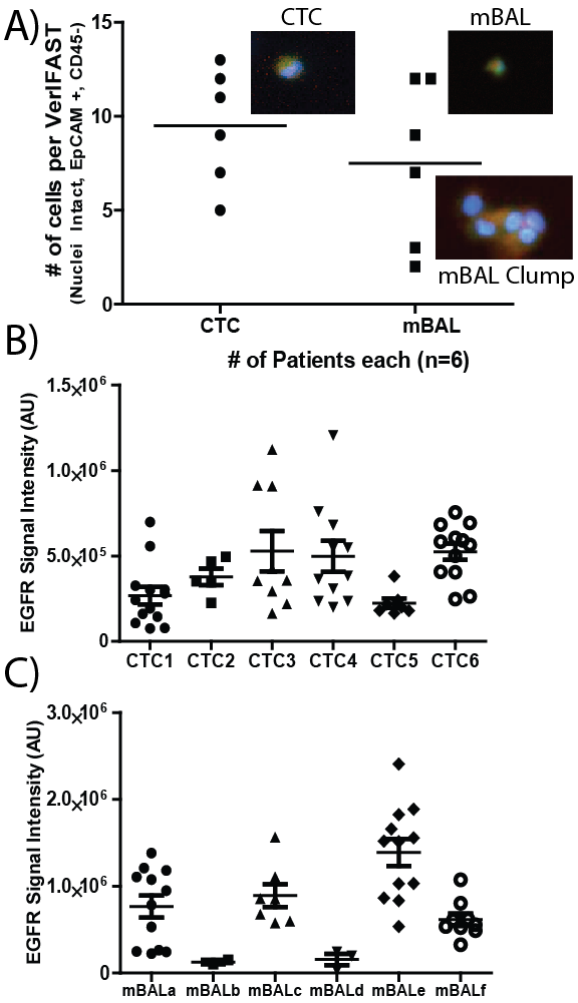

Figure 39-A) Number of cells captured from blood (CTCs) (n=6) or mBALs (n=6) using VerIFAST. Images of a CTC or cells from mBALs. An example of a mBAL cell clump is also given. B) EGFR staining intensity of CTCs cells (n=6) C) EGFR staining intensity of cells from mBAL samples. (n=6)

7.4 Conclusion

Here, we have presented a comprehensive platform that is able to collect and analyze lung cancer samples (both mBAL and blood) using collection techniques that are significantly less invasive than lung biopsies or resections. Leveraging the flexibility of the VerIFAST to use a variety of samples beyond blood, mBAL samples were collected and analyzed as an early collection and diagnostic technique. Blood samples were analyzed for CTCs as a second method towards the

analysis of lung cancer. The ability of the VerIFAST to collect and analyze these patient samples is particularly useful for lung cancer, as minimally invasive sample collection that can be repeated serially allows for safer and longitudinal studies that will obviate the need for repeated biopsies and their attendant complications. TTF-1 was used as a diagnostic target, and revealed the heterogeneity of the lung lavage samples. The variability of EGFR expression in mBAL samples relative to CTC samples is an interesting observation, as patients that have CTCs are more likely to have advanced disease. This study was a proof-of-concept study for the use of mBAL and CTCs for the evaluation of EGFR and TTF-1, rather than only enumeration of discovered cells. The success of this study allows these samples to be used moving forward in a clinical trial to assess the validity of these endpoints. Further, the VerIFAST was enhanced with new features that facilitated, for the first time, the analysis of both mBAL samples and CTCs from blood samples from lung cancer patients.

7.5 Acknowledgements

This work was supported by a grant from the Bill & Melinda Gates Foundation through the Grand Challenges in Global Health initiative, NIH Grant #5R33CA137673, NSF GRFP DGE-0718123, a UW Institute for Clinical and Translational Research-Type 1 Research Pilot Award, UW Carbone Cancer Center Investigator Initiated Pilot grant and a Prostate Cancer Foundation Young Investigator award to Dr. Lang. David J. Beebe holds equity in Salus Discovery, LLC, Bellbrook Labs, LLC and Ratio, Inc.

Chapter 8 – Future Directions: Towards an Multi-analyte Integrated Platform VERSA

8.1 Introduction

8.1.1 Circulating Tumor Cells

Within the past few years the landscape of therapeutic options for cancer patients has dramatically changed. However, this has also presented a new challenge of identifying those patients who will and will not respond to these therapeutic advancements. Therefore, the development of prognostic, predictive and pharmacodynamic biomarkers to determine and monitor patient response is of upmost importance, saving patient's time and resources[145]. A limitation to the development of these biomarker assays is the availability of tumor samples for testing, which can be difficult, expensive and inconvenient for the patient to obtain. Circulating tumor cells (CTCs), a rare population of tumor cells shed into peripheral circulation from primary and metastatic tumor sites, represent an interesting and easily accessible cell population for these kinds of analysis.

Though the specific origin of CTCs is unknown they are associated with the metastatic cascade[146] and remain prognostic of patient survival in many cancers[147-151], as well as serving as a surrogate to drug response. Given that CTCs are a rare cell population, less than one in a billion of the circulating mononuclear cells in the blood[152], several questions including metastatic potential and their use as a biomarker beyond enumeration remain invalidated[153]. Therefore, the development of new technologies to further our understanding of the biological properties of CTCs is critical not only for basic cancer research but to affect clinical outcome[103].

8.1.2 Circulating Tumor Cells Capture Technologies

Currently, the only FDA-approved method for CTC capture and enumeration is the Veridex CellSearch® platform, which uses 7.5 mL of blood to magnetically capture EpCAM positive cells. CTCs are further classified on the basis of morphologic limits and rigorous criteria for staining of cytokeratin (CK-6, 8, 18), display of a nucleus [4′, 6 diamidino 2 phenylindole (DAPI)] and exclusion of white blood cell (CD45 staining)[154]. The success of this platform has led to the development of numerous other CTC capture technologies that rely on capture through either physical or biological aspects of CTCs. These physical characteristics rely on dielectric moment, density gradient centrifugation, filtration based on size or exploit differences in cell plasticity[155]. Biological characteristics can be divided into either direct or indirect capture methods. Direct capture methods include capture with a single antibody or antibody cocktail to cell surface markers that are conjugated to magnetic ferrofluids, magnetic beads, microposts or chips[156, 157]; as well as, separation by flow cytometry. Indirect methods have gained in popularity as CTCs from any cancer can be analyzed as no specific extracellular markers are needed[158]. In addition, EpCAM-based CTC capture methods may have limited ability to identify tumor cells with reduced expression of this epithelial marker as a result of the epithelial-meschymal transition (EMT)[159]. These indirect capture methods include depleting CD45 expressing mononuclear cells leaving behind only the CTC population, depletion of red blood cells with direct deposit of buffy coat to microscope slide for future imaging[160] or ability of CTCs to grow in-vitro[161].

Unfortunately, the current CTC capture technologies have largely focused on CTC enumeration, ignoring the vast amount of valuable biological information these cells potentially

hold. Efforts to integrate methods for further analysis of CTCs have focused on integration directly with capture methods or appending single-cell aspiration to remove cells for off-chip analysis. Endpoints integrated on-chip include intracellular protein staining[162], RNA-ISH gene expression analysis[163], DNA methylation[164], cell secretion[161], mRNA seq[165], and extracellular staining of CTCs directly following enumeration endpoints. A critical shortcoming of these assays is the limited number of endpoints that can be used given the small yield of biological material CTC cells contain.

8.1.3 Prostate Cancer Background

Prostate Cancer (PCa) is the second leading cause of cancer death for men in the United States and is associated with significant healthcare cost[166]. In 1941, Huggins and Hodges demonstrated that PCa is an androgen-dependent disease[167]. The androgen receptor (AR) is a transcription factor, which upon binding of dihydrotestosterone (testosterone modified by 5-alpha reductase) to its ligand binding domain (LBD), translocates from the cell cytoplasm to the nucleus activating a transcription program critical to PCa tumorigenesis[168] (Figure 40). Patients with metastatic PCa first undergo chemical or surgical castration to lower androgen levels, specifically testosterone, which are responsible for activating the AR signaling pathway downstream[169]. Despite an initial response to androgen deprivation therapy (ADT), patients inevitably progress to a prostate cancer castration resistant (CRPC) state where the cancer will progress despite low levels of testosterone[170]. CRPC has a poor prognosis and until recently there were few treatment options besides chemotherapy and palliative care[171]. However, as our understanding of PCa disease biology has improved so too has rational development of targeted approaches mainly focused on the AR signaling pathway.

As traditional androgen deprivation therapy (ADT) does not completely deplete intratumoral androgens or expression of AR target genes[172], one of the most successful targeted approaches and the first FDA approved drug was abiraterone acetate[173]. Abiraterone acetate is an irreversible inhibitor of cytochrome P450-17 (cyp17), inhibiting extragonadal and intratumoral synthesis of androgens[174] (Figure 40). Another drug recently FDA approved is Enzalutamide (formerly known as MDV3100), which acts as an AR antagonist[175, 176] (Figure 40). Together both of these drugs inhibit translocation of AR nuclear localization preventing downstream PCa growth. Unfortunately, these drugs have been shown to be effective for only a percentage of CRPC patients and patients undergoing these therapies eventually become resistant. Mechanisms of intrinsic and acquired resistance to these AR-targeting therapies include, "genomic amplification and overexpression of AR[177, 178], gain of function mutations allowing AR to be activated by promiscuous ligands such as steroids or antiandrogens[179], upregulation of AR enhancer elements[180], alterations in androgen transport[181, 182], increased synthesis of extragonadal androgens[183], abnormalities in AR coactivators and coregulators[184], ligand-independent transactivation of AR by growth factors or cytokines, and AR splice variants that encode for LBD-deficient receptors and are constitutively active but may be dependent upon a full-length receptor for functionality[185-187]." Given the high cost of these drugs and potential ineffectiveness prognostic, predictive and pharmacodynamic biomarkers are critically needed[157].

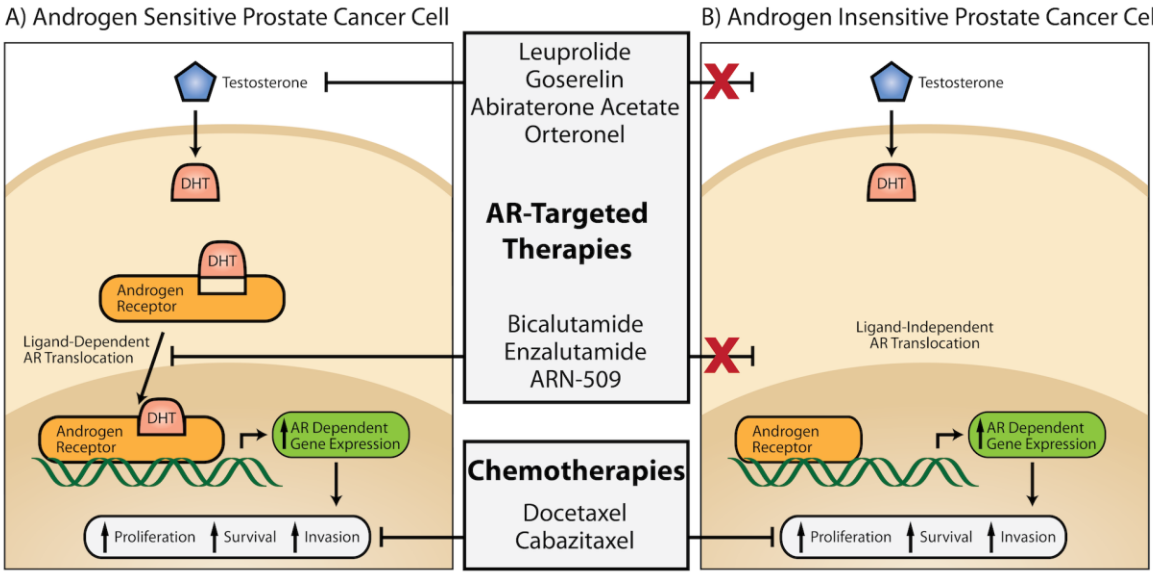

Figure 40-Drugs that Target the Androgen Receptor signaling axis A) Cells sensitive to AR B) Cells insensitive to AR

8.1.4 Prostate Cancer and Circulating Tumor Cells

Based on a prospective trial enrolling patients with metastatic PCa the number of CTCs correlated with prognosis leading the FDA to provide clearance for use of the Veridex CellSearch® platform to be used for monitoring disease status[154]. Importantly, it was shown that the number of CTCs demonstrated only a modest correlation to overall disease burden[148, 188]. Additionally, more CTCs were collected from patients with bone and visceral metastases as compared to patients with lymph node disease[148, 188, 189]. In another study of PCa patients, CTC number was shown to be a prognostic pre and post chemotherapy biomarker[148, 188]. In a separate cohort of PCa patients treated at Memorial Sloan-Kettering Cancer Center, CTC number also considered as a continuous variable was shown to be an independent prognostic factor[189]. Finally, CTC enumeration as a biomarker was incorporated into clinical trials accessing abiraterone acetate and enzulatamide therapeutic efficacy with the number of CTCs correlating

to patient response[174, 176, 190]. More studies are ongoing and needed in order to further disseminate CTC count as a potential efficacy-response biomarker of survival for AR-targeted therapies.

As mentioned previously, in addition to CTC enumeration as a prognostic and predictive biomarker, CTCs have the potential to provide a picture of the molecular make-up of a patient's tumor. Previously, CTCs isolated from patients with CRPC have been shown to exhibit features of PCa, such as expression of PSA, alpha-methylacyl-CoA racemase (AMACR) and prostate-specific genomic abnormalities including AR gene copy number amplification, phosphatase and tensin homolog (PTEN) deletions and TMRRSS-ETV fusion products[191, 192]. While it is likely that further molecular profiling will reveal additional PCa tumor similarities this information could be used to profile for determinants that predict sensitivity or resistance to treatment. But again we are currently limited by the lack of reliable technology to go beyond CTC enumeration. Within this chapter we will introduce a platform with the needed technology for in-depth molecular profiling of PCa CTCs. This platform will also allow us to start accessing potential predictive AR-axis therapeutic biomarkers focused on determining patient response and emerging mechanisms of resistance.

8.1.5 VERSA

The platform utilizes ESP methods, employing surface tension to isolate PMPs bound to specific analytes without diluting or perturbing the sample of interest[17, 22, 23, 53, 86, 87]. Specifically, we utilize surface tension to load immiscible fluids side-by-side without density driven stratification allowing PMPs bound to an analyte of interest to be brought across a virtual wall, facilitating purification. This ESP method termed VERSA (Vertical Exclusion-based Rare Sample Analysis) allows us to streamLine the workflow by removing traditional wash and

centrifugal steps needed for analyte purification. While we have shown effective isolation of single analytes separately using ESP methods (cells, protein, DNA and mRNA), here we sequentially extract important analytes from the same sample. The VERSA platform allows for a comprehensive and flexible CTC endpoint analysis that allows not only enumeration but can access AR activity in-depth using protein localization, mRNA transcript analysis, and DNA sequencing. Specifically, we assess mechanisms of AR activity and therapeutic resistance including, AR nuclear localization percentage, AR splice variant analysis and mutations in the AR gene.

8.2 Materials and Methods

8.2.1 VERSA Fabrication

The VERSA device was injected molded using the services of Proto Labs (USA). Briefly, the front and back sides were fabricated separately from polystyrene to a thickness of 2 and 2.5 mm, each with varying well heights and widths to accommodate different volume capacities. For the front side, the cell capture well held 250 μL, whereas subsequent wells consisting of the extracellular staining well, sieve well and the mRNA extraction well held 30 μL, 50 μL and 15 μL respectively. The back side consists only of the back sieve well that mates to the front sieve well and DNA extraction well, which held 50 μL and 15 μL respectively. All wells were connected via a trapezoid that had a 300 mm depth and height that tapered from 2 mm to 0.8 mm with a channel above for oil loading. However, both the front and back side have an oil well, holding 60 μL, which connected the sieve and two nucleic acid extraction wells. This allowed a multi-operational path for the paramagnetic particles (PMPs) to either the separated mRNA or DNA extraction wells. The front and back sides were solvent bonded using acetonitrile (Sigma-

Aldrich, USA), with a membrane sandwiched between the sieve well and supported by the horizontal crossbar located on the back side. The sieve well was used for PMP removal and intracellular staining employed an 8 μm microporous membrane (Part PET8025100, Sterlitech, USA). A pressure sensitive adhesive was applied to each side of the device to contain the fluids (MicroAmp, Applied Biosystems, USA).

8.2.2 Cell Culture

The prostate cancer cell lines 22Rv1, LNCaPs, PC3, were cultured in Corning Cellgro® RPMI 1640 Medium (VWR, USA) containing 10 % fetal bovine serum (FBS), 1 % Pen-Strep, 1 % Sodium Pyruvate and 1 % α-MEM. The prostate cancer cell lines R1-D567 and R1-AD1 (a kind gift from the laboratory of Dr. Scott Dehm at the University of Minnesota) were cultured in Corning Cellgro®RPMI 1640 Medium and 10 % FBS. The R1-D567 cell line was genetically engineered to remove exon 5, 6 and 7 of the AR LBD, representing a clinically present AR splice variant, V567es. All cells were cultured at 37 °C and maintained under 5 % CO_2 in polystyrene flasks until confluent. Cells were released using a 0.05% trypsin/EDTA solution and collected via centrifugation.

8.2.3 Patient Sample Processing

Blood samples were collected from patients who had signed an informed consent document under a University of Wisconsin IRB approved protocol. From each patient, we collected 7.5 mL of blood into both an EDTA (BD Biosciences, USA) and CellSave® (Veridex, USA) tube, each of which underwent a standard density centrifugation (Ficoll-Paque, GE, USA) to isolate peripheral mononuclear blood cells (PBMCs). The blood samples collected in CellSave® tubes were fixed (BD Cytofix™, USA) for 30 minutes on ice and washed once in phosphate buffered

saline (PBS) with 0.1% BSA + 2 mM EDTA. 100 µL CD45 PMPs (Dynabeads, Life Tech, USA) washed twice and resuspended in 100 µL PBS with 0.1 % BSA + 2mM EDTA, were added to PBMCs collected from EDTA preserved blood and incubated for 15 minutes at 4 °C on tumbler. CD45 PMPs were then removed using a magnetic stand prior to VERSA processing.

8.2.4 Paramagnetic Particle Preparation

Streptavidin coupled PMPs from the Dynabeads® FlowComp™ Flexi (Life Technologies, USA) at a concentration of 250 µg per reaction were used for all experiments. The PMPs were washed twice and resuspended in 0.1% Tween-20 in PBS. 0.4 µg/mL of epithelial cell adhesion molecule (EpCAM, R&D Systems, USA) biotinylated according to the Dynabeads® FlowComp™ Flexi manufacturer's directions were added to the solution. The PMPs and antibodies were mixed for 30 minutes at RT followed by three washes and resuspension in 25 µL of 0.1 % BSA in PBS.

8.2.5 VERSA Operation

CTC Capture

6 µL silicon oil (Fisher Scientific, USA) was added to the first trapezoid where it pinned via interfacial tension. EpCAM labeled PMPs, 20 µL 0.1 % Tween 20 in PBS and samples suspended in 2 mM EDTA, and 0.1% BSA in PBS were added to the input well. The device containing the sample was mixed on a tumbler for 30 min at 4 °C, in order for the cells to bind to the PMPs.

Extracellular Staining

Next, the second trapezoid was filled with silicon oil before the addition of a staining cocktail for extracellular proteins. The staining cocktail consisted of CD45 conjugated to PE (1:15 dilution, Biolegend, USA) and Hoescht (0.4 mg/mL)). A handheld magnet (B333-N52, K&J Magnetics,

USA) transferred the PMPs into the extracellular staining well were it was incubated for 30 minutes at 4°C. For blood samples collected in an EDTA tube no extracellular staining was performed with PMPs being transferred directly to the sieve well.

PMP removal in Sieve Well

PMP release buffer from the Dynabeads® FlowComp™ Flexi kit was added to the sieve well and a magnet was used to transfer the PMPs. The magnet was then used to pull the excess unbound PMPs through the membrane to the back sieve well were they were collected and additional release buffer added. The membrane pore size (8 μm) was chosen so that only PMPs (2.8 μm) and fluid would be able to transfer to the back sieve well while keeping cells (12-20 μm) in the front sieve well. After 30 minutes incubation, PMPs were again pulled through to the back sieve well and removed. For both blood samples collected in either EDTA and CellSave® tubes, PMP removal was performed using the same method.

Intracellular Staining and Enumeration in Sieve Well

Cells were permeabilized in the sieve well for 30 minutes by the addition of 1 % Tween 20 in PBS. Following permeabilization, pan-cytokeratin conjugated to FITC (1:50, Abcam, USA) and androgen receptor (1:100, Cell signaling, USA), was added and incubated overnight at 4 °C in a humidified environment. After 24 hours, the samples were washed 3 times with 0.1 % BSA in PBS. A secondary antibody labeled with AlexaFluor-647 (1:250, Abcam, USA) was added for 1 hour at RT followed by 5 washes with 0.1 % BSA in PBS. Samples were imaged within device and collected using Nikon Eclipse Ti and NIS-Elements AR Microscope Imaging Software (Nikon, USA). Images were processed using *JEX* a software program developed at the University of Wisconsin-Madison and analyzed using RStudio. For blood samples collected in

EDTA tubes no intracellular staining was performed with sample being directly lysed following PMP removal. CTCs were defined as having an intact nucleic, cytokeratin positive and CD45 negative.

Nucleic Acid Extraction

15 µL of nuclease free water was added to both mRNA and DNA extraction wells. Fluid was removed gently from the back sieve well using a pipette until approximately 10 µL of sample was left in the front well. Next, 50 µL of olive oil (Unilever, USA) colored with oil red (Fisher Scientific, USA) for easier visualization was added to the back sieve well. Due to surface tension the olive oil pinned within the back sieve well creating a plug. The plug stops nucleic acids from escaping the front well following cell lysis, where nucleic acid binding to PMPs occurred. 15 µL lysis and mRNA binding buffer (10 mM Tris-HCl, 500 mM lithium chloride , 1 % Igepal® CA-630 (Sigma-Aldrich, USA), 5 mM ethylenediaminetetraacetic acid (EDTA), 5 mM dithiothreitol, pH 7.5) containing 30 µg oligo(dT) Dynabeads® (Life Technologies, USA) was added to the front sieve well. To complete filling of the device, 60 µL silicon oil (Fisher, USA) was added to well connecting sieve and nucleic extraction wells. After 5 minutes, a magnet was used to manually pull olgio(dt) PMPs across the front until the PMPs reached the mRNA output well. Next, 25 µL of DNA binding buffer (10 mM Tris-HCL, 6 M GTC, 0.1 % Igepal® CA-630, pH 7.5) containing 1 µL MagneSil® PMPs (Promega, Madison) was added to the front sieve well. After 5 minutes, the MagneSil® PMPs were transferred to the DNA output well using the permanent magnet. The elution buffers along with PMPs were collected for further downstream analysis.

8.2.6 Cell Capture Efficiency

For quantification experiments LNCaP, DU145 and PC3 cells were incubated for ten minutes with 2 mM calcein AM (Life Technologies, USA) in serum free RPMI media. The cells were centrifuged and washed once in PBS, then counted with a hemocytometer and re-suspended in PBS. Cells were spiked in PBS with 0.1 % BSA and 2 mM EDTA at 1,000 cells per a device. Cells were captured and processed as described above without additional staining.

8.2.7 TaqMan® Reverse Transcription Polymerase Chain Reaction

The mRNA elution sample containing PMPs was reverse transcribed using a High Capacity cDNA Reverse Transcriptase kit (Life Tech, USA) according to manufacturer's directions using Bio-Rad C1000 Thermo Cycler (Bio-Rad, USA). 12.5 µL of the RT reaction was then amplified using TaqMan® PreAmp (Life Tech, USA) according to manufacturer's directions for 10 cycles and diluted 1:5 in 10 mM Tris-HCL buffer. For TaqMan® assays, 5 µL of diluted cDNA template was mixed with 10 µL iTaq® master mix (Bio-Rad, USA), 1 µL TaqMan® Gene Expression Assay (Specified in Table 6, Life Technologies, USA) and 5 µL nuclease free (NF) water. Each reaction was amplified for 40 cycles (denatured at 95 °C for 15 seconds followed by annealing at 60°C for 1 minute) using a CFX Connect® Real-Time PCR System (Biorad, USA).

Table 6-TaqMan® primers and probes

Gene	Life Tech Catalog #
P0	4310879E
AR 1/2	Hs00907242_m1
V1	HUAR_v1
V7	Hs04260217_m1
V567es	Hs04260216_m1

8.2.8 SYBR® Green Reverse Transcription Polymerase Chain Reaction

The mRNA elution sample containing PMPs was reverse transcribed as described above. For SYBR® Green assays, 3.5 µL of cDNA template was mixed with 10 µL SYBR® Green master mix (Bio-Rad, USA), 0.5 µL 10 µM forward and reverse primers (Specified in Table 7, IDT, USA) and 5.5 µL nuclease free (NF) water. Each reaction was amplified for 45 cycles (denatured at 95 °C for 15 seconds, annealed at 60°C for 1 minute, and extended at 72°C for 1 minute) using a CFX Connect® Real-Time PCR System.

Table 7-SYBR® Green primers and probes

Gene	Forward Primer	Reverse Primer
P0	GACAATGGCAGCATCTACAAC	GCAGACAGACACTGGCAAC
AR 1/2	CCATCTTGTCGTCTTCGGAAATGTTATGAAGC	AGCTTCTGGGTTGTCTCCTCAGTGG
V1	CCATCTTGTCGTCTTCGGAAATGTTATGAAGC	CTGTTGTGGATGAGCAGCTGAGAGTCT
V7	CCATCTTGTCGTCTTCGGAAATGTTATGAAGC	TTTGAATGAGGCAAGTCAGCCTTTCT
V567es	CCAAGGCCTTGCCTGATTGC	TTGGGCACTTGCACAGAGAT

8.2.9 Specificity and Sensitivity of Reverse Transcription Polymerase Chain Reaction TaqMan®

Cell dilutions of 100 and 10 cells for R1-AD1 and R1-D567 cell lines were created and mRNA extracted using SNARE as described above. Next, samples were reverse transcribed and TaqMan® RT-PCR assay performed as described above without TaqMan® PreAmp. Raw threshold cycle (Ct) value and relative expression to P0 calculated using the delta Ct method were reported.

8.2.10 Androgen Receptor Ligand Binding Domain RNA Sequencing

Following reverse transcription of mRNA, the AR LBD consisting of exon 5, 6, 7 and 8 was amplified by nested PCR using Phusion Hot Start II High-Fidelity DNA Polymerase (Thermo Scientific, USA) according to manufacturer's directions. The first set of primers forward

(CTTTGCAGCCTTGCTCTCTAGC) and reverse (CCAAGGCACTGCAGAGGAG) was amplified with initial denaturation at 98°C for 30 sec, denature at 98° C for 10 seconds, anneal and extend at 72° C for 20 seconds, which was repeated for 25 cycles with final extension at 72° C for 10 minutes. Following a 1:5 dilution in NF water the second set of primers forward (CAATGAACTGGGAGAGAGACAGC) and reverse (GCCTGTTATAACTCTGCACTA) was amplified using the same settings described above but for 35 cycles. Confirmation of product was performed using the E-Gel® Agarose Gel Electrophoresis system (Life Tech, USA). Samples were sent to the Wisconsin Biotechnology Center where a Big Dye (Life Technologies, USA) reaction was performed and PCR products directly sequenced (ABI 3730xl). Samples were analyzed using ApE (v2. 0.47).

8.2.11 Androgen Receptor Ligand Binding Domain DNA Sequencing

Following enumeration CTCs collected in CellSave® tubes, fluid was gently removed from back sieve well until approximately 10 µL was left. The CTCs were collected and added to 10 µL PKD buffer (Qiagen, USA) and 1 µL proteinase K (Qiagen, USA) for overnight incubation at 37 °C. DNA was then isolated as described above. Each exon of the AR LBD was amplified (primers shown in Supplementary Table 8) as described above for 35 cycles.

Table 8-DNA primers for AR Ligand Binding Domain (LBD)

AR Ligand Binding Domain	Forward Primer	Reverse Primer
Exon 5	ccaacagggactcagacttagctcaacc	gacagtgaagcttagctcatttgatctgc
Exon 6	gggatggcaatcagagacattccctc	gaaaagccagctcctggacatttcc
Exon 7	gtcagaaaacttggtgctttgtctaatgc	gcttctctagagtctggcaccacctgttg
Exon 8	cagaggttggggaagaggctagc	ctctgcactactcctctgcagtgcctt

8.3 Results and Discussion

8.3.1 VERSA Device

Through utilization of the dominance of surface tension over gravity at the microscale, the VERSA device creates virtual walls between immiscible fluids. This forms separate aqueous compartments to replace multiple laborious and time consuming fluid exchanges. By using magnetically actuated PMPs bound to CTCs, we can transfer them across an immiscible barrier leaving behind non-targeted cells. While the VERSA device builds on and incorporates previously developed ESP technologies, its main innovation is integration to extract multiple analytes from a single rare and precious sample (Figure 41).

The first component integrated, the IFAST (described in Chapter 2) demonstrated we could purify cells of interest from a background of non-specific cells without effecting viability[23]. IFAST was then reengineered to a vertical position to incorporate a gravitational settling chamber that enhanced cell purity in a passive process[53]. This new device termed VerIFAST, removed non-specific cells from the magnet's operational path by allowing them to settle (Figure 41.1). The second integrated component, the VerIFAST incorporated a sieve well to allow PMP removal and intracellular staining. The sieve well contained an 8 μm porous membrane dividing the well into a front and back. The membrane allowed low pressure fluid and PMP (2.8 μm) exchanges while preventing larger cells (12-20 μm) of interest from passing through the porous membrane. The fluid exchanges imparted by the sieve well also allowed cellular permeabilization and intracellular staining (Figure 41.2). Another minor technological innovation incorporated into the VerIFAST was the use of oil pinning, which allowed mixing on-chip, preloading of fluids and helped reduce device footprint[86]. The third integrated component

was the SNARE device, which previously demonstrated highly sensitive mRNA and DNA extraction from a single sample. SNARE was incorporated for further CTC molecular interrogation (Figure 41.3). To operate, the back sieve well was plugged with an immiscible fluid to prevent backflow of intercellular analytes when mRNA lysis and binding buffer along with olgio(dT) PMPs were added to the front sieve well. From there, instead of an oil pinning trapezoid, an open oil well was incorporated to allow two separate paths for mRNA and DNA bound PMPs to travel to their respective elution wells. Finally, DNA lysis and binding buffer and silica PMPs were added for DNA isolation and purification. Due to the removal of transfer and wash steps the VERSA greatly simplifies the workflow into one device that is easy to fabricate and use.

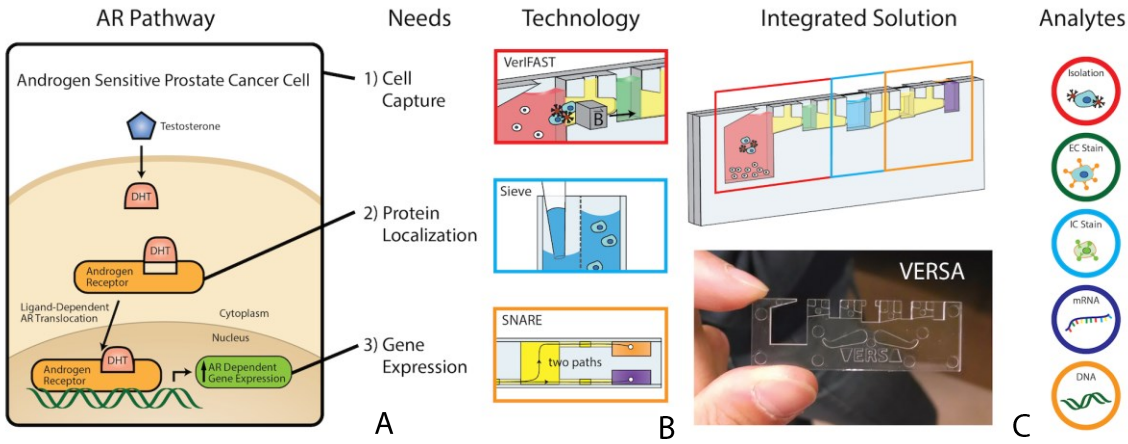

Figure 41-VERSA A) The VERSA integrates an efficient cell capture technique (1-IFAST) with an integrated bead removal and staining well (2-VerIFAST) and a downstream method to capture both mRNA and DNA without dilution steps (3-SNARE). B) Actual VERSA device C) Endpoints enabled in VERSA. Image courtesy of Benjamin Casavant.

With the integration of the previously developed technology into a single VERSA device we can now achieve multiple endpoint analysis assays, including extra and intracellular staining, as well as mRNA and DNA extraction. To demonstrate the importance of integration, Figure 42 shows

more cells were lost if binding occurred off-VERSA, instead of on-VERSA. While the results were not found to be significantly different ($p>0.27$) the removal of an additional pipetting and transfer step helped to further streamLine upstream workflow.

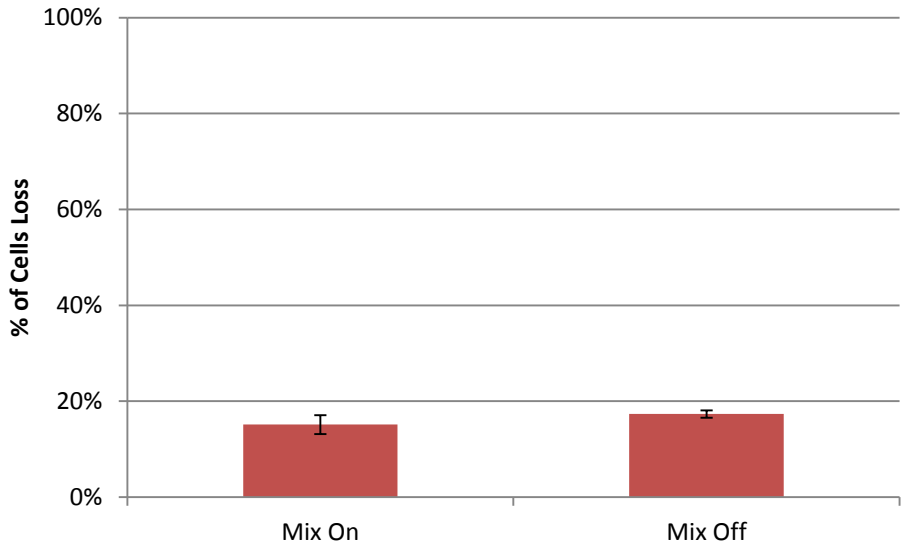

Figure 42-Mixing of cells on and off-device. While there was no statistical difference the integratable nature removed upstream workflow.

Additionally, mRNA extracted from cells on-VERSA showed lower Ct values as compared to samples collected off-VERSA and processed using SNARE (Figure 43). It should be noted that a statistical difference was seen between transferred and non-transferred ($p>0.05$).

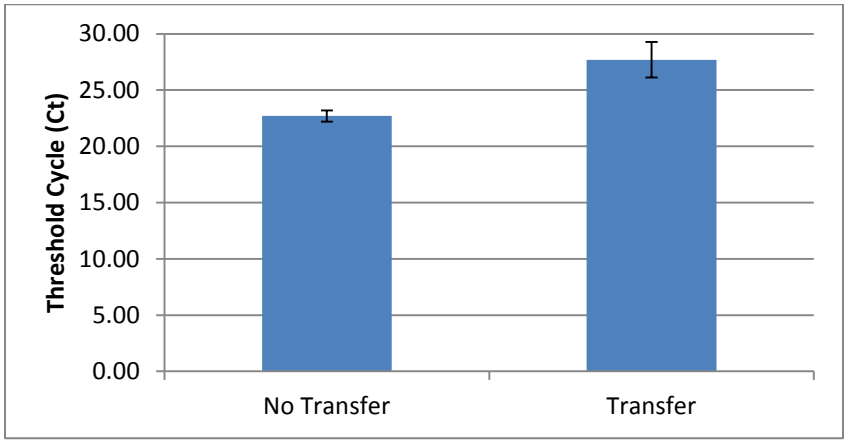

Figure 43-Transfer of cells on and off-VERSA as compared to sample processed directly in SNARE. Data shows that sample transferred is significantly different ($p<0.02$) as compared to SNARE suggesting importance of integration.

While loss of material is inherent in any analytical process the results are more devastating and compounded when starting material is rare. Therefore, the ability to integrate and obtain different types of analytes is of upmost importance when dealing with precious CTC samples.

8.3.2 Cell Capture Efficiency

To validate that VERSA capture efficiency was similar to other capture technologies, different prostate cancer cells lines (LNCaPs, DU145 and PC3) were spiked into the device and quantified. Different prostate cancer cell lines with varying amounts of EpCAM were used as the characteristics of CTCs are not fully define. This allowed us to test the capture efficiency of VERSA when EpCAM expression is either low or high. For LNCaPs, the expression of EpCAM is high with approximately 400,000 molecules per a cell[20] resulting in a capture efficiency of 90±7.7 %. For PC3, the expression of EpCAM is low with approximately 50,000 molecules per a cell[20] resulting in a capture efficiency of 14.2±6.8 % (Figure 44). While in the introduction we showed recovery of PC3 cells near 50 %, the high recovery was found to be due to how

vigorously we pipetted PC3-bound PMPs in the sieve well. Finally, DU145 has a moderate EpCAM expression and result in a capture efficiency of 44.6±5.1 %. This capture efficiency data correlates with other EpCAM capture technologies that report capture efficiencies of 65 % on average across multiple cell lines with varying levels of EpCAM expression[131].

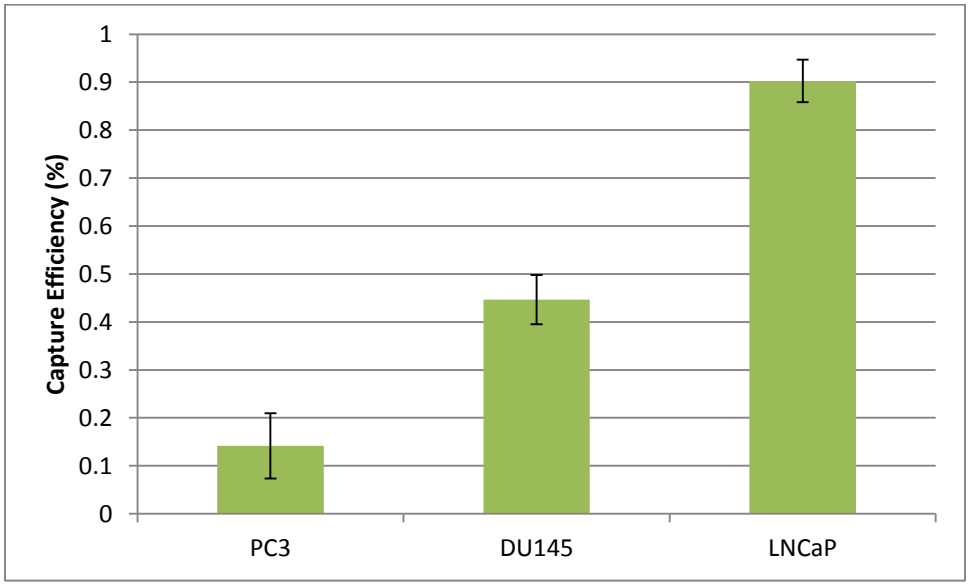

Figure 44-Cell capture efficiency across different PCa cell lines with varying levels of EpCAM expression

8.3.3 AR Nuclear Localization: Manual vs. Automated Imagining Analysis

For AR to enhance expression of downstream PCa tumorgenisis targets it must localize to the nucleus. Therefore, through intracellular staining of the AR, a capability completed within the VERSA, we can quantify AR nuclear localization and intensity, which could serve as a biomarker. Initially, Dr. Benjamin Casavant demonstrated by manual imagining methods the potential predictive nature of AR nuclear localization (Figure 46). However, as manual methods are extremely labor intensive and naturally subjective, we have begun to automate image processing using an in-house developed software program *JEX* with analysis of the raw intensity

data completed in RStudio. Briefly, *JEX* allows us to import multiple images taken of the VERSA sieve well, with each image containing four color channels relating to a specific stain. We stitch these images together and perform background correction, segmentation and thresholding. Using an unique colocalization plug-in we determine the cytoplasm through pan-cytokeration staining and the nucleus through Hoescht staining. By overlaying each pixel determined to be either nuclear or cytoplasm positive with the AR stain we can determine AR localization. This is in contrast to the manual method, in which a ROI of the nucleus and cytoplasm were created and overlaid with the AR stain. Unfortunately, this method was error prone as the cell cytoplasm and nucleus were sometimes difficult to determine.

For validation of the manual versus automated method, two PCa cell lines were treated with Enzalutamide, an AR antagonist, and analyzed for AR nuclear localization and intensity. The first PCa cell line, R1-AD1 has been shown to be sensitive to Enzulatamide[193], however, the second PCa cell line, R1-D567, was genetically engineered to remove exons 5, 6 and 7 comprising the AR LBD. Therefore, as Enzulatamide has no target to act on we would expect it to show no effect. It was shown using both the manual and automated method that AR intensity slightly decreased when R1-AD1 cells were treated with Enzulatamide; however no significant difference was seen. For the R1-D567 cells there was no statistical difference between treated and untreated as expected. Additionally, the error bars using the automated method were tighter suggesting less variation using this technique (Figure 45). Finally, when AR nuclear localization was examined there were no changes in treated and untreated samples. While loss of AR localization was expected when treated with Enzulatamide this has not been reported in the literature and there are several underlying biological mechanisms that could still lead to AR

nuclear localization. To better qualify and quantify AR nuclear localization as a predictive biomarker we will look at a different model system to create a data image analysis validation set. To complete, we will serum starve a PCa cancer cell line, LNCaPs, and treat or not treat with R1881, a synthetic androgen, which has been reported in the literature to cause AR nuclear localization.

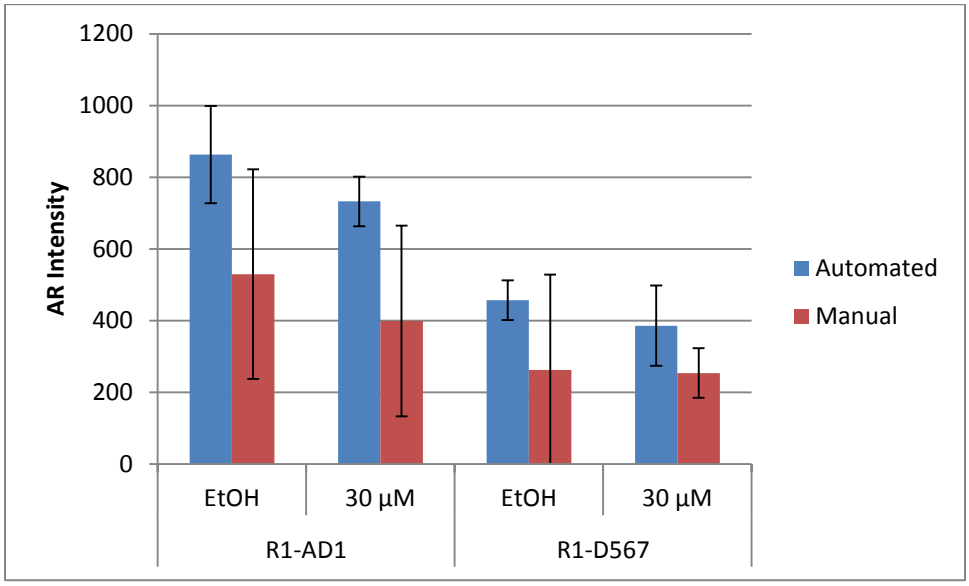

Figure 45-Automated vs. Manual method of AR intensity using PCa cell lines treated or untreated with Enzalutamide, an AR antagonist.

Previously, Dr. Benjamin Casavant used the manual AR analysis method on a small cohort of patients (Figure 46). He demonstrated patients that are responding to various AR-targeting and chemotherapy treatments showed lower percentages of AR within the cell, whereas patients that have progressed on AR-targeting therapies demonstrated high average and maximum AR localized to the nucleus. Further, most CTCs of patients responding to treatment (AR-targeting or broad-range) showed relatively low heterogeneity of percent localization, whereas patients progressing on AR-targeting therapies demonstrated the most heterogeneous

distribution of AR percent localization (Figure 6.2A). Additionally, when each CTC is plotted for total AR intensity and nuclear localization most CTCs exhibit relatively low total AR. Also for patients progressing on AR targeting therapies there is a unique population of cells that do not have much AR (potentially due to the activity of the specific AR-antagonist therapy) but that AR is seemingly highly localized to the nucleus.

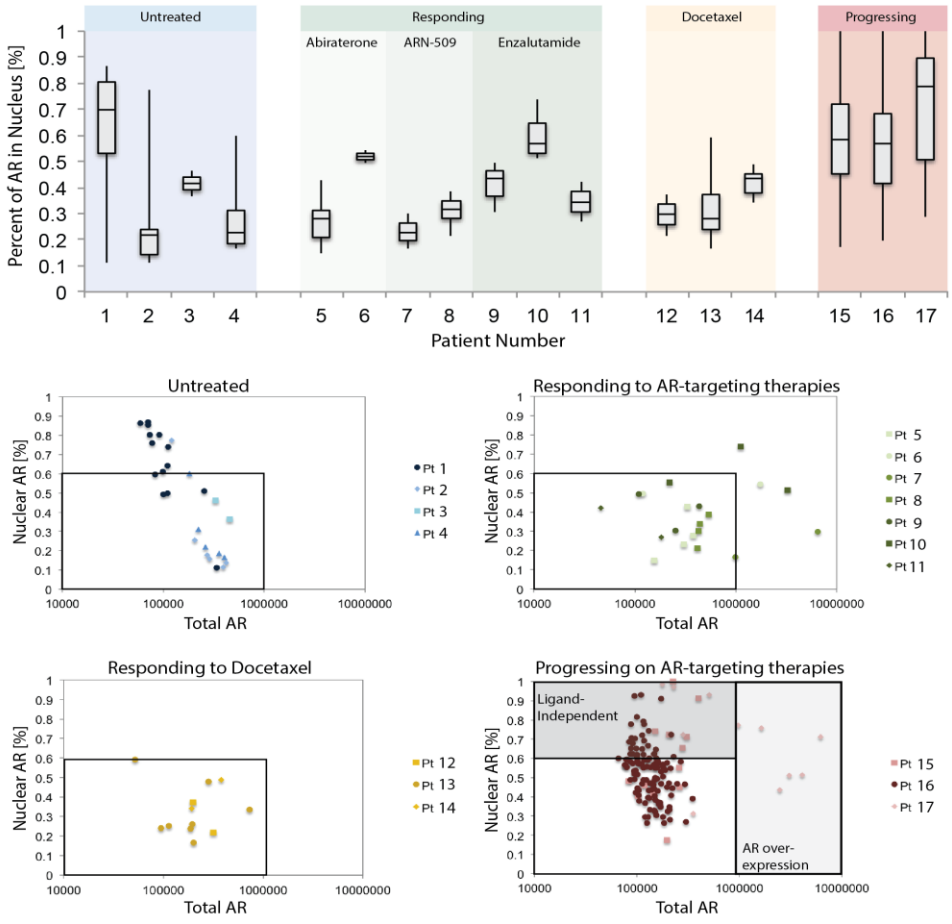

Figure 46-AR total amount and nuclear localization in CRPC patients. A) The percent localization summarizes the 4 patient sets observed. Box plots show average and spread (min to max) of the localization percent within CTCs for each patient. B) Total CTC amount and percent localization were plotted for each patient group. The percentage of cells with low AR expression and low percent localization are able to capture cells in patients that are responding to therapy.

Image courtesy of Benjamin Casavant.

Using the automated image analysis method described previously we are beginning to examine a larger cohort of patients. Unfortunately, there are several bugs and details still being worked out mainly due to dust, which is interfering with threshold calculations that are used to determine CTC positivity. Following completion of the automated CTC image analysis algorithm we will be able to validate it against the manually collected data and start analyzing a larger cohort of patients to determine the potential use of AR nuclear localization and intensity as a predictive and prognostic biomarker. This will be completed by observing patients that have yet to begin AR treatments and following them longitudinally through a treatment to evaluate the predictive value of this observation.

8.3.4 mRNA AR Splice Variants

The VERSA platform enables purification and isolation of mRNA from CTCs, allowing downstream interrogation techniques such as qPCR and RNA sequencing. Here, we probe for AR splice variants in CTCs using qPCR, which represent mutations in the AR that can cause ligand-independent activity and translocation of the AR[194]. AR splice variants are only one possible mechanism of therapeutic resistance and have been found in prostate cancer tumors[195] and metastatic sites[196] but have not yet been reported in the literature within CTCs. We specifically explore AR splice variants reported within the literature, including V1[197], V7[197, 198] and V567es[196] (Figure 47). In addition, Figure 47 shows wild type AR, consisting of the NH_2-terminal domain (exon 1), DNA binding domain (exon 2 & 3) and the COOH-terminal domain, which harbors the ligand binding domain and transcriptional activation function 2 co-regulator binding interface (exon 4-8)[194].

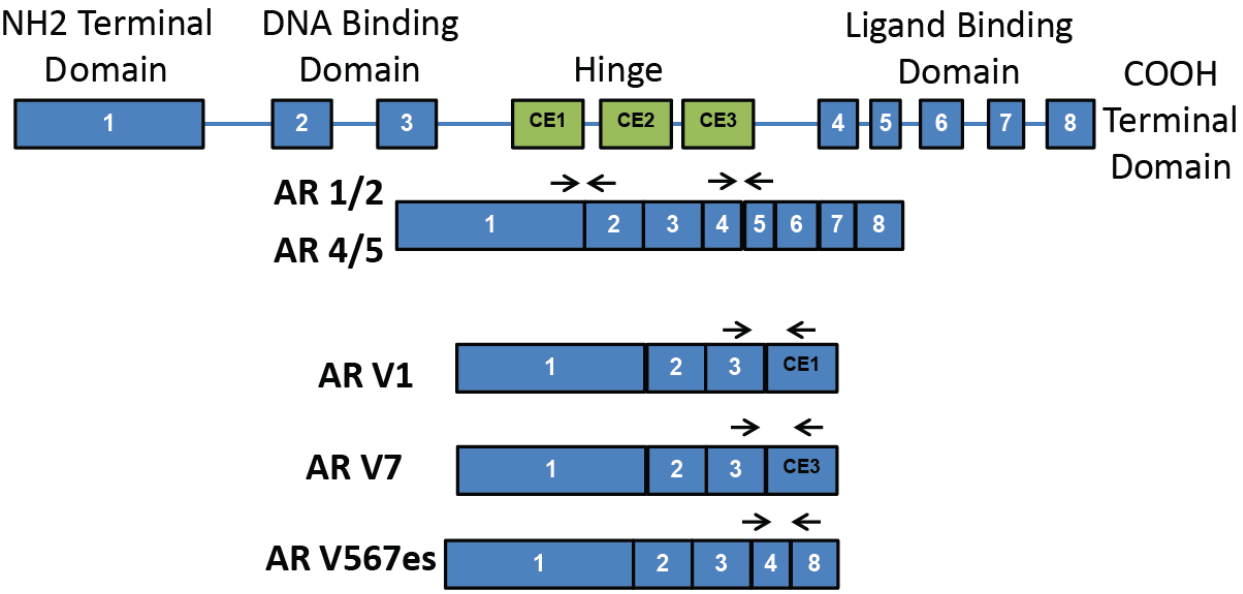

Figure 47–Location of primers used for studies below. Top row shows wild type AR structure. AR 1/2 and AR 4/5 represent full length AR with AR 4/5 not or minimally being detected if AR splice variants present. AR V1, V7 and V567es represent AR Splice variants tested in the following studies.

In order to determine the sensitivity and specificity of VERSA, mRNA was purified and isolated from cell lines expressing the specific AR splice variants (22Rv1: V1 & V7, R1-AD1:V1 and V7 & R1-D567: V1, V7 & 567es). Initially, both TaqMan® and SYBR® Green RT-PCR assays were utilized. While the SYBR® Green assay exhibited greater sensitivity as exhibited by the lower threshold cycle values, the specificity was not acceptable (Figure 48). For example, the R1-AD1 cell line does not express AR V567es but did for all cell dilutions in contrast to the TaqMan® assay. The decrease in specificity of SYBR® Green was expected due to differences in fluorescence chemistries.

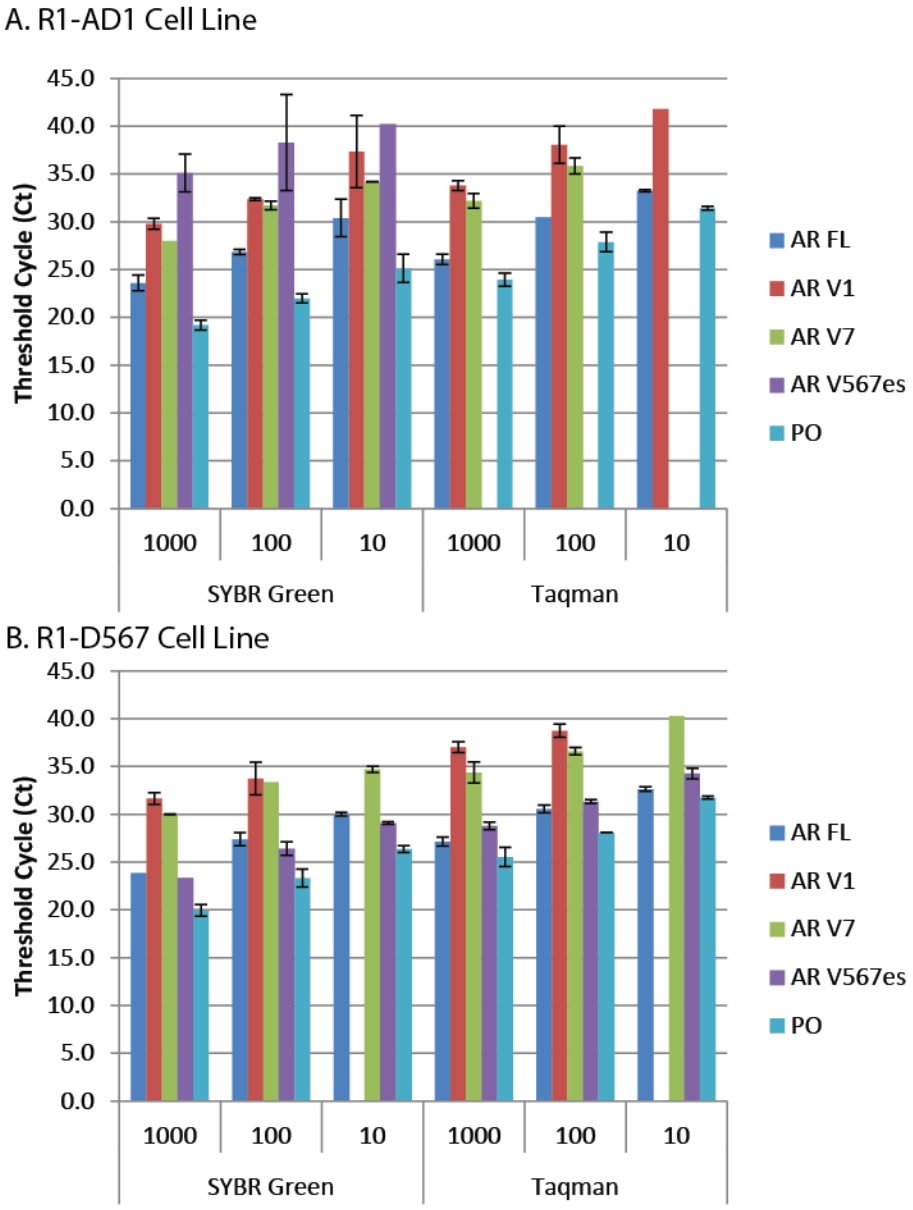

Figure 48-SYBR® Green vs. TaqMan® assay sensitivity and specificity A) Ct values of AR full length (AR 1/2), AR splice variants and housekeeping gene P0 for R1-AD1 cell dilutions (1000, 100 & 10) of SYBR® Green vs. TaqMan®. B) Ct values of AR full length (AR ½), AR splice variants and housekeeping gene P0 for R1-D567 cell dilutions (1000, 100 & 10) of SYBR® Green vs. TaqMan®.

Based on the above data, TaqMan® assays were pursued to determine AR splice variant expression in CTCs. A further TaqMan® assay specificity and sensitivity experiment was pursued using all three cell lines expressing splice variants for 10 and 100 cell dilutions (Figure

49). The same data is also shown as normalized to P0 (Figure 49). It should be noted that AR splice variants V1 and V7 demonstrate low expression in all the cell lines with V7 showing higher expression in 22Rv1. Additionally, when these cell lines were spiked into a background of 5000 PBMCs to simulate live VERSA conditions the specificity and sensitivity remained with no statistical difference seen (data not shown). Unfortunately, when we started testing patient samples we discovered our sensitivity greatly decreased, therefore amplification methods were pursued.

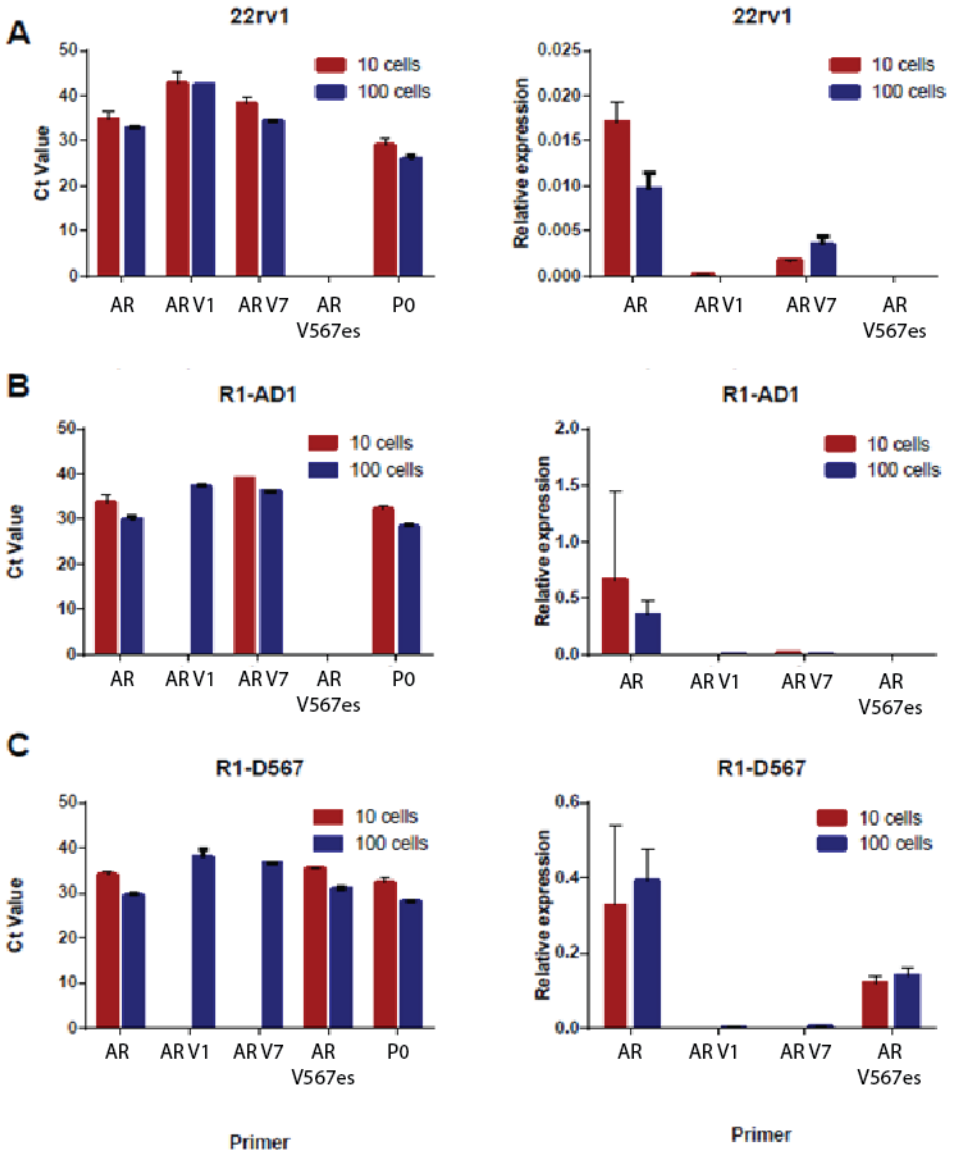

Figure 49-Sensitivity TaqMan® Assay A) 22Rv1 Ct values for AR full length (AR 1/2), AR splice variants and housekeeping gene P0 and relative expression to P0. B) R1-AD1 Ct values for AR full length (AR 1/2), AR splice variants and housekeeping gene P0 and relative expression to P0. C) R1-D567 Ct values for AR full length (AR 1/2), AR splice variants and housekeeping gene P0 and relative expression to P0.

Three different amplification methods were pursued. The first, Qiagen QuantiTect Whole Transcriptome kit, converts mRNA to cDNA, ligates the cDNA and performs isothermal

multiple displacement amplification (MDA). Using this kit we saw a preference for amplifying highly abundant transcripts and therefore did not pursue it further (data not shown). Secondly, the Nugen Ovation® Pico WTA system, which uses less starting mRNA template (500 pg) was pursued. Following cDNA synthesis the Nugen kit employed single primer isothermal amplification (SPIA), which used DNA/RNA chimeric primers, DNA polymerase and RNase H. Using this kit we found a bias towards the 3' end and given the cost of an assay, approximately $100 dollars per a sample, this kit was also not pursued further (Figure 50). Finally, we tried TaqMan® PreAmp, which amplifies cDNA targets using AmpliTaq Gold® DNA polymerase. The cost per a sample was $30 dollars and was shown to increase the sensitivity without introducing bias (Figure 50) as determined by comparison with an unamplified sample. Using a non-prostate cancer cell line as a negative control, no amplification of any AR splice variant was seen suggesting specificity of assay (data not shown).

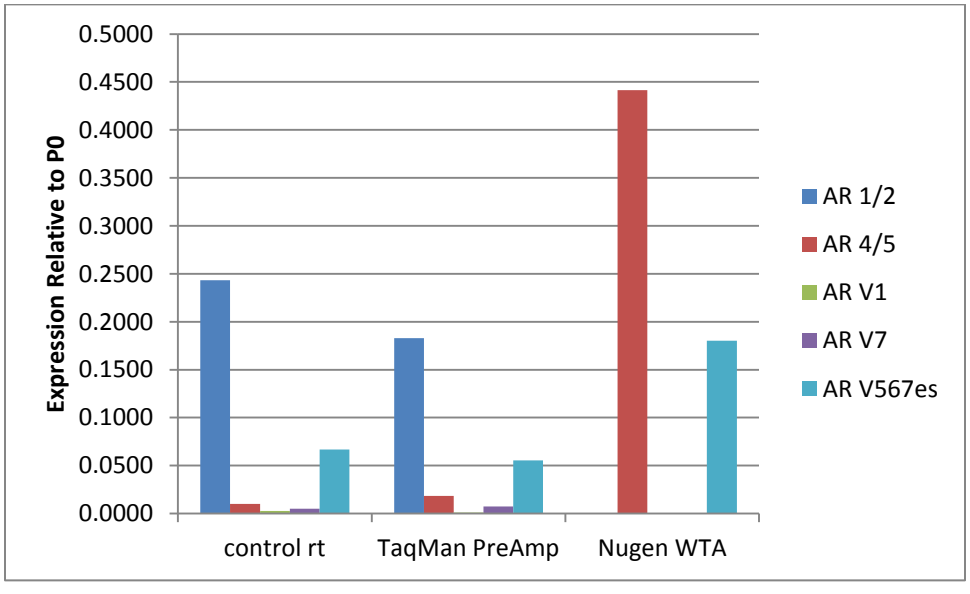

Figure 50-Comparison of TaqMan® PreAmp, Nugen Ovation Pico Kit and no amplification. TaqMan® PreAmp shows unbiased amplification as compared to non-amplified sample, whereas Nugen Ovation Pico Kit does not.

Finally, small cohorts of patients were tested for AR splice variant, cytokeratin and EpCAM expression (Figure 51). Currently, the data shows expression of full length AR but no splice variants. It is important to note that no EpCAM expression was seen but cytokeratin expression was. The data suggests several potential possibilities as to why AR splice variants are not being seen. First there is the potential that the patients are not expressing any AR splice variants; however other groups have started reporting seeing expression of them in CTCs but the data has not been published. Secondly, the higher cytokeratin expression does show we are enriching for CTCs of epithelial origin but could potentially be missing cells undergoing EMT that are more likely to have metastatic potential. Thirdly, no EpCAM expression could also mean the cells are apoptosing. Finally, the data suggests potential problems with the assay, including problems with RNA degradtion, no CTC capture, low mRNA extraction efficiency and qPCR sensitivity issues. Continued work to access these potential problems is ongoing.

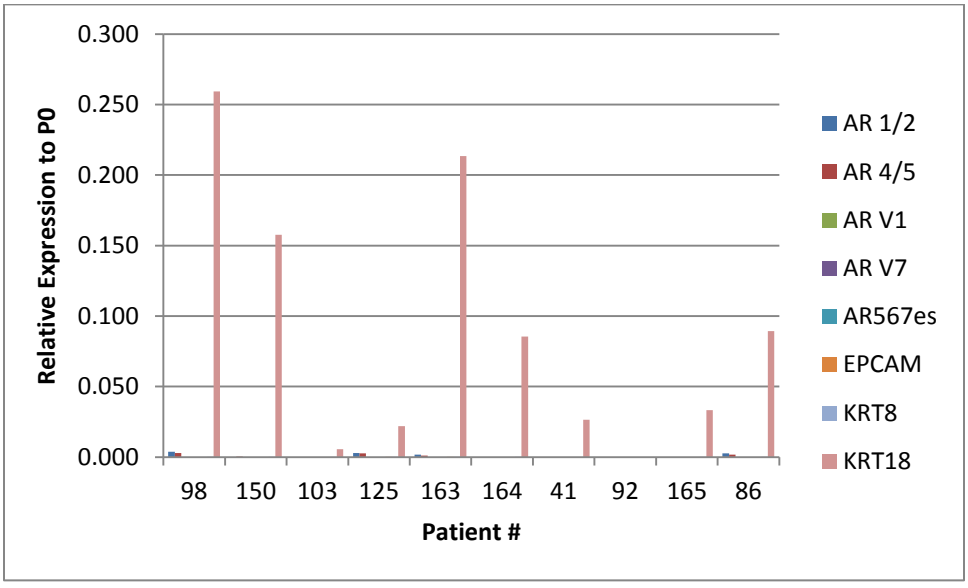

Figure 51: AR splice variant, cytokeratin and EpCAM expression in CTCs isolated from CRPC using VERSA

8.3.5 DNA AR sequencing

Finally, within the VERSA we can isolate and purify DNA from the CTCs for additional downstream assays. Here, we pursued DNA sequencing that is heavily reliant on the purity of the sample as we cannot differentiate background PBMC DNA. In the VerIFAST, fixed cells were processed in a background of PBMCs and carryover PBMCs was determined to be between 100-1000 cells; however, when live patient samples were processed the carryover PBMCs greatly increased to 1000-25,000. Several strategies were pursued to increase the purity of live samples; including, Fc blocker, negative CD45 selection, etc. Throughout testing it was determined that PBMCs bound either non-specifically to PMPs or were phagocytizing the PMPs as several additional wash steps never removed these background PBMCs. It was found that a negative CD45 selection step before VERSA processing reduced the PBMC carryover (Figure 52) without significantly increasing the cost of the assay.

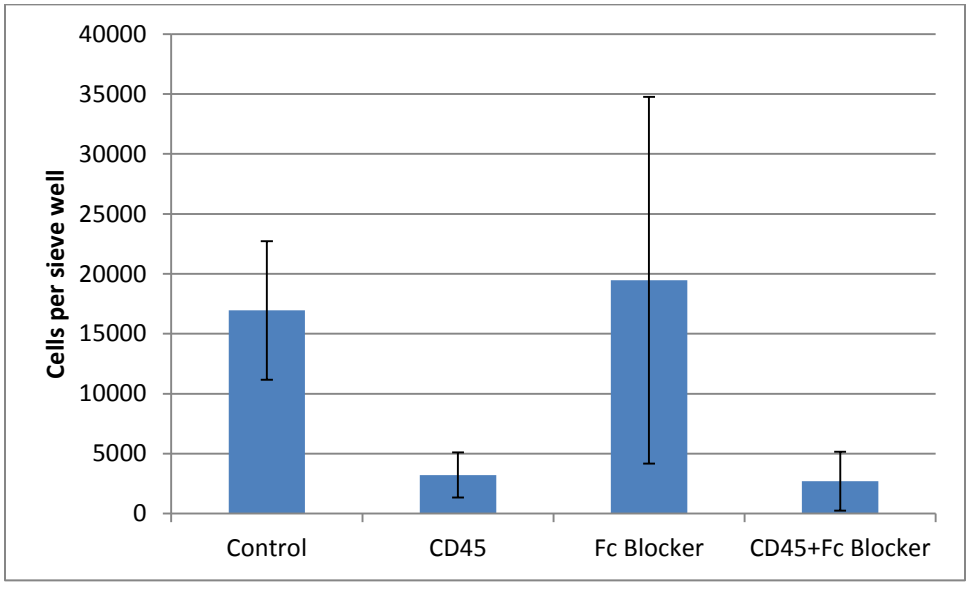

Figure 52-Background PBMCs per a VERSA device when CD45 PMPs (utilized for negative selection of PBMCs), Fc blocker and combination of CD45 PMPs + Fc blocker are used. Results show CD45 and combination significantly reduce background PBMCs.

In Figure 53, 1000 green cell tracked LNCaP cells were spiked into a background of PBMCs and captured cells counted. No significant loss of CTCs was shown with the addition of this CD45 negative selection step (Figure 53).

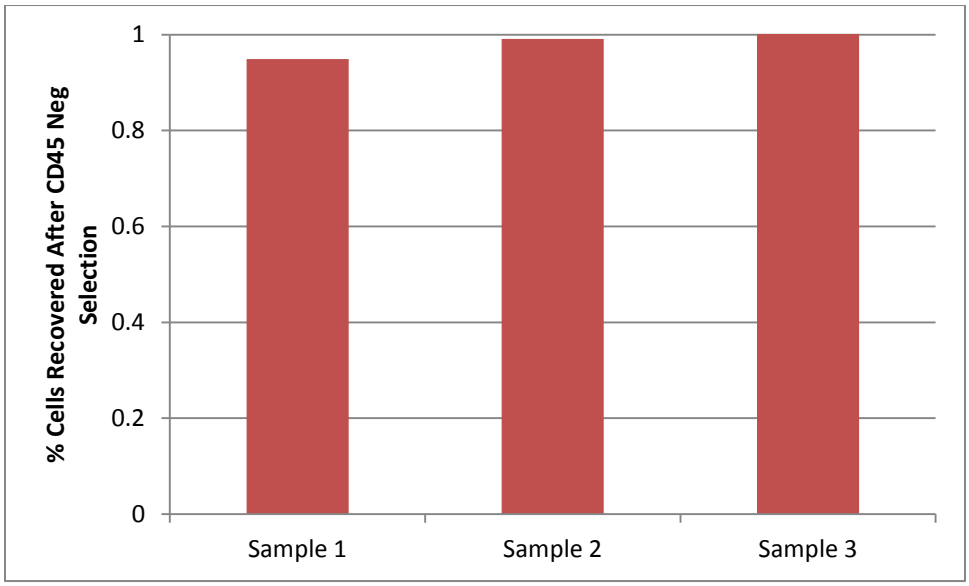

Figure 53-LNCaPs recovered when spiked into a background of PBMCs and CD45 negative selection performed across 3 different samples. Results show little loss of cells when a CD45 negative selection method is appended.

Additionally, to determine the main population of PBMCs causing background contamination, the isolated and purified patients CTCs were collected from the sieve well. The cells were then stained for various white blood cell markers and run through FACS. The main population of contaminating cells was shown to be monocytes and macrophages (data not shown) as previously reported in the literature[199]. This information could be leveraged in the future to help increase purity by using PMPs targeted to these specific PBMC populations.

Given the difficulty in isolating a pure population of CTCs with live patient samples we turned towards isolating DNA from fixed patient samples. For proof of principle we isolated and purified DNA using VERSA from 100 live and fixed LNCaP cells. For fixed LNCaP cells, we

used heat and proteinase K to reverse the crosslinks created from using paraformaldehyde to fix samples. Figure 54, shows that live samples had the lowest Ct value suggested best DNA capture and purification efficiency; however fixed samples processed resulted in a lower threshold cycle value then samples not processed. While the data suggests the potential to use fixed DNA from CTCs, the assay does not provide any relevant biological information.

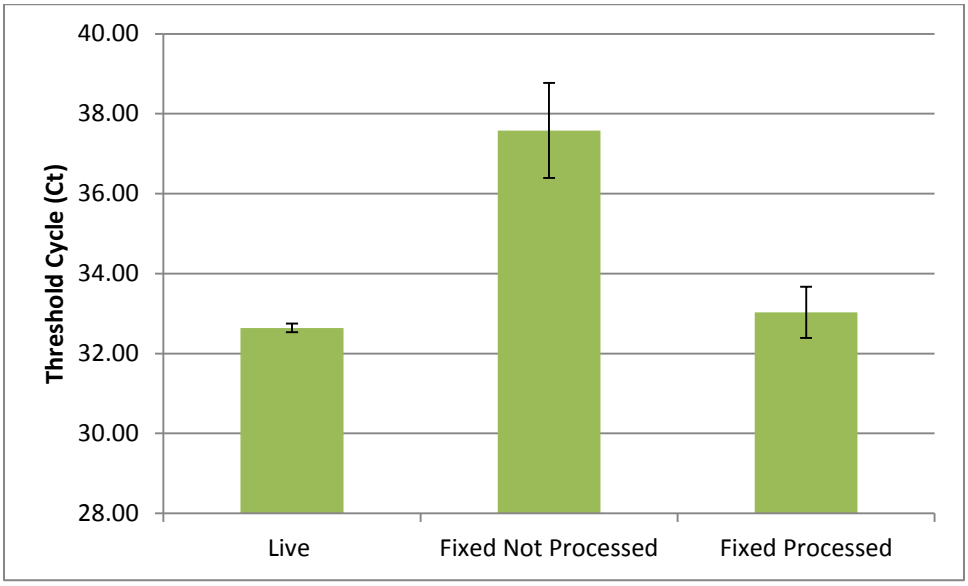

Figure 54-GAPDH DNA Threshold Cycle (Ct) value isolated from 100 LNCaP cells using VERSA. Samples were either live or fixed processed (proteinase K & heat) and unprocessed (no proteinase K & heat).

Therefore, we started pursing DNA sequencing of the AR ligand binding domain to search for mutations. For proof of principle, we isolated DNA from 100 LNCaPs in a background of 100 PBMCs and amplified exon 8 of the AR to search for a known mutation, T887a, using Sanger sequencing (Figure 55). The mutation was discovered but when the LNCaP cell number was reduced to 10 cells the mutation could no longer be seen. In a small cohort of patients, exon 5, 6, 7 and 8 of the AR ligand binding domain was amplified and sequenced. All chromatograms of

patient samples showed wild type AR with no mutations seen. For next generation sequencing, it is estimated that 50 % purity is needed from a sample to analyze.

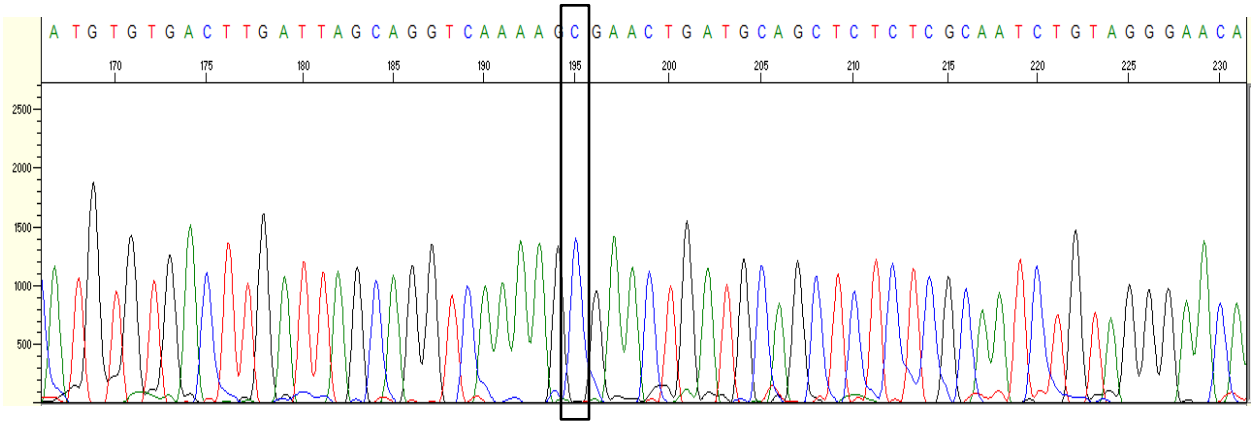

Figure 55-Chromatogram of exon 8 from AR extracted from 100 LNCaPS in a background of 100 PMBCs. A known mutation, T887a, was seen.

Given the current difficultly of obtaining a pure sample and the probability of seeing a mutational event through Sanger sequencing other methods must be pursued.

8.4 Conclusions

To fully understand a pathway that is a highly valuable therapeutic target one must be able to interrogate CTCs at the genomic, transcriptional and translational level. The VERSA platform represents a streamLined workflow and operational process that enables CTC enumeration, extra and intracellular protein analysis, as well as mRNA and DNA extraction. While this can be done on biopsies they are difficult to obtain and cannot be accessed frequently overtime. While we have just begun to access the full range of analytical endpoints demonstrated in Table 9 below, it begins to show the information we can obtain. We will continue to use the VERSA to access the multiple endpoints we discussed to begin to access their potential as a prognostic and predictive biomarker.

Table 9-Comprehensive patient analysis of the AR Two patients with CRPC are evaluated for AR localization, total AR amount, and analyzed for the expression of AR splice variants.

Patient	Age	Gleason Score	PSA	Disease Status	AR+ CTCs	% Nuclear AR Median	% Nuclear AR Min	% Nuclear AR Max	RNA Splice Variant
45	55	4+5	228	CRPC-Progressing on Abiraterone	11	76%	29%	100%	Full Length AR Exon 5 Mutation
71	64	3+3	6.93	CRPC-Post Chemo and Orterenol	5	41%	21%	79%	Full length, V1 and V7

8.5 Future Directions

We will continue to incorporate VERSA into several ongoing clinical trials to extract CTCs and their biological information for identification of potential prognostic, predictive and pharmacodynamics biomarkers. We are also currently expanding VERSA into other cancer types including renal cancer and melanoma. Currently, VERSA is performed manually which is valuable for labs in need of a cost effective device to isolate CTCs, however repeatability and robustness can be difficult to obtain, especially from operator induced variance. Therefore, we have begun the process of automating the VERSA platform. Shown below in Figure 56 is the current embodiment we are pursuing for automation using an existing standard robotic liquid handling instrument (Pipetmax, Gilson). Automation will be critical to achieve sufficient robustness and reproducibility needed for CLIA lab certification and thus FDA approval. Without CLIA certification VERSA cannot begin to be used for CTC biomarker qualification that could eventually effect clinical decisions and thus patient care.

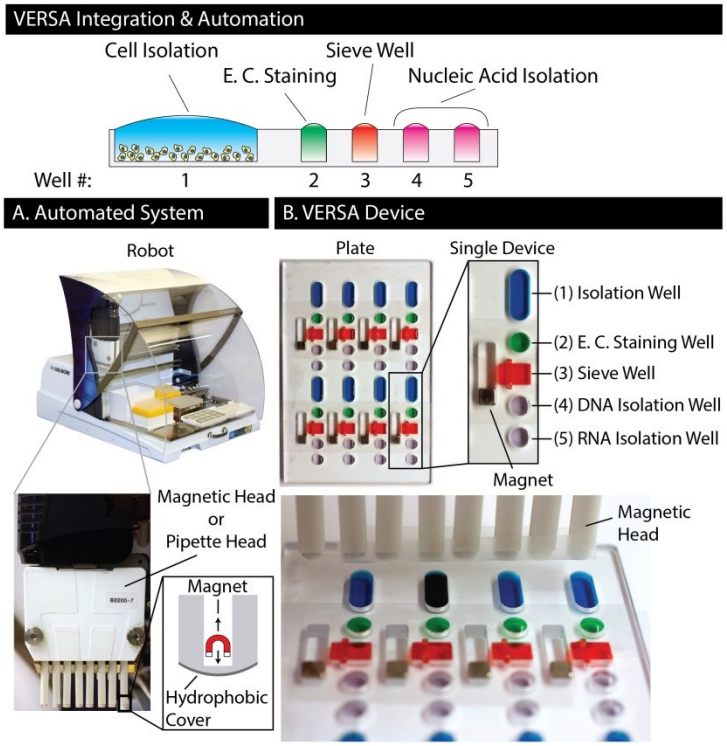

Figure 56-Side View of Automated VERSA A) Gilson PipetMax robot with magnet head attached to pipette head. B) Array of automated VERSA devices

8.6 Acknowledgements

I would like to specifically thank Ben Casavant for being a team partner throughout the past few years and with helpful brainstorming and discussions. I would also really like to thank Jamie Sperger for all the help with the experiments performed in this section and helping to teach me her knowledge of designing nucleic acid assays. Finally, I would also like to thank both David Beebe and Josh Lang for giving me a chance to pursue my ideas and helping me move them forward. This work was supported by a grant from the Bill & Melinda Gates Foundation through the Grand Challenges in Global Health initiative, NIH Grant #5R33CA137673, NSF GRFP DGE-0718123, a UW Institute for Clinical and Translational Research-Type 1 Research Pilot Award, UW Carbone Cancer Center Investigator Initiated Pilot grant and a Prostate Cancer

Foundation Young Investigator award to Dr. Lang. David J. Beebe holds equity in Salus Discovery, LLC, Bellbrook Labs, LLC and Ratio, Inc.

Chapter 9 Appendix – Development of Primary Murine Fetal Leydig Cell Culture

9.1 Introduction

It has been over sixty years since the discovery that the testis provided resources responsible for the perpetuation of the Wolffian duct and secondary sex characteristics in male embryos[200]. Since then, we have learned that testosterone is the primary androgen necessary to masculinize the brain, maintain the Wolffian duct system, and facilitate proper formation of the internal and external genitalia in mammalian male fetuses. Complete disruption of androgenic activity results in feminized external genitalia and brain, and nonfunctional internal genitalia. Although such extreme cases are rare, some of the most common birth defects are caused by subtle deficiencies in masculinization, including hypospadias and cryptorchidism[201]. Disorders of masculinization are attributed to abnormal fetal androgen synthesis or activity, and are increasing at an alarming rate in industrialized countries exposed to widespread use of endocrine disruptors, suggesting a causal link. Unfortunately, our understanding of mechanisms giving rise to deficiencies in androgen production or activity during fetal development has been severely limited by the lack of appropriate experimental models. Our progress towards an understanding, diagnosis, and treatment or prevention of these disorders would greatly benefit from experimental tools to study androgen-producing cells during development within the fetal testis.

Both fetal and adult testes produce testosterone; however, the source and regulation of steroid synthesis differs depending on life stage. In the adult testis, testosterone is synthesized within the interstitial Leydig cell under control of luteinizing hormone and the hypothalamic-pituitary-gonadal axis. Adult Leydig cells originate from undifferentiated mesenchymal-like

stem cells shortly after birth and progress through distinct stages of development to produce terminally differentiated cells that generate high levels of testosterone[202]. The current view is that adult Leydig cells arise as a distinct population from fetal Leydig cells; however, it is hypothesized that adult and fetal Leydig cells both originate from common precursor cells[203-205].

In contrast to the adult Leydig cell, the onset of fetal Leydig cell androgen synthesis is gonadotropin-independent [206-208]. Increasing numbers of fetal Leydig cells appear within the mouse testis interstitium approximately twenty-four hours after Sertoli cells differentiate and initiate expression of the morphogen, Desert hedgehog (*Dhh*)[207, 209, 210]. The numbers of fetal Leydig cells increase dramatically between embryonic day 12.5-15.5 in the mouse; however, they do not proliferate during this time[211, 205, 212, 213]. Instead, their expanded numbers have been attributed to differentiation of progenitor cells that have migrated into the testis from the coelomic epithelium and the gonad-mesonephros border[211, 214, 215, 216, 217]. Recent studies suggested that fetal Leydig cell numbers and activity are initially controlled by a balance between DHH stimulatory and Notch inhibitory signals that act upon a population of interstitial cells that express Steroidogenic Factor 1 (SF1)[218 217, 219, 220].

Another distinction of the fetal Leydig cell is that they do not synthesize testosterone on their own. While adult Leydig cells express all steroidogenic enzymes required for testosterone synthesis, fetal Leydig cells produce androstenedione, which must be converted to testosterone by 17ß-hydroxysteroid dehydrogenase-type 3 (HSD17B3) activity that is expressed exclusively within fetal Sertoli cells[221, 222]. In sum, maintenance and regulation of fetal Leydig cell identify and steroidogenic activity is extremely complex and includes interactions with Sertoli cells and

neighboring interstitial cells that may include peritubular myoid, endothelial, perivascular, and inflammatory cell types[217, 220].

Adult Leydig cell biology has been extensively characterized due to the availability of established methods to isolate and purify primary cell cultures, and relevant immortalized cell lines [223-226]. In contrast, significant barriers limit our ability to study fetal Leydig cells: 1) their small population size; 2) their rapidly changing biology within developing testes; and 3) the lack of fetal Leydig cell lines. Here we report a genetic approach that utilized two commercially available strains of mice that facilitated isolation of fetal Leydig cells from developing testes. To overcome the problem of working with a small cell population, we developed microfluidic channel devices that enabled high cell density culture conditions. A key feature of the platform is the ability to compartmentalize small populations of cells in controlled microenvironments that can better reflect physiological conditions and enable cell-cell interaction studies. To that end, we measured testosterone synthesis as an indicator of fetal Leydig cell activity in microchannels that contained either a mixture of all testicular cells to allow direct cell-cell contacts or in co-culture devices that physically isolated fetal Leydig cells from remaining testicular cells, but allowed shared media between cell populations. Our results show that fetal Leydig cells can facilitate testosterone synthesis whether they are in direct or indirect contact with other testicular cells. Isolated fetal Leydig cells make androstenedione whereas mixed testicular cells fail to make androgens without the presence of fetal Leydig cells. In summary, we present new tools that facilitate study of the fetal Leydig cell population and enable the technology to discover molecular targets of fetal testis steroidogenesis so that we may prevent and treat disorders of masculinization that impact both fetal and adult male health.

9.2 Materials and Methods

9.2.1 Mice

Two strains of mice were crossed in order to produce the appropriate recombinant pups. The first of these strains was an mT/mG double fluorescent reporter mouse[227]. These mice contain a floxed membrane-targeted tomato red marker linked to a stop signal that precedes a membrane targeted green fluorescent protein gene. When Cre recombination occurs this GFP protein will be expressed. The second mouse used was a Cre recombinase strain with a Cyp11a1 promoter. Because Cyp11a1 is expressed specifically in steroidogenic cells, we were able to specifically marked fetal Leydig cells. Mice were housed together and the checked regularly for vaginal plugs. If present, this was designated as embryonic day 0.5 (E0.5). Gonads of the embryos were harvested on the appropriate days between E13.5 and E16.5 when testosterone production is on the rise in the gonads. Samples for immunohistochemistry were fixed in a 4% paraformaldehyde solution for several hours and later kept in PBS. After viewing the harvested gonads under a fluorescent microscope, gonads were put into frozen blocks and sectioned.

9.2.2 Immunohistochemistry

Gonads of the embryos were harvested on E13.5 and E16.5 to compare efficiency of the Cre recombinase. Samples for immunohistochemistry were fixed in a 4% paraformaldehyde solution overnight and placed in paraffin blocks for sectioning. To colocalize the endogenous GFP with a known fetal Leydig cell marker, the primary antibodies used were a rabbit anti-3BHSD and a rabbit anti-GFP biotinylated antibody. Secondary antibodies included a FITC anti-rabbit and an anti-biotin antibody.

9.2.3 FACS

Gonads were harvested from embryos between E13.5 and E15.5 when testosterone levels are rising in the gonad. The gonads were then dispersed using 250 µL of the following mixture: 1mL total volume containing DMEM, 125 µL type 1 collagenase, 100 µL FBS, 10 µL pen/strep. Cells were then incubated for one hour at 37 °C. Finally the dispersed cells were submitted to fluorescent activated cell sorting on the BD Biosciences FACSAria II SORP.

9.2.4 Quantitative RT-PCR analyses

Isolation of mRNA was accomplished using TRIzol Reagent after submitting cells to FACS. The amount of reagents used in the RNA isolation protocol were modified to adjust for such a small population of cells. cDNA was then synthesized using reverse transcriptase Superscript protocol (Invitrogen) and oligo(dT) (Promega). Power SYBR® Green quantitative PCR mix (Applied Biosystems) was then used to complete the QT-PCR. Primers used include VASA, SF1, 3BHSD, CYP 17, SOX9, MIS, and DHH.

9.2.5 Monoculture and Coculture Channel Fabrication

Both monoculture (2x3) and coculture (3x3) device arrays consisted of three layers of polystyrene (PS, Goodfellow, UK). The top layers enclosed the channels and provided through holes for pipette tips to fit for loading cells, changing media and allowing oxygen permeation. Both top layers were CNC (PCNC770, Tormach, USA) milled from 0.125 mm thick polystyrene. The middle layers consisted of channels that were milled from 1.2 mm thick polystyrene. The coculture channel had a specific diffusion port, 100 µm in length and 50 µm in depth, located at the top of the middle layer between the horseshoe ring and center channel. The diffusion port created a physical separation between both the TmRed and GFP cell populations while still

allowing paracrine signaling. Finally, the bottom layers were simply a 0.125 mm thin polystyrene layer with no additional fabrication. Thermal bonding was used to bond the layers. Briefly, the bottom layer, middle layer and top layer were stacked and aligned. Next, acetate, COC (Topaz) and a silicon sheet were layered on top of the devices to distribute pressure and limit channel collapse. The devices were pressed (XX) together at a pressure of 3000 lbs for 40 minutes at 90 °C. Finally, monoculture and coculture devices were plasma treated (XX) for cell culture and device sterilization.

9.2.6 Cell culture

After harvesting gonads between E13.5 and E16.5, the whole gonad, including the mesonephros was dispersed as previously described. Mixed cell cultures were plated at a cell density of 25,000 cells/15 µL well based on studies we performed. Media consisted of DMEM with 10% FBS and 10 µL Pen/Strep and was collected every 24 hours and stored at -20°C. For the coculture systems, cells were dispersed, submitted to FACS, counted and then plated. mT positive cells, which consisted of the stromal and others, were seeded at a concentration of 21,750 cells/10 µL in the horseshoe ring. And mG positive cells, which consisted of the Leydig cells, was seeded at a concentration of 500 cells/5 µL in the center channel.

9.2.7 Testosterone ELISA

Both monoculture and coculture channels were treated with and without hCG, which increases testosterone production. Media was collected from each of the mono and coculture channels each day and replaced with fresh media. Testosterone was measures using an ELISA (Life Tech, USA) and detected using a spectrophotometer.

9.3 Results and Discussion

9.3.1 Mouse Model

The Jorgenson lab developed a mouse model to achieve GFP (mG, green) expression specific to steroidogenic cells with all non-steroidogenic cells expressing Tomato Red (mT, red). The model was created crossing a Cyp11a1-Cre and mT/mG reporter mice. Figure 57A shows fluorescent images of only the mT expressing cells for both the adrenal and fetal testis of the mouse model. Figure 57B shows the steroidogenic cells expressing mG for both the adrenal and fetal testis of the mouse model. Figure 57C overlays the two, to demonstrate that the fluorescent is specific to the steroidogenic producing cells.

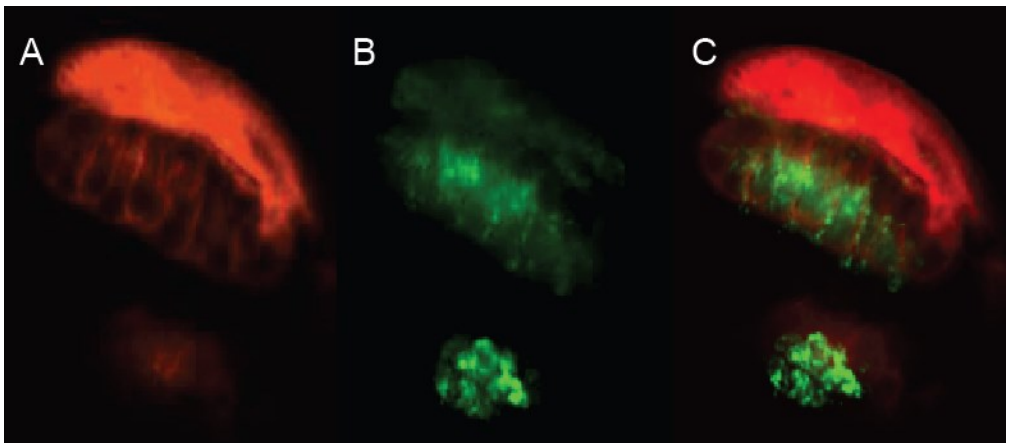

Figure 57-Cyp11a1-Cre and mT/mG reporter mice were crossed to achieve GFP (mG, green) expression specific to steroidogenic cells. Fetal testis (above) and adrenal (below) were harvested at E13.5 and imaged live. A) Cells initially express Tomato Red (mT, red) B) Cre-recombinase activity facilitates cell-specific excision of mT to promote mG expression in fetal Leydig cells of the testis and cortical cells of the adrenal. C) Merged image demonstrates mG+ steroidogenic cells surrounded by mT+ cells.

The specificity of the mG being associated with the steroidogenic cells was further confirmed using RT-qPCR. Following flow sorting of the mT and mG into separate populations, the RNA was extracted and examined for specific expression of known Sertoli and fetal testis specific

genes. Figure 58A shows the mG cell population upregulated specific genes (Sf1, Cyp17 and Hsd3b) associated with fetal Leydig cells and mT cell population did not. Figure 58b shows that the mT cell population upregulated specific genes (Sox9, Dhh and Mix) associated with Sertoli cells and the mG cell population did not. These data combined with the fluorescent images confirms that the mG cell population is the steroidogenic producing fetal Leydig cell population.

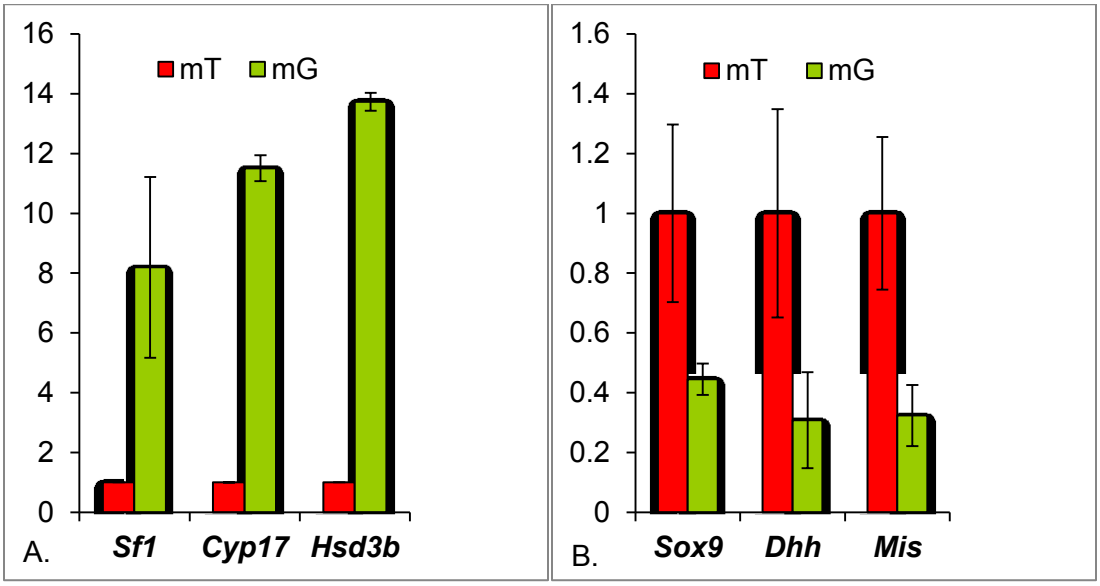

Figure 58-Isolated mG+ cells express fetal Leydig cell-specific transcripts: mG and mT cells were separated by FACS for RNA harvest and qPCR analysis. A) Fetal Leydig cell-specific transcripts were enriched and B) Sertoli cell-specific markers were decreased

9.3.2 Monoculture & Coculture Channels

Currently, there are no fetal Leydig cell line models and few methods for culturing fetal Leydig cells exist due to their limited cell numbers. Microfluidic cell culture systems can meet this need as they require limited cells per a channel, allowing multiple channels to be seeded. Here, we utilized microfluidics to create two different devices, a monoculture and coculture channel arrays (Figure 59). The monoculture channels allowed for both Sertoli, other cells and fetal Leydig cells to be cultured in direct contact (Figure 59A). The coculture channels allow for

both the Sertoli and other cells to be cultured with no direct contact with the fetal Leydig cells (Figure 59B). However, a diffusion channels was designed allowing paracrine signaling between the different cell populations. By separating these two populations we can begin to examine biological mechanisms that lead to differentiation of the fetal Leydig cells during development.

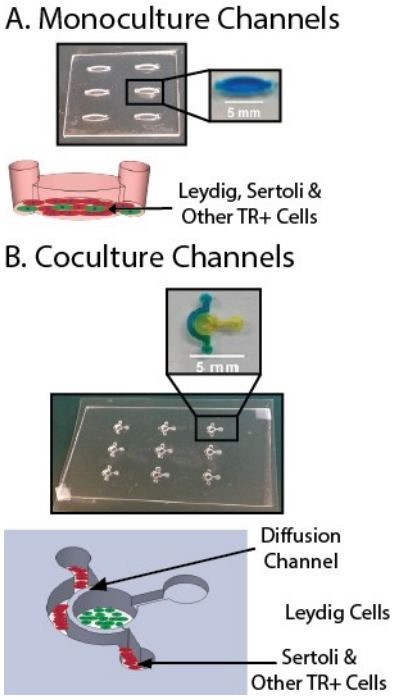

Figure 59-A) Monoculture device array with an exploded view of a single channel. Both fetal Leydig, Sertoli and all other mT positive cells were seeded and cultured in one channel. Cells were not separated using FACS B) Coculture device array with an exploded view of a single channel. Following FACS sorting, fetal Leydig cells were seeded and cultured in the center with Sertoli and all other mT positive cells seeded and cultured into the horseshoe ring. No direct contact was made but a diffusion port allowed paracrine signaling.

9.3.3 Testosterone Measurements

For both monoculture and coculture channels testosterone was measured on days 2, 3, 4 and 5. hCG treated channels showed increased testosterone measurements as expected compared to untreated channels (Vehicle) (Figure 60). Testosterone measurements showed similar concentrations at the same time points with testosterone concentrations decreasing each day

(Figure 60). The ability to measure testosterone in both monoculture and coculture channels shows their ability to be used as tools for researchers; in order, to start accessing questions surrounding fetal testis development.

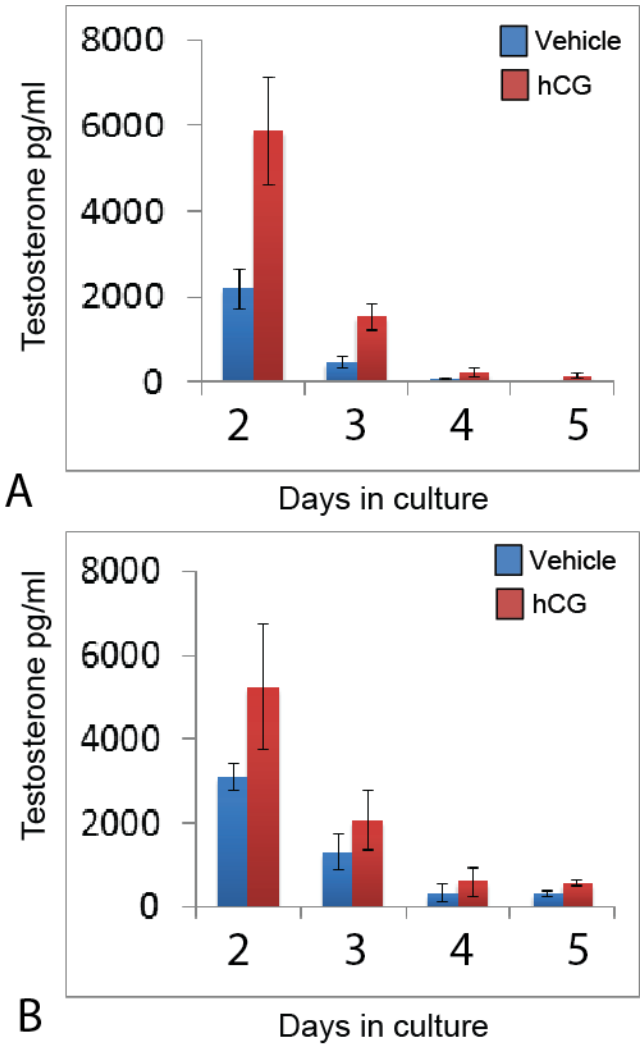

Figure 60-Testosterone Measurements A) Monoculture of hCG and non-hCG channels with hCG increasing testosterone production but decreasing overtime B) Coculture shows similar testosterone concentrations as compared to monoculture.

9.4 Conclusions

In conclusion, using a mouse model in which steroid producing cells fluorescence green and every other cell tomato red we were able to separate the two populations using FACS. We specifically focused on mouse fetal testis were we either cultured them in microfluidic platforms using either a monoculture or coculture platform. These platforms allowed us to culture fetal Leydig cells either through direct or indirect contact with other testis cells, which could be used to determine the necessary mechanisms of fetal Leydig cell development. Finally, we showed that fetal Leydig cells could produce testosterone up to five days in culture suggesting their ability to maintain functionability. Based on the ground work laid we believe this platform, which uses limited cells could help to access fetal Leydig cell developmental biology.

9.5 Acknowledgements

I would like to specifically thank Joan Jorgenson and the people in her lab, Colleen Carney and Jess Muszynski, for all their work dissecting the testis and using the microfluidic platforms designed by the Beebe Lab for cell culture. I would also like to thank Rachel O'Connell and Sam Schultz for all their hardwork designing and fabricating the devices. Finally I would like to thank Ashleigh Theberge for pulling me onto this project and all the helpful discussions.

References

1. L. Novakova and H. Vlckova, *Analytica chimica acta*, 2009, **656**, 8-35.
2. A. J. de Mello and N. Beard, *Lab on a chip*, 2003, **3**, 11N-19N.
3. B. Canas, C. Pineiro, E. Calvo, D. Lopez-Ferrer and J. M. Gallardo, *Journal of chromatography. A*, 2007, **1153**, 235-258.
4. Y. Chen, Z. Guo, X. Wang and C. Qiu, *Journal of chromatography. A*, 2008, **1184**, 191-219.
5. N. Simpson, *Solid-Phase Extraction: Principles, Applications, Techniques*, Marcel Dekker, New York, 2000.
6. N. Lion, F. Reymond, H. H. Girault and J. S. Rossier, *Current opinion in biotechnology*, 2004, **15**, 31-37.
7. R. A. Kemshead J, Ugelstad J., presented in part at the ASCO Annual Meeting, St. Louis, Missouri, April 25-27, 1982, 1982.
8. S. C. Tan and B. C. Yiap, *Journal of biomedicine & biotechnology*, 2009, **2009**, 574398.
9. S. Berensmeier, *Applied microbiology and biotechnology*, 2006, **73**, 495-504.
10. M. C. Hennion, *Journal of chromatography. A*, 1999, **856**, 3-54.
11. J. Lichtenberg, N. F. de Rooij and E. Verpoorte, *Talanta*, 2002, **56**, 233-266.
12. M. Madou, J. Zoval, G. Jia, H. Kido, J. Kim and N. Kim, *Annual review of biomedical engineering*, 2006, **8**, 601-628.
13. Q. Ramadan and M. A. Gijs, *The Analyst*, 2011, **136**, 1157-1166.
14. D. J. Beebe, G. A. Mensing and G. M. Walker, *Annual review of biomedical engineering*, 2002, **4**, 261-286.
15. B. Zhao, J. S. Moore and D. J. Beebe, *Science*, 2001, **291**, 1023-1026.
16. J. Atencia and D. J. Beebe, *Nature*, 2005, **437**, 648-655.
17. L. Strotman, R. O'Connell, B. P. Casavant, S. M. Berry, J. M. Sperger, J. M. Lang and D. J. Beebe, *Analytical chemistry*, 2013, **85**, 9764-9770.
18. S. M. Berry, K. J. Regehr, B. P. Casavant and D. J. Beebe, *Journal of laboratory automation*, 2013, **18**, 206-211.
19. S. M. Berry, E. N. Chin, S. S. Jackson, L. N. Strotman, M. Goel, N. E. Thompson, C. M. Alexander, S. Miyamoto, R. R. Burgess and D. J. Beebe, *Analytical biochemistry*, 2014, **447**, 133-140.
20. C. G. Rao, D. Chianese, G. V. Doyle, M. C. Miller, T. Russell, R. A. Sanders, Jr. and L. W. Terstappen, *International journal of oncology*, 2005, **27**, 49-57.
21. E. S. Stalder, L. H. Nagy, P. Batalla, T. M. Arthur, N. E. Thompson and R. R. Burgess, *Protein expression and purification*, 2011, **77**, 26-33.
22. S. M. Berry, E. T. Alarid and D. J. Beebe, *Lab on a chip*, 2011, **11**, 1747-1753.
23. S. M. Berry, L. N. Strotman, J. D. Kueck, E. T. Alarid and D. J. Beebe, *Biomedical microdevices*, 2011, **13**, 1033-1042.
24. K. Sur, S. M. McFall, E. T. Yeh, S. R. Jangam, M. A. Hayden, S. D. Stroupe and D. M. Kelso, *The Journal of molecular diagnostics : JMD*, 2010, **12**, 620-628.
25. T. K. Shikida M, Inouchi K, Honda H, Sato K, *Sensors and Actuators B: Chemical*, 2006, **113**, 563-569.
26. A. A. Chen H, Faghri M, *Microfluidics and Nanofluidics* 2011, **10**, 593-605.

27. H. Bordelon, N. M. Adams, A. S. Klemm, P. K. Russ, J. V. Williams, H. K. Talbot, D. W. Wright and F. R. Haselton, *ACS applied materials & interfaces*, 2011, **3**, 2161-2168.
28. C. W. Price, D. C. Leslie and J. P. Landers, *Lab on a chip*, 2009, **9**, 2484-2494.
29. J. Kim, M. Johnson, P. Hill and B. K. Gale, *Integrative Biology*, 2009, **1**, 574-586.
30. D. R. Franz, P. B. Jahrling, A. M. Friedlander, D. J. McClain, D. L. Hoover, W. R. Bryne, J. A. Pavlin, G. W. Christopher and E. M. Eitzen, Jr., *JAMA : the journal of the American Medical Association*, 1997, **278**, 399-411.
31. S. S. Arnon, R. Schechter, T. V. Inglesby, D. A. Henderson, J. G. Bartlett, M. S. Ascher, E. Eitzen, A. D. Fine, J. Hauer, M. Layton, S. Lillibridge, M. T. Osterholm, T. O'Toole, G. Parker, T. M. Perl, P. K. Russell, D. L. Swerdlow, K. Tonat and B. Working Group on Civilian, *JAMA : the journal of the American Medical Association*, 2001, **285**, 1059-1070.
32. D. DG, *PCR Primer A laboratory manual*, Cold Spring Harbor Laboratory, New York, 2003.
33. L. M. Wein and Y. Liu, *Proceedings of the National Academy of Sciences of the United States of America*, 2005, **102**, 9984-9989.
34. L. Rossen, P. Norskov, K. Holmstrom and O. F. Rasmussen, *International journal of food microbiology*, 1992, **17**, 37-45.
35. J. Bickley, J. K. Short, D. G. McDowell and H. C. Parkes, *Letters in applied microbiology*, 1996, **22**, 153-158.
36. P. Belgrader, W. Benett, D. Hadley, J. Richards, P. Stratton, R. Mariella, Jr. and F. Milanovich, *Science*, 1999, **284**, 449-450.
37. J. A. Higgins, S. Nasarabadi, J. S. Karns, D. R. Shelton, M. Cooper, A. Gbakima and R. P. Koopman, *Biosensors & bioelectronics*, 2003, **18**, 1115-1123.
38. C. Zhang, J. Xu, W. Ma and W. Zheng, *Biotechnology advances*, 2006, **24**, 243-284.
39. S. S. Arnon, R. Schechter, T. V. Inglesby and et al., *JAMA : the journal of the American Medical Association*, 2001, **285**, 1059-1070.
40. S. Bandyopadhyay, A. W. Clark, B. R. DasGupta and V. Sathyamoorthy, *The Journal of biological chemistry*, 1987, **262**, 2660-2663.
41. G. Schiavo, M. Matteoli and C. Montecucco, *Physiological reviews*, 2000, **80**, 717-766.
42. S. K. Sharma and R. C. Whiting, *Journal of food protection*, 2005, **68**, 1256-1263.
43. M. Lindstrom and H. Korkeala, *Clinical microbiology reviews*, 2006, **19**, 298-314.
44. S. Cai, B. R. Singh and S. Sharma, *Critical reviews in microbiology*, 2007, **33**, 109-125.
45. M. L. Frisk, G. Lin, E. A. Johnson and D. J. Beebe, *Biosensors & bioelectronics*, 2011, **26**, 1929-1935.
46. W. S. Hong, E. W. Young, W. H. Tepp, E. A. Johnson and D. J. Beebe, *Toxicological sciences : an official journal of the Society of Toxicology*, 2013, **134**, 64-72.
47. L. N. Strotman, G. Lin, S. M. Berry, E. A. Johnson and D. J. Beebe, *The Analyst*, 2012, **137**, 4023-4028.
48. K. H. Ching, A. Lin, J. A. McGarvey, L. H. Stanker and R. Hnasko, *Journal of immunological methods*, 2012, **380**, 23-29.
49. M. Szilagyi, V. R. Rivera, D. Neal, G. A. Merrill and M. A. Poli, *Toxicon : official journal of the International Society on Toxinology*, 2000, **38**, 381-389.

50. J. C. Jokerst, J. A. Adkins, B. Bisha, M. M. Mentele, L. D. Goodridge and C. S. Henry, *Analytical chemistry*, 2012, **84**, 2900-2907.
51. S. M. Berry, L. J. Maccoux and D. J. Beebe, *Analytical chemistry*, 2012, **84**, 5518-5523.
52. M. Okochi, H. Tsuchiya, F. Kumazawa, M. Shikida and H. Honda, *Journal of Bioscience and Bioengineering*, 2010, **109**, 193-197.
53. B. P. Casavant, D. J. Guckenberger, S. M. Berry, J. T. Tokar, J. M. Lang and D. J. Beebe, *Lab on a chip*, 2013, **13**, 391-396.
54. C. Schrader, A. Schielke, L. Ellerbroek and R. Johne, *Journal of Applied Microbiology*, 2012, **113**, 1014-1026.
55. C. W. Price, D. C. Leslie and J. P. Landers, *Lab on a Chip*, 2009, **9**, 2484-2494.
56. A. W. Martinez, S. T. Phillips, G. M. Whitesides and E. Carrilho, *Analytical Chemistry*, 2010, **82**, 3-10.
57. A. W. Martinez, S. T. Phillips, M. J. Butte and G. M. Whitesides, *Angewandte Chemie-International Edition*, 2007, **46**, 1318-1320.
58. L. Lafleur, D. Stevens, K. McKenzie, S. Ramachandran, P. Spicar-Mihalic, M. Singhal, A. Arjyal, J. Osborn, P. Kauffman, P. Yager and B. Lutz, *Lab on a Chip*, 2012, **12**, 1119-1127.
59. Y. Lu, W. Shi, J. Qin and B. Lin, *Analytical Chemistry*, 2010, **82**, 329-335.
60. S. A. Klasner, A. K. Price, K. W. Hoeman, R. S. Wilson, K. J. Bell and C. T. Culbertson, *Analytical and Bioanalytical Chemistry*, 2010, **397**, 1821-1829.
61. E. Fu, B. Lutz, P. Kauffman and P. Yager, *Lab on a Chip*, 2010, **10**, 918-920.
62. S. R. Jangam, D. H. Yamada, S. M. McFall and D. M. Kelso, *Journal of Clinical Microbiology*, 2009, **47**, 2363-2368.
63. A. V. Govindarajan, S. Ramachandran, G. D. Vigil, P. Yager and K. F. Boehringer, *Lab on a Chip*, 2012, **12**, 174-181.
64. S. M. Berry, E. T. Alarid and D. J. Beebe, *Lab on a Chip*, 2011, **11**, 1747-1753.
65. K. Sur, S. M. McFall, E. T. Yeh, S. R. Jangam, M. A. Hayden, S. D. Stroupe and D. M. Kelso, *Journal of Molecular Diagnostics*, 2010, **12**, 620-628.
66. F. Shen, B. Sun, J. E. Kreutz, E. K. Davydova, W. Du, P. L. Reddy, L. J. Joseph and R. F. Ismagilov, *Journal of the American Chemical Society*, 2011, **133**, 17705-17712.
67. H. Bordelon, N. M. Adams, A. S. Klemm, P. K. Russ, J. V. Williams, H. K. Talbot, D. W. Wright and F. R. Haselton, *Acs Applied Materials & Interfaces*, 2011, **3**, 2161-2168.
68. C. Marangoni, *Ann. Phy. Chem*, 1871, **143**, 337.
69. J. Bico and D. Quere, *Europhysics Letters*, 2000, **51**, 546-550.
70. J. Bico and D. Quere, *Journal of Fluid Mechanics*, 2002, **467**, 101-127.
71. *PCR Primer: A Laboratory Manual*, CSHL Press, 2003.
72. D. C. Hay Burgess, J. Wasserman and C. A. Dahl, *Nature*, 2006, **444 Suppl 1**, 1-2.
73. M. A. Dineva, L. MahiLum-Tapay and H. Lee, *The Analyst*, 2007, **132**, 1193-1199.
74. M. Urdea, L. A. Penny, S. S. Olmsted, M. Y. Giovanni, P. Kaspar, A. Shepherd, P. Wilson, C. A. Dahl, S. Buchsbaum, G. Moeller and D. C. Hay Burgess, *Nature*, 2006, **444 Suppl 1**, 73-79.
75. A. V. Govindarajan, S. Ramachandran, G. D. Vigil, P. Yager and K. F. Bohringer, *Lab on a chip*, 2012, **12**, 174-181.
76. *Technical Brief on HIV Viral Load Technologies*, 2010.

77. P. Yager, T. Edwards, E. Fu, K. Helton, K. Nelson, M. R. Tam and B. H. Weigl, *Nature*, 2006, **442**, 412-418.
78. A. K. Yetisen, M. S. Akram and C. R. Lowe, *Lab on a chip*, 2013, **13**, 2210-2251.
79. H. Guio, H. Okayama, Y. Ashino, H. Saitoh, P. Xiao, M. Miki, N. Yoshihara, S. Nakanowatari and T. Hattori, *The international journal of tuberculosis and lung disease : the official journal of the International Union against Tuberculosis and Lung Disease*, 2006, **10**, 906-910.
80. S. R. Jangam, D. H. Yamada, S. M. McFall and D. M. Kelso, *Journal of clinical microbiology*, 2009, **47**, 2363-2368.
81. C. J. Easley, J. M. Karlinsey and J. P. Landers, *Lab on a chip*, 2006, **6**, 601-610.
82. S. I. Han, K. H. Han, A. B. Frazier, J. P. Ferrance and J. P. Landers, *Biomedical microdevices*, 2009, **11**, 935-942.
83. J. W. Hong, V. Studer, G. Hang, W. F. Anderson and S. R. Quake, *Nature biotechnology*, 2004, **22**, 435-439.
84. J. Min, J. H. Kim, Y. Lee, K. Namkoong, H. C. Im, H. N. Kim, H. Y. Kim, N. Huh and Y. R. Kim, *Lab on a chip*, 2011, **11**, 259-265.
85. L. F. Diaz, G. M. Savage and L. L. Eggerth, *Waste management*, 2005, **25**, 626-637.
86. B. P. Casavant, L. N. Strotman, J. J. Tokar, S. M. Thiede, A. M. Traynor, J. S. Ferguson, J. M. Lang and D. J. Beebe, *Lab on a chip*, 2013, **14**, 99-105.
87. S. F. Moussavi-Harami, D. S. Annis, W. Ma, S. M. Berry, E. E. Coughlin, L. N. Strotman, L. M. Maurer, M. S. Westphall, J. J. Coon, D. F. Mosher and D. J. Beebe, *Journal of proteome research*, 2013, **12**, 3393-3404.
88. C. Xu, J. R. Houck, W. Fan, P. Wang, Y. Chen, M. Upton, N. D. Futran, S. M. Schwartz, L. P. Zhao, C. Chen and E. Mendez, *The Journal of molecular diagnostics : JMD*, 2008, **10**, 129-134.
89. P. D. Cirilo, F. A. Marchi, C. Barros Filho Mde, R. M. Rocha, M. A. Domingues, I. Jurisica, A. Pontes and S. R. Rogatto, *PloS one*, 2013, **8**, e57901.
90. C. Curtis, S. P. Shah, S. F. Chin, G. Turashvili, O. M. Rueda, M. J. Dunning, D. Speed, A. G. Lynch, S. Samarajiwa, Y. Yuan, S. Graf, G. Ha, G. Haffari, A. Bashashati, R. Russell, S. McKinney, M. Group, A. Langerod, A. Green, E. Provenzano, G. Wishart, S. Pinder, P. Watson, F. Markowetz, L. Murphy, I. Ellis, A. Purushotham, A. L. Borresen-Dale, J. D. Brenton, S. Tavare, C. Caldas and S. Aparicio, *Nature*, 2012, **486**, 346-352.
91. C. Wu, A. W. Wyatt, A. V. Lapuk, A. McPherson, B. J. McConeghy, R. H. Bell, S. Anderson, A. Haegert, S. Brahmbhatt, R. Shukin, F. Mo, E. Li, L. Fazli, A. Hurtado-Coll, E. C. Jones, Y. S. Butterfield, F. Hach, F. Hormozdiari, I. Hajirasouliha, P. C. Boutros, R. G. Bristow, S. J. Jones, M. Hirst, M. A. Marra, C. A. Maher, A. M. Chinnaiyan, S. C. Sahinalp, M. E. Gleave, S. V. Volik and C. C. Collins, *The Journal of pathology*, 2012, **227**, 53-61.
92. W. Mathieson and G. A. Thomas, *Analytical biochemistry*, 2013, **433**, 10-18.
93. M. Grzendowski, M. J. Riemenschneider, E. Hawranke, A. Stefanski, H. E. Meyer, G. Reifenberger and K. Stuhler, *Proteomics*, 2009, **9**, 4985-4990.
94. P. Chomczynski, *BioTechniques*, 1993, **15**, 532-534, 536-537.
95. J. M. Tolosa, J. E. Schjenken, T. D. Civiti, V. L. Clifton and R. Smith, *BioTechniques*, 2007, **43**, 799-804.

96. A. B. Hummon, S. R. Lim, M. J. Difilippantonio and T. Ried, *BioTechniques*, 2007, **42**, 467-470, 472.
97. C. A. Klein, S. Seidl, K. Petat-Dutter, S. Offner, J. B. Geigl, O. Schmidt-Kittler, N. Wendler, B. Passlick, R. M. Huber, G. Schlimok, P. A. Baeuerle and G. Riethmuller, *Nature biotechnology*, 2002, **20**, 387-392.
98. J. J. Kim, M.; Hill, P.; Gale B.K., *Integrative Biology*, 2009, **1**, 574–586.
99. J. J. Kim, M.; Hill, P.; Sonkul, R.S.; Kim, J.; Gale B.K., *JOURNAL OF MICROMECHANICS AND MICROENGINEERING*, 2011, **22**.
100. M. A. Witek, M. L. Hupert, D. S. Park, K. Fears, M. C. Murphy and S. A. Soper, *Analytical chemistry*, 2008, **80**, 3483-3491.
101. M. Zborowski and J. J. Chalmers, *Analytical chemistry*, 2011, **83**, 8050-8056.
102. E. S. Lianidou and A. Markou, *Clinical chemistry*, 2011, **57**, 1242-1255.
103. U. Dharmasiri, M. A. Witek, A. A. Adams and S. A. Soper, *Annual review of analytical chemistry*, 2010, **3**, 409-431.
104. L. E. Lowes, D. Goodale, M. Keeney and A. L. Allan, *Methods in cell biology*, 2011, **102**, 261-290.
105. C. D. Steele, R. J. Wapner, J. B. Smith, M. K. Haynes and L. G. Jackson, *Clinical obstetrics and gynecology*, 1996, **39**, 801-813.
106. N. Daniele, M. C. Scerpa, M. Caniglia, M. E. Bernardo, C. Rossi, C. Ciammetti, G. Palumbo, F. Locatelli, G. Isacchi and F. Zinno, *Pathology, research and practice*, 2012, **208**, 67-73.
107. X. Cheng, Y. S. Liu, D. Irimia, U. Demirci, L. Yang, L. Zamir, W. R. Rodriguez, M. Toner and R. Bashir, *Lab on a chip*, 2007, **7**, 746-755.
108. N. N. Gangopadhyay, H. Shen, R. Landreneau, J. D. Luketich and M. J. Schuchert, *Journal of immunological methods*, 2004, **292**, 73-81.
109. D. C. Rio, M. Ares, Jr., G. J. Hannon and T. W. Nilsen, *Cold Spring Harbor protocols*, 2010, **2010**, pdb prot5454.
110. T. W. Friedlander and C. J. Ryan, *The Urologic clinics of North America*, 2012, **39**, 453-464.
111. J. Veldscholte, C. A. Berrevoets, C. Ris-Stalpers, G. G. Kuiper, G. Jenster, J. Trapman, A. O. Brinkmann and E. Mulder, *The Journal of steroid biochemistry and molecular biology*, 1992, **41**, 665-669.
112. B. Alberts, *Molecular Biology of the Cell*, Garland Science, New York, 2002.
113. Z. Gibas, R. Becher, E. Kawinski, J. Horoszewicz and A. A. Sandberg, *Cancer genetics and cytogenetics*, 1984, **11**, 399-404.
114. T. Berg, R. A. Bradshaw, O. A. Carretero, J. Chao, L. Chao, J. A. Clements, M. Fahnestock, H. Fritz, F. Gauthier, R. J. MacDonald and et al., *Agents and actions. Supplements*, 1992, **38 (Pt 1)**, 19-25.
115. R. Siegel, D. Naishadham and A. Jemal, *CA Cancer J Clin*, 2013, **63**, 11-30.
116. F. C. Detterbeck, P. J. Mazzone, D. P. Naidich and P. B. Bach, *Chest*, 2013, **143**, e78S-92S.
117. D. A. Eberhard, G. Giaccone and B. E. Johnson, *J Clin Oncol*, 2008, **26**, 983-994.
118. L. V. Sequist, B. A. Waltman, D. Dias-Santagata, S. Digumarthy, A. B. Turke, P. Fidias, K. Bergethon, A. T. Shaw, S. Gettinger, A. K. Cosper, S. Akhavanfard, R. S. Heist, J.

Temel, J. G. Christensen, J. C. Wain, T. J. Lynch, K. Vernovsky, E. J. Mark, M. Lanuti, A. J. Iafrate, M. Mino-Kenudson and J. A. Engelman, *Sci Transl Med*, 2011, **3**, 75ra26.
119. D. W. Hsia, K. W. Jensen, D. Curran-Everett and A. I. Musani, *J Bronchology Interv Pulmonol*, 2012, **19**, 5-11.
120. L. S. Poulou, P. Tsagouli, P. D. Ziakas, D. Politi, R. Trigidou and L. Thanos, *Acta Radiol*, 2013.
121. S. S. Dhillon and E. U. Dexter, *J Carcinog*, 2012, **11**, 19.
122. S. A. Ahrendt, J. T. Chow, L. H. Xu, S. C. Yang, C. F. Eisenberger, M. Esteller, J. G. Herman, L. Wu, P. A. Decker, J. Jen and D. Sidransky, *J Natl Cancer Inst*, 1999, **91**, 332-339.
123. D. Ha, H. Choi, F. A. Almeida, A. Arrossi, J. Brainard, J. Cicenia, C. Farver, T. Gildea, M. S. Machuzak and P. Mazzone, *J Bronchology Interv Pulmonol*, 2013, **20**, 10-15.
124. G. Attard and J. S. de Bono, *Curr Opin Genet Dev*, 2011, **21**, 50-58.
125. G. R. Mundy, *Nat Rev Cancer*, 2002, **2**, 584-593.
126. V. S. Nair, K. V. Keu, M. S. Luttgen, A. Kolatkar, M. Vasanawala, W. Kuschner, K. Bethel, A. H. Iagaru, C. Hoh, J. B. Shrager, B. W. Loo, Jr., L. Bazhenova, J. Nieva, S. S. Gambhir and P. Kuhn, *PLoS One*, 2013, **8**, e67733.
127. M. G. Krebs, J. M. Hou, R. Sloane, L. Lancashire, L. Priest, D. Nonaka, T. H. Ward, A. Backen, G. Clack, A. Hughes, M. Ranson, F. H. Blackhall and C. Dive, *J Thorac Oncol*, 2012, **7**, 306-315.
128. J. M. Hou, M. G. Krebs, L. Lancashire, R. Sloane, A. Backen, R. K. Swain, L. J. Priest, A. Greystoke, C. Zhou, K. Morris, T. Ward, F. H. Blackhall and C. Dive, *J Clin Oncol*, 2012, **30**, 525-532.
129. M. G. Krebs, R. Sloane, L. Priest, L. Lancashire, J. M. Hou, A. Greystoke, T. H. Ward, R. Ferraldeschi, A. Hughes, G. Clack, M. Ranson, C. Dive and F. H. Blackhall, *J Clin Oncol*, 2011, **29**, 1556-1563.
130. D. C. Danila, K. Pantel, M. Fleisher and H. I. Scher, *Cancer J*, **17**, 438-450.
131. S. Nagrath, L. V. Sequist, S. Maheswaran, D. W. Bell, D. Irimia, L. Ulkus, M. R. Smith, E. L. Kwak, S. Digumarthy, A. Muzikansky, P. Ryan, U. J. Balis, R. G. Tompkins, D. A. Haber and M. Toner, *Nature*, 2007, **450**, 1235-1239.
132. D. Issadore, J. Chung, H. Shao, M. Liong, A. A. Ghazani, C. M. Castro, R. Weissleder and H. Lee, *Sci Transl Med*, 2012, **4**, 141ra192.
133. I. J. Vishal Gupta, Miguel Garza, Vladislava O. Melnikova, David K. Hasegawa, Ronald Pethig, and Darren W. Davis, *Biomicrofluidics*, 2012, **6**.
134. B. P. Casavant, D. J. Guckenberger, S. M. Berry, J. T. Tokar, J. M. Lang and D. J. Beebe, *Lab on a Chip*, 2013.
135. D. Tan, Q. Li, G. Deeb, N. Ramnath, H. K. Slocum, J. Brooks, R. Cheney, S. Wiseman, T. Anderson and G. Loewen, *Hum Pathol*, 2003, **34**, 597-604.
136. T. John, G. Liu and M. S. Tsao, *Oncogene*, 2009, **28 Suppl 1**, S14-23.
137. J. S. Lee, H. R. Kim, C. Y. Lee, M. Shin and H. S. Shim, *Ann Surg Oncol*, 2013.
138. B. Zhao, N. O. Viernes, J. S. Moore and D. J. Beebe, *Journal of the American Chemical Society*, 2002, **124**, 5284-5285.
139. S. Derer, P. Bauer, S. Lohse, A. H. Scheel, S. Berger, C. Kellner, M. Peipp and T. Valerius, *J Immunol*, 2012, **189**, 5230-5239.

140. R. L. Bitting, R. Boominathan, C. Rao, G. Kemeny, B. Foulk, M. A. Garcia-Blanco, M. Connelly and A. J. Armstrong, *Methods*, 2013.
141. T. Kanematsu, S. Yano, H. Uehara, Y. Bando and S. Sone, *Oncol Res*, 2003, **13**, 289-298.
142. R. Pirker, J. R. Pereira, A. Szczesna, J. von Pawel, M. Krzakowski, R. RamLau, I. Vynnychenko, K. Park, C. T. Yu, V. Ganul, J. K. Roh, E. Bajetta, K. O'Byrne, F. de Marinis, W. Eberhardt, T. Goddemeier, M. Emig and U. Gatzemeier, *Lancet*, 2009, **373**, 1525-1531.
143. F. A. Shepherd, J. Rodrigues Pereira, T. Ciuleanu, E. H. Tan, V. Hirsh, S. Thongprasert, D. Campos, S. Maoleekoonpiroj, M. Smylie, R. Martins, M. van Kooten, M. Dediu, B. Findlay, D. Tu, D. Johnston, A. Bezjak, G. Clark, P. Santabarbara and L. Seymour, *N Engl J Med*, 2005, **353**, 123-132.
144. R. Rosell, E. Carcereny, R. Gervais, A. Vergnenegre, B. Massuti, E. Felip, R. Palmero, R. Garcia-Gomez, C. Pallares, J. M. Sanchez, R. Porta, M. Cobo, P. Garrido, F. Longo, T. Moran, A. Insa, F. De Marinis, R. Corre, I. Bover, A. Illiano, E. Dansin, J. de Castro, M. Milella, N. Reguart, G. Altavilla, U. Jimenez, M. Provencio, M. A. Moreno, J. Terrasa, J. Munoz-Langa, J. Valdivia, D. Isla, M. Domine, O. Molinier, J. Mazieres, N. Baize, R. Garcia-Campelo, G. Robinet, D. Rodriguez-Abreu, G. Lopez-Vivanco, V. Gebbia, L. Ferrera-Delgado, P. Bombaron, R. Bernabe, A. Bearz, A. Artal, E. Cortesi, C. Rolfo, M. Sanchez-Ronco, A. Drozdowskyj, C. Queralt, I. de Aguirre, J. L. Ramirez, J. J. Sanchez, M. A. Molina, M. Taron and L. Paz-Ares, *Lancet Oncol*, 2012, **13**, 239-246.
145. S. Medic, R. L. Pearce, P. J. Heenan and M. Ziman, *Pigment cell research / sponsored by the European Society for Pigment Cell Research and the International Pigment Cell Society*, 2007, **20**, 80-91.
146. M. Y. Kim, T. Oskarsson, S. Acharyya, D. X. Nguyen, X. H. Zhang, L. Norton and J. Massague, *Cell*, 2009, **139**, 1315-1326.
147. T. Fehm, V. Muller, C. Alix-Panabieres and K. Pantel, *Breast cancer research : BCR*, 2008, **10 Suppl 1**, S1.
148. J. S. de Bono, H. I. Scher, R. B. Montgomery, C. Parker, M. C. Miller, H. Tissing, G. V. Doyle, L. W. Terstappen, K. J. Pienta and D. Raghavan, *Clinical cancer research : an official journal of the American Association for Cancer Research*, 2008, **14**, 6302-6309.
149. D. C. Danila, A. Anand, C. C. Sung, G. Heller, M. A. Leversha, L. Cao, H. Lilja, A. Molina, C. L. Sawyers, M. Fleisher and H. I. Scher, *European urology*, 2011, **60**, 897-904.
150. F. Tanaka, K. Yoneda, N. Kondo, M. Hashimoto, T. Takuwa, S. Matsumoto, Y. Okumura, S. Rahman, N. Tsubota, T. Tsujimura, K. Kuribayashi, K. Fukuoka, T. Nakano and S. Hasegawa, *Clinical cancer research : an official journal of the American Association for Cancer Research*, 2009, **15**, 6980-6986.
151. R. J. Amato, V. Melnikova, Y. Zhang, W. Liu, S. Saxena, P. K. Shah, B. T. Jensen, K. E. Torres and D. W. Davis, *Urology*, 2013, **81**, 1303-1307.
152. D. C. Danila, M. Fleisher and H. I. Scher, *Clinical cancer research : an official journal of the American Association for Cancer Research*, 2011, **17**, 3903-3912.
153. F. L. Carvalho, B. W. Simons, E. S. Antonarakis, Z. Rasheed, N. Douglas, D. Villegas, W. Matsui and D. M. Berman, *Oncotarget*, 2013, **4**, 413-421.

154. W. J. Allard, J. Matera, M. C. Miller, M. Repollet, M. C. Connelly, C. Rao, A. G. Tibbe, J. W. Uhr and L. W. Terstappen, *Clinical cancer research : an official journal of the American Association for Cancer Research*, 2004, **10**, 6897-6904.
155. H. I. Scher, M. J. Morris, S. Larson and G. Heller, *Nature reviews. Clinical oncology*, 2013, **10**, 225-234.
156. J. P. Gleghorn, E. D. Pratt, D. Denning, H. Liu, N. H. Bander, S. T. Tagawa, D. M. Nanus, P. A. Giannakakou and B. J. Kirby, *Lab on a chip*, 2010, **10**, 27-29.
157. D. C. Danila, K. Pantel, M. Fleisher and H. I. Scher, *Cancer journal*, 2011, **17**, 438-450.
158. E. Ozkumur, A. M. Shah, J. C. Ciciliano, B. L. Emmink, D. T. Miyamoto, E. Brachtel, M. Yu, P. I. Chen, B. Morgan, J. Trautwein, A. Kimura, S. Sengupta, S. L. Stott, N. M. Karabacak, T. A. Barber, J. R. Walsh, K. Smith, P. S. Spuhler, J. P. Sullivan, R. J. Lee, D. T. Ting, X. Luo, A. T. Shaw, A. Bardia, L. V. Sequist, D. N. Louis, S. Maheswaran, R. Kapur, D. A. Haber and M. Toner, *Science translational medicine*, 2013, **5**, 179ra147.
159. R. Kalluri and R. A. Weinberg, *The Journal of clinical investigation*, 2009, **119**, 1420-1428.
160. S. J. Tan, R. L. Lakshmi, P. Chen, W. T. Lim, L. Yobas and C. T. Lim, *Biosensors & bioelectronics*, 2010, **26**, 1701-1705.
161. C. Alix-Panabieres, X. Rebillard, J. P. Brouillet, E. Barbotte, F. Iborra, B. Segui, T. Maudelonde, C. Jolivet-Reynaud and J. P. Vendrell, *Clinical chemistry*, 2005, **51**, 1538-1541.
162. D. T. Miyamoto, R. J. Lee, S. L. Stott, D. T. Ting, B. S. Wittner, M. Ulman, M. E. Smas, J. B. Lord, B. W. Brannigan, J. Trautwein, N. H. Bander, C. L. Wu, L. V. Sequist, M. R. Smith, S. Ramaswamy, M. Toner, S. Maheswaran and D. A. Haber, *Cancer discovery*, 2012, **2**, 995-1003.
163. M. Yu, A. Bardia, B. S. Wittner, S. L. Stott, M. E. Smas, D. T. Ting, S. J. Isakoff, J. C. Ciciliano, M. N. Wells, A. M. Shah, K. F. Concannon, M. C. Donaldson, L. V. Sequist, E. Brachtel, D. Sgroi, J. Baselga, S. Ramaswamy, M. Toner, D. A. Haber and S. Maheswaran, *Science*, 2013, **339**, 580-584.
164. T. W. Friedlander, V. T. Ngo, H. Dong, G. Premasekharan, V. Weinberg, S. Doty, Q. Zhao, E. G. Gilbert, C. J. Ryan, W. T. Chen and P. L. Paris, *International journal of cancer. Journal international du cancer*, 2013.
165. G. M. Cann, Z. G. Gulzar, S. Cooper, R. Li, S. Luo, M. Tat, S. Stuart, G. Schroth, S. Srinivas, M. Ronaghi, J. D. Brooks and A. H. Talasaz, *PloS one*, 2012, **7**, e49144.
166. C. G. Roehrborn and L. K. Black, *BJU international*, 2011, **108**, 806-813.
167. C. Huggins and C. V. Hodges, *The Journal of urology*, 2002, **168**, 9-12.
168. C. A. Heinlein and C. Chang, *Endocrine reviews*, 2004, **25**, 276-308.
169. D. Rathkopf and H. I. Scher, *Cancer journal*, 2013, **19**, 43-49.
170. H. I. Scher and G. Heller, *Urology*, 2000, **55**, 323-327.
171. S. Halabi, E. J. Small, P. W. Kantoff, M. W. Kattan, E. B. Kaplan, N. A. Dawson, E. G. Levine, B. A. Blumenstein and N. J. Vogelzang, *Journal of clinical oncology : official journal of the American Society of Clinical Oncology*, 2003, **21**, 1232-1237.
172. R. B. Montgomery, E. A. Mostaghel, R. Vessella, D. L. Hess, T. F. Kalhorn, C. S. Higano, L. D. True and P. S. Nelson, *Cancer research*, 2008, **68**, 4447-4454.

173. J. S. de Bono, C. J. Logothetis, A. Molina, K. Fizazi, S. North, L. Chu, K. N. Chi, R. J. Jones, O. B. Goodman, Jr., F. Saad, J. N. Staffurth, P. Mainwaring, S. Harland, T. W. Flaig, T. E. Hutson, T. Cheng, H. Patterson, J. D. Hainsworth, C. J. Ryan, C. N. Sternberg, S. L. Ellard, A. Flechon, M. Saleh, M. Scholz, E. Efstathiou, A. Zivi, D. Bianchini, Y. Loriot, N. Chieffo, T. Kheoh, C. M. Haqq, H. I. Scher and C.-A.-. Investigators, *The New England journal of medicine*, 2011, **364**, 1995-2005.
174. A. H. Reid, G. Attard, E. Barrie and J. S. de Bono, *Nature clinical practice. Urology*, 2008, **5**, 610-620.
175. H. I. Scher, K. Fizazi, F. Saad, M. E. Taplin, C. N. Sternberg, K. Miller, R. de Wit, P. Mulders, K. N. Chi, N. D. Shore, A. J. Armstrong, T. W. Flaig, A. Flechon, P. Mainwaring, M. Fleming, J. D. Hainsworth, M. Hirmand, B. Selby, L. Seely, J. S. de Bono and A. Investigators, *The New England journal of medicine*, 2012, **367**, 1187-1197.
176. H. I. Scher, T. M. Beer, C. S. Higano, A. Anand, M. E. Taplin, E. Efstathiou, D. Rathkopf, J. Shelkey, E. Y. Yu, J. Alumkal, D. Hung, M. Hirmand, L. Seely, M. J. Morris, D. C. Danila, J. Humm, S. Larson, M. Fleisher, C. L. Sawyers and C. Prostate Cancer Foundation/Department of Defense Prostate Cancer Clinical Trials, *Lancet*, 2010, **375**, 1437-1446.
177. C. D. Chen, D. S. Welsbie, C. Tran, S. H. Baek, R. Chen, R. Vessella, M. G. Rosenfeld and C. L. Sawyers, *Nature medicine*, 2004, **10**, 33-39.
178. H. I. Scher and C. L. Sawyers, *Journal of clinical oncology : official journal of the American Society of Clinical Oncology*, 2005, **23**, 8253-8261.
179. M. E. Taplin, G. J. Bubley, T. D. Shuster, M. E. Frantz, A. E. Spooner, G. K. Ogata, H. N. Keer and S. P. Balk, *The New England journal of medicine*, 1995, **332**, 1393-1398.
180. C. Cai, H. H. He, S. Chen, I. Coleman, H. Wang, Z. Fang, S. Chen, P. S. Nelson, X. S. Liu, M. Brown and S. P. Balk, *Cancer cell*, 2011, **20**, 457-471.
181. J. L. Wright, E. M. Kwon, E. A. Ostrander, R. B. Montgomery, D. W. Lin, R. Vessella, J. L. Stanford and E. A. Mostaghel, *Cancer epidemiology, biomarkers & prevention : a publication of the American Association for Cancer Research, cosponsored by the American Society of Preventive Oncology*, 2011, **20**, 619-627.
182. M. Yang, W. Xie, E. Mostaghel, M. Nakabayashi, L. Werner, T. Sun, M. Pomerantz, M. Freedman, R. Ross, M. Regan, N. Sharifi, W. D. Figg, S. Balk, M. Brown, M. E. Taplin, W. K. Oh, G. S. Lee and P. W. Kantoff, *Journal of clinical oncology : official journal of the American Society of Clinical Oncology*, 2011, **29**, 2565-2573.
183. J. A. Locke, E. S. Guns, M. L. Lehman, S. Ettinger, A. Zoubeidi, A. Lubik, K. Margiotti, L. Fazli, H. Adomat, K. M. Wasan, M. E. Gleave and C. C. Nelson, *The Prostate*, 2010, **70**, 239-251.
184. B. S. Taylor, N. Schultz, H. Hieronymus, A. Gopalan, Y. Xiao, B. S. Carver, V. K. Arora, P. Kaushik, E. Cerami, B. Reva, Y. Antipin, N. Mitsiades, T. Landers, I. Dolgalev, J. E. Major, M. Wilson, N. D. Socci, A. E. Lash, A. Heguy, J. A. Eastham, H. I. Scher, V. E. Reuter, P. T. Scardino, C. Sander, C. L. Sawyers and W. L. Gerald, *Cancer cell*, 2010, **18**, 11-22.
185. S. Haile and M. D. Sadar, *Cellular and molecular life sciences : CMLS*, 2011, **68**, 3971-3981.
186. R. Hu, W. B. Isaacs and J. Luo, *The Prostate*, 2011, **71**, 1656-1667.

187. P. A. Watson, Y. F. Chen, M. D. Balbas, J. Wongvipat, N. D. Socci, A. Viale, K. Kim and C. L. Sawyers, *Proceedings of the National Academy of Sciences of the United States of America*, 2010, **107**, 16759-16765.
188. H. I. Scher, X. Jia, J. S. de Bono, M. Fleisher, K. J. Pienta, D. Raghavan and G. Heller, *The lancet oncology*, 2009, **10**, 233-239.
189. D. C. Danila, G. Heller, G. A. Gignac, R. Gonzalez-Espinoza, A. Anand, E. Tanaka, H. Lilja, L. Schwartz, S. Larson, M. Fleisher and H. I. Scher, *Clinical cancer research : an official journal of the American Association for Cancer Research*, 2007, **13**, 7053-7058.
190. D. C. Danila, M. J. Morris, J. S. de Bono, C. J. Ryan, S. R. Denmeade, M. R. Smith, M. E. Taplin, G. J. Bubley, T. Kheoh, C. Haqq, A. Molina, A. Anand, M. Koscuiszka, S. M. Larson, L. H. Schwartz, M. Fleisher and H. I. Scher, *Journal of clinical oncology : official journal of the American Society of Clinical Oncology*, 2010, **28**, 1496-1501.
191. G. Attard, J. F. Swennenhuis, D. Olmos, A. H. Reid, E. Vickers, R. A'Hern, R. Levink, F. Coumans, J. Moreira, R. Riisnaes, N. B. Oommen, G. Hawche, C. Jameson, E. Thompson, R. Sipkema, C. P. Carden, C. Parker, D. Dearnaley, S. B. Kaye, C. S. Cooper, A. Molina, M. E. Cox, L. W. Terstappen and J. S. de Bono, *Cancer research*, 2009, **69**, 2912-2918.
192. D. R. Shaffer, M. A. Leversha, D. C. Danila, O. Lin, R. Gonzalez-Espinoza, B. Gu, A. Anand, K. Smith, P. Maslak, G. V. Doyle, L. W. Terstappen, H. Lilja, G. Heller, M. Fleisher and H. I. Scher, *Clinical cancer research : an official journal of the American Association for Cancer Research*, 2007, **13**, 2023-2029.
193. Y. Li, S. C. Chan, L. J. Brand, T. H. Hwang, K. A. Silverstein and S. M. Dehm, *Cancer research*, 2013, **73**, 483-489.
194. S. M. Dehm and D. J. Tindall, *Endocrine-related cancer*, 2011, **18**, R183-196.
195. S. J. Libertini, C. G. Tepper, V. Rodriguez, D. M. Asmuth, H. J. Kung and M. Mudryj, *Cancer research*, 2007, **67**, 9001-9005.
196. S. Sun, C. C. Sprenger, R. L. Vessella, K. Haugk, K. Soriano, E. A. Mostaghel, S. T. Page, I. M. Coleman, H. M. Nguyen, H. Sun, P. S. Nelson and S. R. Plymate, *The Journal of clinical investigation*, 2010, **120**, 2715-2730.
197. R. Hu, T. A. Dunn, S. Wei, S. Isharwal, R. W. Veltri, E. Humphreys, M. Han, A. W. Partin, R. L. Vessella, W. B. Isaacs, G. S. Bova and J. Luo, *Cancer research*, 2009, **69**, 16-22.
198. Z. Guo, X. Yang, F. Sun, R. Jiang, D. E. Linn, H. Chen, H. Chen, X. Kong, J. Melamed, C. G. Tepper, H. J. Kung, A. M. Brodie, J. Edwards and Y. Qiu, *Cancer research*, 2009, **69**, 2305-2313.
199. A. M. Sieuwerts, J. Kraan, J. Bolt-de Vries, P. van der Spoel, B. Mostert, J. W. Martens, J. W. Gratama, S. Sleijfer and J. A. Foekens, *Breast cancer research and treatment*, 2009, **118**, 455-468.
200. A. Jost, *Proceedings of the Society for Experimental Biology and Medicine. Society for Experimental Biology and Medicine*, 1947, **66**, 302.
201. H. M. Scott, J. I. Mason and R. M. Sharpe, *Endocr Rev*, 2009, **30**, 883-925.
202. H. Chen, R. S. Ge and B. R. Zirkin, *Molecular and cellular endocrinology*, 2009, **306**, 9-16.

203. H. Chen, E. Stanley, S. Jin and B. R. Zirkin, *Birth defects research. Part C, Embryo today : reviews*, 2010, **90**, 272-283.
204. L. Dong, S. A. Jelinsky, J. N. Finger, D. S. Johnston, G. S. Kopf, C. M. Sottas, M. P. Hardy and R. S. Ge, *Annals of the New York Academy of Sciences*, 2007, **1120**, 16-35.
205. I. B. Barsoum and H. H. Yao, *Journal of andrology*, 2010, **31**, 11-15.
206. P. J. O'Shaughnessy, P. Baker, U. Sohnius, A. M. Haavisto, H. M. Charlton and I. Huhtaniemi, *Endocrinology*, 1998, **139**, 1141-1146.
207. H. H. Yao, W. Whoriskey and B. Capel, *Genes & development*, 2002, **16**, 1433-1440.
208. J. Brennan, C. Tilmann and B. Capel, *Genes Dev.*, 2003, **17**, 800-810.
209. R. Habert, H. Lejeune and J. M. Saez, *Molecular and cellular endocrinology*, 2001, **179**, 47-74.
210. I. Barsoum and H. H. Yao, *Trends in endocrinology and metabolism: TEM*, 2006, **17**, 223-228.
211. J. M. Orth, *The Anatomical record*, 1982, **203**, 485-492.
212. A. G. Byskov, *Physiological reviews*, 1986, **66**, 71-117.
213. S. Migrenne, C. Pairault, C. Racine, G. Livera, A. Geloso and R. Habert, *Molecular and cellular endocrinology*, 2001, **172**, 193-202.
214. H. Merchant-Larios and N. Moreno-Mendoza, *Experimental cell research*, 1998, **244**, 230-238.
215. J. Brennan, C. Tilmann and B. Capel, *Genes & development*, 2003, **17**, 800-810.
216. J. Karl and B. Capel, *Developmental biology*, 1998, **203**, 323-333.
217. T. DeFalco, S. Takahashi and B. Capel, *Developmental biology*, 2011, **352**, 14-26.
218. I. B. Barsoum, J. Kaur, R. S. Ge, P. S. Cooke and H. H. Yao, *FASEB journal : official publication of the Federation of American Societies for Experimental Biology*, 2013, **27**, 2657-2666.
219. H. Tang, J. Brennan, J. Karl, Y. Hamada, L. Raetzman and B. Capel, *Development*, 2008, **135**, 3745-3753.
220. T. Defalco, A. Saraswathula, A. Briot, M. L. Iruela-Arispe and B. Capel, *Biology of reproduction*, 2013, **88**, 91.
221. Y. Shima, K. Miyabayashi, S. Haraguchi, T. Arakawa, H. Otake, T. Baba, S. Matsuzaki, Y. Shishido, H. Akiyama, T. Tachibana, K. Tsutsui and K. Morohashi, *Molecular endocrinology*, 2013, **27**, 63-73.
222. P. J. O'Shaughnessy, P. J. Baker, M. Heikkila, S. Vainio and A. P. McMahon, *Endocrinology*, 2000, **141**, 2631-2637.
223. G. R. Klinefelter, P. F. Hall and L. L. Ewing, *Biol Reprod*, 1987, **36**, 769-783.
224. A. Salva, G. R. Klinefelter and M. P. Hardy, *J Androl*, 2001, **22**, 665-671.
225. M. Ascoli and D. Puett, *Proc Natl Acad Sci U S A*, 1978, **75**, 99-102.
226. J. P. Mather, *Biol Reprod*, 1980, **23**, 243-252.
227. M. D. Muzumdar, B. Tasic, K. Miyamichi, L. Li and L. Luo, *Genesis*, 2007, **45**, 593-605.